Development of a microfluidic, segmented-flow, single molecule, enzyme activity assay and improvement of separation efficiency of basic proteins by application of a water-proofing agent as a coating in capillary electrophoresis

A DISSERTATION
SUBMITTED TO THE FACULTY OF THE GRADUATE SCHOOL
OF THE UNIVERSITY OF MINNESOTA
BY

Eric Rigoberto Castro Barahona

IN PARTIAL FULFILLMENT OF THE REQUIREMENTS
FOR THE DEGREE OF
DOCTOR OF PHILOSOPHY

Michael T. Bowser, Research Advisor

August 2012

Acknowledgements

No scientific project is done in isolation, with the researcher walking a lonely path to discovery. More than ever, research is a communal undertaking and as such the support and assistance of many groups and individuals must be acknowledged. This list is by no means exhaustive, but has merely sought to include those whose influence on the author looms largest.

In my choice of academic advisor, I could not have done better than Dr. Michael Bowser. In my time in his research group, he has taught me much, not least of which is the understanding that how you present your work is at least as important of the work itself. I thank him for his patience, support, energy, boundless curiosity and his commitment to training young chemists.

Great advisors strive to put together great research groups. This is very much the case for the Bowser group. I thank present and past members for their probing questions, suggestions and stimulating conversation both in and out of the lab. In particular, I am grateful to Dr. Bryan Fonslow, Dr. Chanda Ciriacks-Klinker, Dr. Neil Graf and Dr. Anne Bobich for both scientific knowledge and friendship without which graduate school would have been a much drearier proposition.

My parents, Rigo and Lizette, have that parent's faith that their children could accomplish anything they set their minds to. To them I owe everything: Life, a first rate education, unwavering support and the confidence that only comes from having parents that love you and believe in you. My sister Lorena, the other only-child, whom I don't

see nearly often enough, I thank just for being herself. Just knowing someone out there shares not only half your genes, but your character and history is a great comfort and a gift.

Throughout my academic career, I have been fortunate to have many excellent teachers, too many to enumerate here. I would, however, like to mention the two who had the greatest impact on my academic development. Dr. John Walters and Dr. John Evans teach the facts of chemistry as well how to think like an analytical chemist. They both are also good men of great humor and I remember them fondly always.

Finally, I thank my wife Karen. No one has been more patient or supportive throughout the writing of this work than she has. I count myself lucky in many ways, but having found my truly better-half is my greatest fortune. Thanks to her, I could write this thesis in such exciting circumstances as the moving to, not only a different country, but a new continent. I know that with her I will never lack for new things to try, which is the very spirit of discovery and science. *Ich liebe dich.*

To my grandparents, Rolando and Argentina

Abstract

A novel, microfluidic platform for segmented flow assays has been developed using commercially available Teflon tubing and PEEK connectors. Such a system can be used to generate arrays of nano to pico liter sized droplets separated from each other by plugs of a fluourous solvent. Each droplet becomes an individual reaction vessel suitable for high-throughput applications. We have applied this method to the development of a single enzyme molecule fluorescence assay.

Characterization of the droplet generation platform was done with the use of a 100 μm ID PEEK T-junction connector. When two immiscible streams, such as water and a fluorous solvent, meet at the T-junction an array of aqueous droplets separated by plugs of the solvent is generated inside the Teflon tubing. Experiments have shown that, like previous microfabricated segmented flow devices, our system can control the size of the droplets generated solely by changing the ratio of the flow rates of the two phases. Using this approach droplets can be produced with good reproducibility (better than 6% in all cases and better than 3% in most) over a wide range of flow rates. Rates of droplet generation of 10.37 ± 0.17 drops/s are easily achieved for good high-throughput potential. Fast on-line mixing of reagents and long term droplet stability of up to 7 days has also been demonstrated.

The discovery of the heterogeneity of enzyme molecules with respect to activity has resulted in the development of a variety of single enzyme molecule assays, with the aim of investigating the prevalence and origin of this phenomenon. The segmented flow platform we have developed is well suited to the application of single enzyme assays. It

has the advantage of high-throughput, as well as ease of fabrication compared to PDMS or silica based devices and elimination of exposure of the enzyme analyte to the walls of the channel or well. A segmented flow, single molecule assay has been developed for the enzyme alkaline phosphatase (AP). Single AP molecules were sequestered inside 100 pL droplets generated in a PEEK tee and stored in a length of 50 μm ID Teflon tubing. The droplet array was allowed to incubate for a suitable time period, during which the AP molecules converted the weakly fluorescent substrate AttoPhos® into a strongly fluorescent product. AP molecules were found, as in previous studies, to display heterogenous activity with up to a 9-fold difference between individual enzymes

In the last section of this work we have used the commercial glass treatment Aquapel as a capillary wall coating agent to reduce protein absorption in capillary electrophoresis (CE). Due to their large number of potential sites for interactions with the fused-silica wall, protein separations with CE can often be difficult. For this reason, much effort is expended on the development on wall coating agents for the prevention of such interactions. Aquapel is a fluorous polymer used commercially to render glass surfaces hydrophobic. The efficacy of the coating was investigated using a suite of three basic proteins: lysozyme, cytochrome c and α-chymotrypsinogen. Separation efficiencies of up to 130,000 theoretical plates were achieved over a pH range of 4.0 to 7.0, a significant improvement over bare fused silica capillary. Electroosmotic flow (EOF) was reduced by the Aquapel coating but not entirely suppressed. The stability of the coating was also examined. 62 protein injections were performed over a two day period during which

analyte migration times varied by less than 3.5%. Due to the ease of application and low cost, coating with Aquapel is an attractive alternative to available capillary coatings.

Table of Contents

List of Tables

List of Figures

Chapter 1

Chapter 2

Chapter 3

Chapter 4

List of Abbreviations

α chym	α-chymotrypsinogen
AP	Alkaline phosphatase
β-Gal	β-Galactosidase
BBT	2′-[2-benzothiazoyl]-6´-hydroxybenzothiazole
CE	Capillary electrophoresis
CIAP	Calf intestinal alkaline phosphatase
CTAB	Cetyltrimethylammonium bromide
Cyt c	Cytochrome c
DDAB	Didodecyldimethylammonium bromide
DMSO	Dimethylsulfoxide
ELISA	Enzyme-linked immunosorbent assay
EOF	Electroosmotic flow
FDG	Fluorescein di-galactopyranoside
HRP	Horse radish peroxidase
ID	Inner diameter
LDH-1	Lactose dehydrogenase 1
LIF	Laser induced fluorescence
Lys	Lysozyme
NAD+	Nicotinamide adenine dinucleotide

PCR	Polymerase chain reaction
PDMS	Polydimethylsiloxane
PEEK	Polyether ether ketone
PEI	Polyethyleneimine
PEO	Polyethylene oxide
PMT	Photomultiplier tube
PTFE	Polytetrafluoroethylene
PVP	Polyvinylpyrrolidone
Q_p	Perfluorodecaline flow rate
Q_w	Aqueous phase flow rate
RSD	Relative standard deviation
TEMED	*N*,*N*,*N*′,*N*′-tetramethylethylenediamine
THF	Tetrahydrofuran

Chapter I. Introduction to segmented flow microfluidics, single enzyme molecule assays and capillary electrophoresis coatings for protein analysis.

Introduction

Among biological macromolecules, proteins show the widest range of functional diversity[2, 3]. Proteins such as collagen and α-keratin serve important structural roles, being the main constituents of mammalian connective tissue and hair and nails respectively[2]. Hemoglobin transports oxygen throughout the body, while other proteins make up the channels that regulate the flow of ions across cellular membranes[4]. Peptide hormones, such as insulin and thyrotropin, also serve important regulatory functions while ovalbumin and casein are used as nutrient storage proteins in the growing egg and in milk[3]. Immunoglobulins and antibodies, along with blood clotting factors are vital parts of an organism's defense system against disease and other invaders[2]. Proteins also take part in the transduction of chemical signals into the cell, acting as both receptors and messenger molecules[5]. Finally, enzymes catalyze most metabolically important reactions, allowing them to occur at rates far above the uncatalyzed rate, that is, fast enough to sustain life. There are, thus, few cellular processes that do not involve proteins.

As the "Central Dogma of Molecular Biology" became established, proteins were cast as the principal agents of cellular activity, carrying out their functions as per instructions coded in the genome. That is, the function of a given protein is determined by its structure, which is in turn determined by its amino-acid sequence， translated by the ribosome from RNA transcribed from the DNA blueprint. After the early days of protein structure elucidation by x-ray diffraction, protein research exploded in the 1990s with the advent of the field of proteomics which aims to measure and characterize the expression of every protein encoded in a genome[6-8]. Among proteins, enzyme structure

and function continue to receive particular attention as they are often involved in diseased states and are, thus, suitable targets for many drug therapies[9-13]. The present work concerns itself with two areas of protein research: Single molecule enzyme activity assays and protein separations by capillary electrophoresis (CE).

In the present chapter we provide brief introductions to microfluidics and two-phased or segmented flow, single enzyme molecule assays and capillary electrophoresis and capillary coating strategies for biomolecule separations. In chapter 2 we introduce a microfluidic system for generating segmented flow arrays using commercially available Teflon tubing and PEEK T-junction connectors. These arrays consist of aqueous droplets separated by plugs of an immiscible liquid, which act as barriers to mass transfer between adjacent droplets. In this way, each droplet can act as a picoliter sized vessel in which chemical reactions can be contained. Size, reproducibility and stability of the droplets, as well as the in-droplet mixing efficiency were assessed.

Starting in the 1990s the groups of Yeung and Dovichi independently used capillary electrophoresis to measure the activity of single molecules of lactose dehydrogenase and alkaline phosphatase[14, 15], respectively. Their results demonstrated the existence of populations of enzyme molecules with distinct activities, which had been previously obscured by bulk assay measurements. Understanding the source of these differences has important implications for our understanding of enzymatic catalysis and protein structure. Chapter 3 describes the application of the previously described droplet array method to the measurement of the activity of single molecules of the enzyme alkaline phosphatase (AP). By sequestering single molecules of the enzyme within

individual droplets in an array containing a fluorogenic substrate, it was possible to use laser induced fluorescence (LIF) to detect single molecule activities.

In the final chapter we change focus to the separation of proteins by capillary electrophoresis and the use of coatings to reduce adsorption to the walls of the fused silica capillary. Protein adsorption to the capillary walls is a common problem in CE separations, particularly for proteins with a large numbers of positively charged residues. Many methods have been developed to reduce these analyte-wall interactions, including a wide selection of coatings. Here we assess the use of a commercial water-proofing agent, Aquapel, as an effective coating for capillary electrophoresis in the separation of a suite of basic proteins.

Fabrication of microfluidic devices

Microfluidic or lab-on-a-chip devices use fabricated microchannels to manipulate small volumes, on the order of nano-to-picoliters, in order to carry out chemical operations such as crystallization, synthesis or analysis[16, 17]. Besides the obvious benefit of reducing both reagent use and sample size, microfluidics presents many advantages to the analytical chemist, such as increased efficiency, decreased mixing and analysis time, and the potential for integrating multiple steps in precise sequence and for high-throughput analysis. The early development of microfluidic devices benefited greatly from microfabrication advances in the microelectronics industry[18-20]. These first microfluidic devices consisted mainly of microchannels etched into glass or silicon substrates using well-developed photolithography techniques (Figure 1.1).

The fabrication of microchannels in glass chips is normally carried out in a series of three basic operations: deposition, patterning and etching[19]. First, a photosensitive polymer, or photoresist, is deposited onto a silicon wafer. The photoresist coating is then exposed to UV light through a mask of the desired pattern. Upon exposure, a positive photoresist becomes soluble in a developer solution which is then used to remove the unwanted regions. Once developed, these exposed regions are used to pattern the glass wafer, usually by chemical etching. After etching, the remaining photoresist is removed. The process can be repeated as necessary until the desired design is completed[21]. Chips fabricated in this fashion have been used for a variety of analytical and biochemical operations such as open-tubular liquid chromatography[22], electrophoretic separations in free solution[1, 23, 24] and in gels[25], PCR amplification[26, 27], DNA sequencing[28, 29], high-throughput genetic analysis[30], and enzyme activity assays[31].

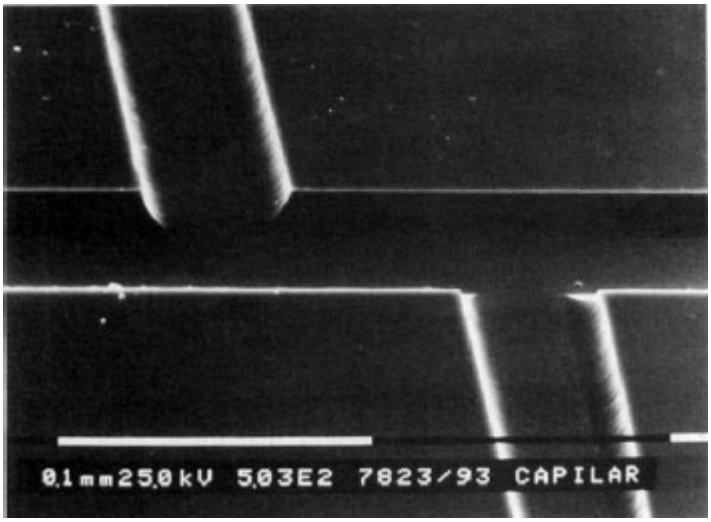

Figure 1.1. Scanning electron micrograph of channels in a glass chip. This design was used for integrated sample injection and electrophoretic separation[1]**.** Channels shown have a width of 50 μm and depth of 12 μm.

Despite their success, the glass or silicon wafers used initially have several disadvantages, such as the relatively high cost of the substrate, the need for specialized microfabrication facilities and clean rooms, the use of harsh reagents and the limited geometry of patterns that can be produced[32]. These disadvantages led to much interest in

alternatives such as polymeric substrates. The most widely used polymer to date is polydimethylsiloxane (PDMS). PDMS has physical and chemical properties that make it highly suitable for microfluidic devices: it is inexpensive, non-toxic, optically transparent, can be made to seal reversibly or irreversibly and has controllable surface chemistry[18]. Finally, PDMS can be readily molded into complex patterns using soft lithography techniques[33, 34], which do not normally require the use of clean rooms.

As can be seen in Figure 1.2, the soft lithography process is relatively simple, but can be used for the fabrication of geometrically complex microfluidic structures. In soft lithography, a master having the desired surface features is prepared, usually by photolithography. The elastomer, such as PDMS, is then poured over the master, cured and peeled off. The resulting cast can be sealed by bonding to another surface such as glass or PDMS. Recently, the use of soft lithography has become even simpler through the development of rapid prototyping, in which masters can be quickly and cheaply made from printed photomasks. Thus, in the last decade soft lithography has overtaken photolithography as the method of choice for many microfluidic applications due to its low cost and relative ease of manufacture. Regardless of the fabrication material, microfluidic devices could prove to be of particular importance in fields in which high-throughput is crucial, such as genomics[35], proteomics[36, 37], single cell sorting and analysis and drug discovery[38].

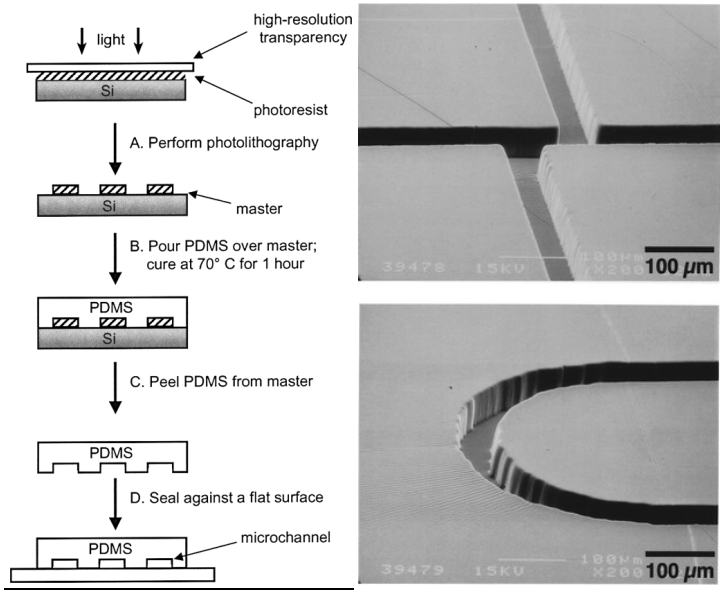

Figure 1.2 Device.fabrication using soft lithography. On the left, general scheme for rapid prototyping of microchannels on PDMS[34]**.** On the right, scanning electron micrograph of channels molded in PDMS on a device for CE**.**[18]

Microfluidic compartmentalization by segmented flow

Due to their small inner diameters, microfluidic channels are the ideal microreactors for applications where small sample volumes are desired. Channel networks also offer efficient mixing and the ability to perform sequential operations on the sample as it flows through the device. For these reasons, devices consisting of microfluidic channels have been used in various applications including combinatorial synthesis[38, 39], multiphase catalytic reactions[40], single cell genome extraction and analysis[41], controlled polymerization[42] and protein crystalization[43].

As well as channels, microwells and vials can also be fabricated on microfluidic chips and used as sample reservoirs for further analysis, much like the commercial 96 or 384 well-plate readers, but with the advantage of much smaller volumes and thus higher throughput capacity. Microfluidic arrays of wells have been used for electrochemical

analysis[44], screening ligand libraries against single cells[45], high-throughput PCR[46], as DNA hybridization sensors[47], and to assay single enzyme molecule activity[48]. In these microarrays, however, the microwells are normally filled with the complete reaction mixture, as sequential additions of reagents are not usually possible.

Compartmentalization of analytes and reactants can also be achieved through the generation of oil-water emulsions. Microfluidic chips have been fabricated that can generate, store and manipulate arrays of aqueous droplets suspended in an immiscible solvent. When these arrays are generated within a microchannel, the result is a segmented flow of aqueous droplets separated from each other by plugs of the immiscible solvent. The solvent is typically chosen so that it preferentially wets the surface of the channel, making certain that the aqueous droplets are truly suspended in the solvent, which acts then as a carrier fluid. These segmented-flow devices possess the benefits of continuous flow devices, such as rapid mixing, low sample volume, and the ability for serial processing. They also retain the advantages microwell-array based chips, such as the complete compartmentalization of the analyte or reaction and the suppression of diffusion. Additionally, the use of droplet arrays also suppresses analyte-wall interactions, as the sequestered analyte never comes in contact with the channel walls. Segmented flow chips have been used for screening sample volumes against multiple reagents[49], single cell analysis, protein crystallyzation[50], nanoparticle synthesis[51], enzyme kinetics assays[52] and compartmentalization of bands separated by CE[53].

T-junction vs flow focusing

Droplet arrays in microfluidic chips are generated through two main methods: Flow focusing[54-56] and by means of a T-junction[57, 58]. Figure 1.3 shows a typical flow focusing geometry. The central channel contains a liquid immiscible with the liquid flowing through the two outside channels. Where the three streams meet, they are forced through a narrow aperture. The two outside streams then focus the middle one into a narrow thread which breaks up into drops whose size can be tuned by adjusting the relative flow rates of the two phases.

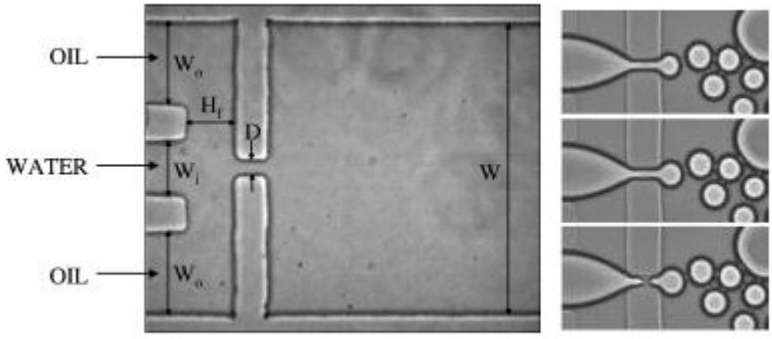

Figure 1.3 Example of flow-focusing geometry used to generate micro-droplets. The micrograph on the left shows a top view of a device which employs three channels: an inner one carrying water and flanked by two outer ones carrying an immiscible oil. The micrograph on the right shows how the oil streams focus the aqueous stream through a small aperture, where droplet break-up occurs. Adapted from Anna[55].

More commonly in segmented flow devices, droplets are generated via a T-junction geometry (Figure 1.4). In a T-junction, a stream of fluid is introduced perpendicularly into a stream of a second immiscible liquid, which acts as a carrier fluid. If the carrier fluid is selected so that it preferentially wets the surface of the channel where the two liquids mix, the result is an array of droplets separated by plugs of the carrier fluid. Typically, in this type of device, channels must be rendered hydrophobic

before use with the oils and fluorous solvents commonly selected as carrier fluids. Both methods, T-junctions and flow focusing geometries, have been shown to produce highly monodisperse emulsions, with many applications.

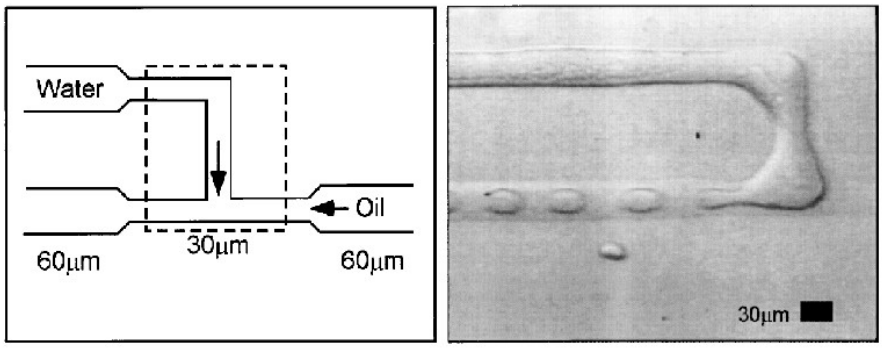

Figure 1.4 Example of a T-junction geometry used in segmented flow generation. Adapted from Quake[57].

Mechanism of droplet break-up

The physical mechanisms involving droplet formation and break-up have been well-studied for both T-junctions and flow focusing geometries[54-57, 59-63]. It was observed early on that the size of the droplets varied predictably with the total flow rate of the streams and the ratio of the flow rates of the dispersed liquid to the carrier fluid[54, 55, 57]. It was also observed in flow focusing geometries that there is a critical ratio of flow rates beyond which droplet break-up becomes unstable, generating polydisperse emulsions. Simulations and experiments by De Menech et al[60], have shown that the mechanism for droplet formation is determined by the capillary number, *Ca*:

$$Ca = \frac{\mu u}{\gamma} \qquad \text{Eq. 1.1}$$

where μ is the viscosity, u is the mean velocity of the carrier fluid and γ is the interfacial tension.

At low values of *Ca* (less than 0.015), droplet formation is under what is termed the "squeezing" regime and produces highly monodisperse emulsions. In this squeezing regime, droplet break-up, and thus droplet size and frequency, is dominated by the pressure drop across the droplet as it obstructs the channel in which it forms. Droplet size scaling in this regime is, then, dependent only on the ratio of the flow rates of the two phases and the dimensions of the channel. This scaling can be expressed in a simple equation[59]:

$$\frac{L}{w} = 1 + \alpha \frac{Q_{in}}{Q_{out}} \qquad \text{Eq. 1.2}$$

where L is the length of the droplet, w is the width of the channel, Q_{in} and Q_{out} are the flow rates of the dispersed phase and the carrier phase respectively and α is a constant of order one. Above the critical value for *Ca,* droplet formation enters the "dripping" regime, where shear stresses become important[60]. Emulsions in the dripping regime become polydisperse, and no simple scaling relation can be derived. For this reason, most applications of segmented flow devices operate within the squeezing regime. When *Ca* is much higher than the critical value, jetting may occur, where both fluids can flow side by side for several channel widths before droplet breakup occurs. The transition between "squeezing" and "dripping" regimes is shown in Figure 1.5.

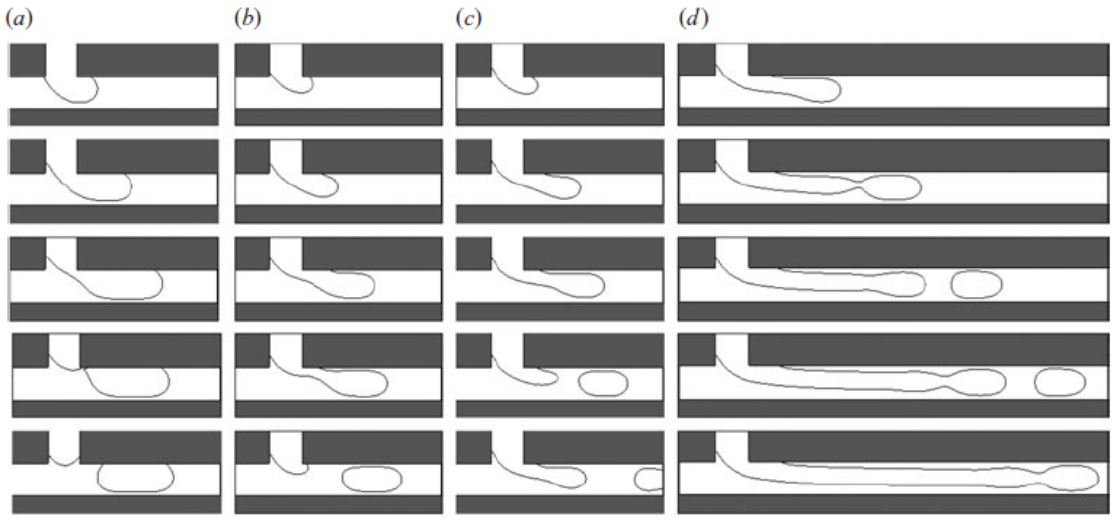

Figure 1.5. Effect of capillary number on droplet formation[60]. a) At low capillary numbers (*Ca* = 0.004) the squeezing regime is observed b,c) At high capillary numbers (*Ca* = 0.035) the dripping regime dominates d) At even higher capillary numbers (*Ca* = 0.05) jetting is observed.

Introduction to single molecule enzymology

Enzyme mediated catalysis is ubiquitous in nature. Nearly all cellular reactions necessary to sustain life require enzymes to occur at fast enough rates. Evolution has shaped enzymes into the ultimate catalysts, increasing reactions rates up to 10^{16} times over the uncatalyzed rate[64]. A few enzymes have even reached catalytic perfection: Diffusion-limited catalysis, in which the reaction rate is limited only by how fast the substrate can reach the enzyme's catalytic site[65, 66]. Due to their prevalence, enzymes are crucial to our understanding of biochemical processes. In particular, their critical role in metabolic pathways makes enzymes obvious targets for drug therapies[67-70]. Finally, enzymes and their functions are important not only in biomedical and pharmaceutical research, but also in many other industries, such as agriculture[71, 72], food production[73-75], waste treatment[76, 77] and biofuel research[78, 79].

As with other proteins, the structure of a particular enzyme is determined by its amino acid sequence. The enzyme's structure, in turn, determines its function, that is, which reaction it will catalyze and on which substrate. Until recently it was assumed that identical amino acid sequences would lead to identical molecular structure, and so all molecules of a given enzyme would behave identically and exhibit the same reaction rate. Traditional enzyme activity assays measure only bulk rates, by adding volumes containing millions or billions of enzyme molecules to a substrate and then monitoring the formation of product over time, usually by spectrophotometric detection. Such bulk assays conceal any variation between individual molecules behind the average activity measured.

In 1995, Yeung and Xue reported the use of capillary electrophoresis in a novel activity assay for individual enzyme molecules[15]. With this assay, they were able to observe four-fold differences in activity between individual molecules of lactose dehydrogenase, an enzyme widely used as a marker for tissue damage. The following year, Dovichi et al. using another CE-based method, also reported the observation of activity heterogeneity between molecules of alkaline phosphatase[14]. Though the causes remained unclear, it was proposed that this heterogeneity could result from post-translational modification or from conformational differences. It was clear, in any case, that this was a real phenomenon and so with these studies, single molecule enzymology was born. Later studies have extended the single enzyme assay to include a variety of enzymes, using many different techniques which will be discussed in the following sections.

Enzyme compartmentalization in emulsions

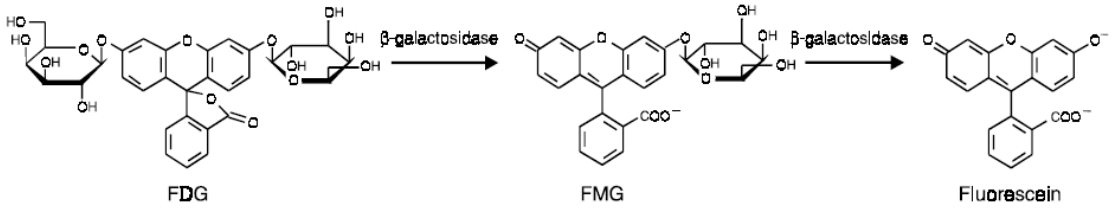

Figure 1.6. Sequential, enzymatic cleavage of FDG to yield fluorescent product, fluorescein. From Molecular Probes user document MP01179**.**

The earliest report of a single enzyme activity measurement was in 1961 by Rotman[80]. The enzyme β-galactosidase catalyzes the hydrolysis of β-galactosides into monosaccharides and is frequently used as marker for gene expression in molecular biology. In the Rotman experiments, two solutions were rapidly mixed in a 1 to 5 ratio: the first containing a very dilute concentration of β-galactosidase, the other containing 0.12 mM of the recently synthesized fluorogenic substrate 6-hydroxyfluoran-β-D-galactopyranoside, later found to be fluorescein di-galactopyranoside (FDG)[81]. The reaction mixture was sprayed into a chamber and covered with silicone oil. The concentration of the enzyme was low enough so that upon dispersion some of the droplets sprayed into the chamber contained an enzyme molecule, while most contained none. The actual distribution of enzyme molecules in the droplets

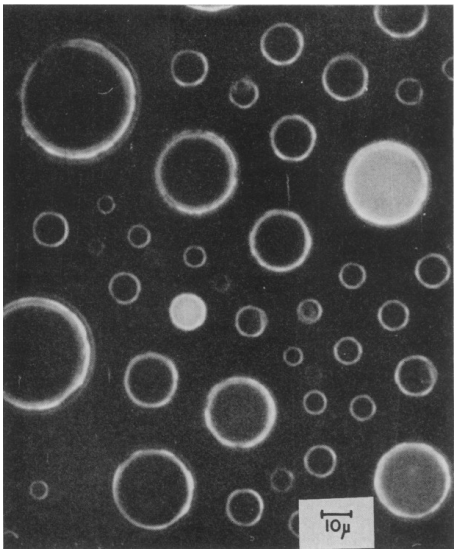

Figure 1.7 Micrograph of droplet microreactors in silicone oil. Droplets containing a single molecule of β-galactosidase are seen to be highly fluorescent. (Rotman, 1961)

(i.e. whether a droplet contains none, one, two and so on) is predicted by Poisson statistics. The sprayed droplets were allowed to incubate for 15 hrs. During this incubation, the enzyme molecules which occupied some of the droplets converted the FDG substrate into the highly fluorescent product, fluorescein and the less fluorescent intermediate, fluorescein mono-galactopyranoside[82, 83] (See Figure 1.6). The droplets generated by spraying spanned a wide volume range, thus for analysis only droplets between 14 and 15 μm in diameter were selected. Fluorescence intensity was measured for the selected droplets by microscopy. Figure 1.7 is a micrograph of one such experiment, clearly demonstrating the difference in fluorescence between occupied and unoccupied droplets.

Single molecule enzymology by capillary electrophoresis

Rotman applied his emulsion based method to distinguishing single enzyme activities of heat inactivated enzyme and alluded to further applications in investigating enzyme homogeneity with regards to activity[80]. It wasn't, however, until the mid 1990s when independent work by the Yeung and Dovichi research groups provided evidence of what was termed micro-heterogeneity[14, 15]. Yeung and Xue filled a 65 cm, 20 μm ID fused silica capillary with a reaction mixture containing 5 mM NAD+ and a very low concentration of the enzyme lactose dehydrogenase 1 (LDH-1). The concentration of LDH-1 was on the order of 10^{-17} M and so for each experiment a filled capillary was expected to contain between 10 and 13 molecules of the enzyme. After filling, the capillary was incubated for an hour. During the incubation period, each single enzyme in

the capillary generated a discreet zone of the fluorescent product NADH. After an hour, the fluorescent product zones were moved electrophoretically past a detection window at the end of the capillary for detection by laser induced fluorescence (LIF). Figure 1.8a, shows these product zones as peaks in an electropherogram. The intensity of these peaks is proportional to the activity of the enzyme molecules that generated them and figure 1.8b shows a histogram of the activities of 81 distinct LDH-1 molecules, and in which the enzyme's heterogeneity can be clearly observed.

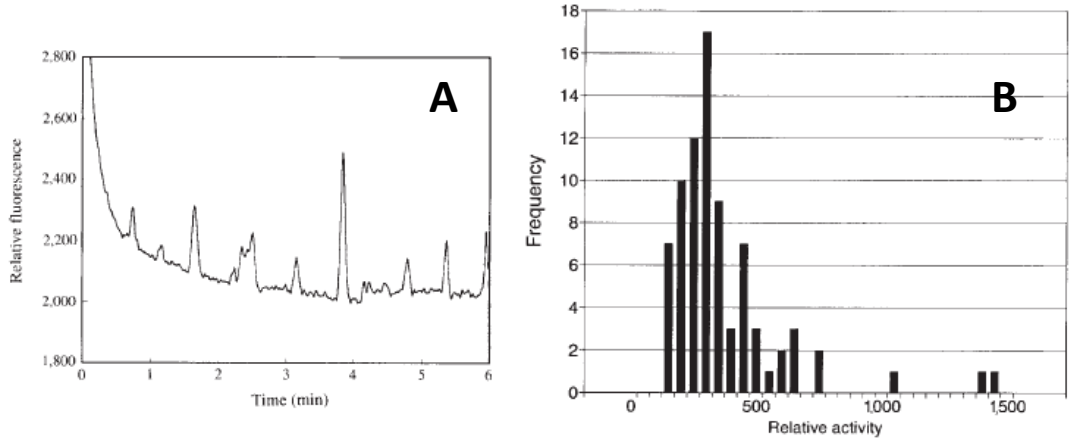

Figure 1.8 Single enzyme molecule detection by CE[15]. A) Sample electropherogram showing fluorescent product bands generated by individual molecules of LDH-1. B) Histogram of relative activities of 81 different molecules. The broad range of single molecule activities can be clearly seen.

Shortly after, Dovichi et al.[14] found microheterogeneity in activity amongst single molecules of the enzyme alkaline phosphatase. Like Yeung and Xue's assay, their experiments used a narrow bore capillary as a reaction chamber for the generation of a fluorescent product. A reaction mixture containing 1 mM of the fluorogenic substrate AttoPhos® and a concentration of alkaline phosphatase on the order of 10^{-16} M was injected electrophoretically onto a 10 μm fused silica capillary for a period of three minutes. After an incubation period of 1 to 30 minutes the fluorescent product bands

were moved electrophoretically past an LIF detector. Figure 1.9a shows an electropherogram from one such incubation, in which the peaks correspond to bands of fluorescent product generated by single AP molecules, much like in the Yeung and Xue experiments. The activities measured for 83 molecules of AP also show significant heterogeneneity, up to a 10-fold difference in activity, as is illustrated in the histogram in Figure 1.9b.

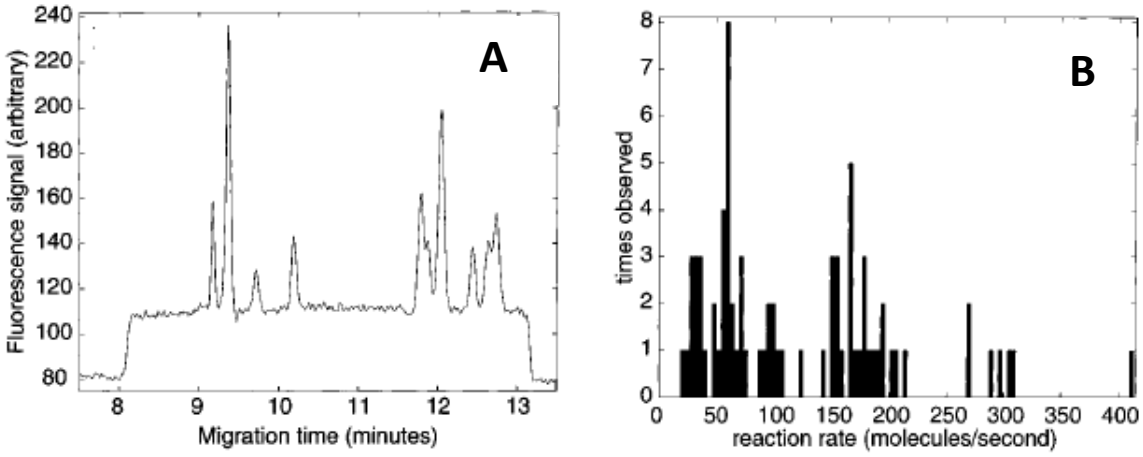

Figure 1.9 Single enzyme molecule detection by CE[14]. A) Sample of electropherogram of fluorescent product bands generated by single molecules of AP. B) Histogram of reaction rates of 83 molecules of AP

While Yeung and Xue suggested that distinct, stable structural conformations of LDH-1 were responsible for the observed catalytic heterogeneity, Dovichi et al.'s studies of the heat denaturation of AP offered no evidence for the existence of low-activity, but stable conformations[14]. Rather, they suggested the variance measured in AP single molecule activity was more consistent with different states of post-translational modification (such as glycosylation) of the molecules. A later study provided further evidence for this hypothesis, by showing that different isoforms of highly-purified, non-glycosylated *E.Coli* AP exhibited identical activities[84].

Subsequent research has found heterogeneity with respect to activity in β-galactosidase[48, 85, 86], horseradish peroxidase[48, 87] and chymotrypsin[88]. β-galactosidase, in particular, has been well-studied by Craig, continuing his work begun in the Dovichi lab. Craig et al., have studied the effect of induction conditions[89, 90], age of enzyme[89, 90], source[90-92], crystallization[93], protease inhibitors[94], different substrates[94], translational error[95, 96] and substrate concentration[97] on β-galactosidase activity and activity heterogeneity. Recent work by this group has also found that single β-galactosidase molecules are also heterogeneous with respect to electrophoretic mobility, providing further evidence of the structural differences that underlie activity heterogeneity[98, 99].

Single molecule enzymology in femtoliter-volume wells

Single enzyme molecules have been carried out successfully not only inside fused silica capillaries, but also inside fabricated femtoliter volume wells. Like the earlier Rotman experiments, this method relies on the confinement of individual enzyme molecules by using very dilute solutions of the enzyme to be studied. When the wells are filled with the solution, which also contains a fluorogenic substrate, only a fraction of them will contain an enzyme molecule. In an early report using this

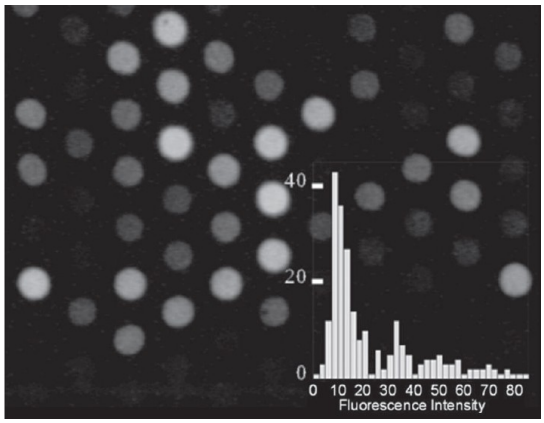

Figure 1.10 Micrograph of femtoliter well array after incubation with horse radish peroxidase (HRP). Fluorescent wells contain one or more enzyme molecules, while dark wells contain none. Insert shows a histogram of distribution of fluorescent intensity in the wells (Rondelez, 2005).

method, Yeung and Tan have confirmed the activity heterogeneity of LDH-1[100]. Using two different types of wells, pores in a membrane and wells fabricated on silica substrate by photolithography, Yeung and Tan isolated individual enzyme molecules and monitored the formation of fluorescent product NADH from NAD+. A significant advantage of this method is that by using a microscope equipped with a CCD camera for detection, a large number of wells can be monitored simultaneously over extended periods of time. Similar assays have been used to study the single enzyme kinetics of chymotrypsin[88], β-galactosidase and horseradish peroxidase[48]. Figure 1.10 shows a micrograph of one such picowell array.

Walt et al. have taken this approach further with the fabrication of a 50,000 femtoliter well array capable of high-throughput single enzyme analysis[86]. The array was fabricated by acid etching the distal end of a bundled array of 50,000 optical fibers. Since the silica core of each fiber is etched more rapidly than the surrounding germania-doped silica, the result is a femto-liter volume reaction vessel at the end of individual optical fibers[101]. Each optical fiber can be used for excitation and monitoring of emission of its respective well, eliminating any cross-talk between wells[102]. The use of this method has been extended to improve the sensitivity of ELISA assays[103], perform single enzyme mechanistic studies[87] and the detection of hybridization of single molecules of DNA. Walt's approach is shown schematically in Figure 1.11.

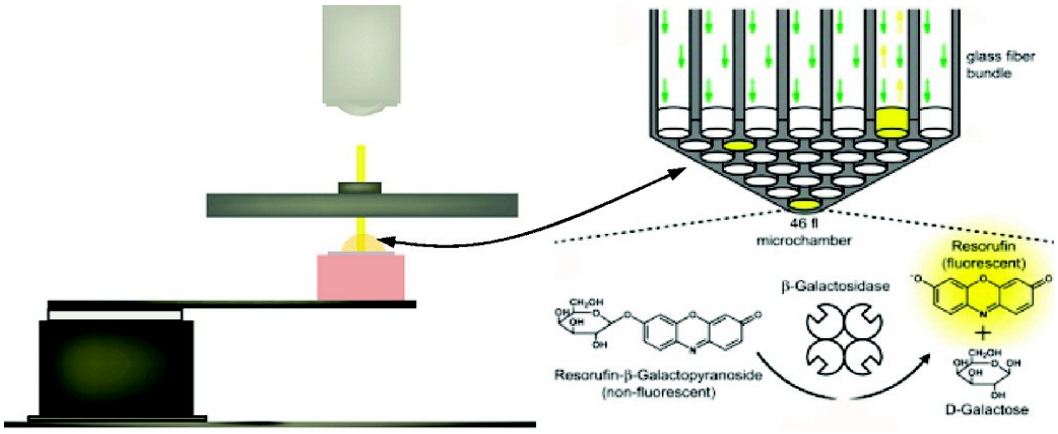

Figure 1.11 Schematic illustration of single enzyme detection using femtoliter wells etched into an optical fiber array[86]

One potential limitation with the use of these femtoliter well arrays is that the wells must typically be filled with a reaction mixture and then enclosed, making it difficult to add reagents in situ, to initiate or quench the reaction. It is also difficult to recover the contents of the well, be it the enzyme or the product, if it is desired to do so. In order to overcome these issues, Noji et al. have fabricated a femtoliter droplet array on a hydrophilic-in-hydrophobic micropatterned surface[104]. The droplets in the array are held in place by the hydrophilic surface and separated from each by oil place over them (Figure 1.12). Since there are no walls retaining the droplets, these are easily accessible by a micropipette tip for content recovery or reagent introduction.

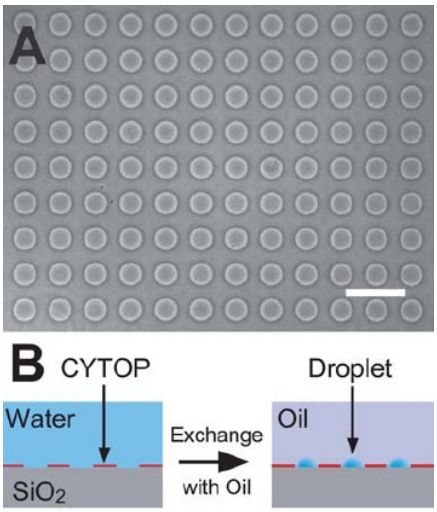

Figure 1.12. Micrograph and schematic of droplet array on a micropatterned surface. (Sakakihara, 2010)

Introduction to capillary electrophoresis

Electrophoresis, or the differential migration of ions under the influence of an applied electric field, has been used as a separation technique since the 1930s[105]. In its early days, the separation efficiency of electrophoresis in free solution was limited by convective currents induced in the separation buffer by Joule heating. As a result, most electrophoretic separations until the 1980s were done using a solid support (usually a gel) to reduce the effect of these convective currents. Gel electrophoresis, however, is not without its drawbacks[106]. Gels typically require a larger sample volume, are work intensive and do not easily lend themselves to automation. Starting in the 1970s, however, researchers such as Virtanen and Mikkers, Everaerts and Verheggen[107] pioneered the use of narrow bore tubing in electrophoretic separations. It was found that using tubing with smaller inner diameters (less than 400 μm) and thus increasing the surface to volume ratio, thermal convection could be much reduced. Soon afterwards, Jorgenson and Lukacs[108] demonstrated that by using even narrower capillaries (75 μm ID) applied voltages of up to 30,000 kV could be used to achieve separation efficiencies greater than 400,000 plates. Since then capillary zone electrophoresis (CZE) has become a major analytical technique, indispensable in the separation of both small and large biological molecules.

Principles of Operation and Instrumentation

Modern capillary electrophoresis is generally carried out in fused silica capillaries with inner diameters (ID) ranging from 25 to 150 μm. Capillary lengths are usually between 10 and 100 cm. Figure 1.13, shows a schematic of a typical CE instrument[109]. The capillary is first filled with a suitable separation buffer. Next, the sample is injected at one end of the capillary (the inlet) either by pressure or by the application of a voltage. Both ends of the capillary are then submerged in two separate buffer-filled reservoirs and a voltage is applied. Under the influence of the field, ionic analytes in the sample will begin to migrate towards the opposite end of the capillary (the outlet). Detection of the migrating ions is done near the outlet end, commonly by an optical detector through the capillary wall. In normal polarity conditions, the positive electrode (anode) is at the inlet and the negative electrode (cathode) is at the outlet. Inside the capillary, an ion will move towards the oppositely charged electrode with a velocity (v) proportional to its electrophoretic mobility (μ_e) and the applied electric field (E):

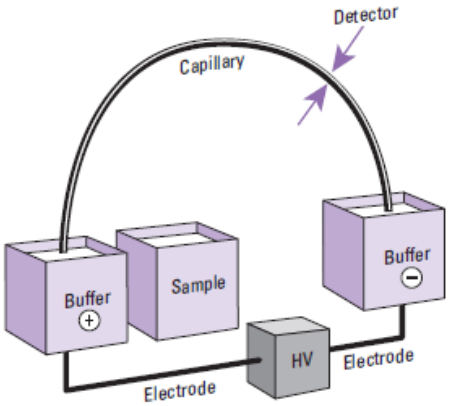

Figure 1.13 Schematic illustration of a capillary electrophoresis instrument. From Agilent's High Performance Capillary Electrophoresis: A Primer (Heiger).

$$v = \mu_e E \qquad \text{Eq.1.3}$$

A particular ion's mobility is constant and is the result of the balance between the coulombic force (F_e) generated by the electric field:

$$F_e = qE \quad \text{Eq.1.4}$$

where q is the ionic charge, and the opposing frictional forces (F_f):

$$F_f = -6\pi\eta r v \quad \text{Eq.1.5}$$

Where η is the density of the medium and r is the ionic radius. When equilibrium is reached, the two opposing forces are equal:

$$qE = 6\pi\eta r v \quad \text{Eq.1.6}$$

Substituting equation 1.3 into equation 1.6, yields an expression for the electrophoretic mobility, μ:

$$\mu_e = \frac{q}{6\pi\eta r} \quad \text{Eq.1.7}$$

It can be readily seen from this equation that a given ion's mobility will be proportional to its charge and inversely proportional to its size and the viscosity of the separation medium. When the separation voltage is applied, ions with different mobilities will migrate towards the detector at different velocities, resulting in a trace referred to, by analogy to a chromatogram, as an electropherogram.

Electroosmotic flow

Besides electrophoresis, there is another related phenomenon that affects separations in free solution. The surface of the silica is covered by silanol groups, which can become deprotonated leaving the surface with an excess negative charge. Due to the presence of different types of silanols (such as geminal or vicinal) the pka of silica difficult to measure and is often reported as a range, as high as 6.3 and as low as 3.5[110].

Surface charge density will depend then on the properties of the silica and on the pH of the buffer used in the separation. This excess negative charge must be balanced by the formation of an electrical double layer at the capillary-aqueous interface[111]. Closest to the silica surface, positive counter ions aggregate into a compact, rigid layer known as the Stern layer. This separation of charges generates a potential difference, known as the zeta potential. The incomplete shielding of the surface silanols by the counter ions in the rigid layer causes the formation a second, more diffuse layer beyond it. This diffuse layer is sometimes also referred to the Gouy-Chapman layer[112]. Application of a voltage to the capillary induces the motion of the cations in the diffuse layer towards the cathode. As these cations are solvated in solution, they drag along their associated water molecules causing a bulk flow of solution in the same direction. This bulk flow or electroosmotic flow (EOF) has the effect of moving all ions in solution in the same direction. Thus, if the magnitude of EOF is large enough to overcome the electrophoretic mobilities of the anions in a sample, it is possible to separate samples containing cations, anions and neutral molecules in a single run. When working in normal polarity conditions, the smallest, most positively charged ions will reach the outlet (and the detector) first, followed by the neutral molecules and lastly the smallest, most negatively charged ions. Though strong EOF is often desirable, if it is too strong it can also have detrimental effects on the separation. As Jorgenson[108] has pointed out, strong EOF can decrease resolution by decreasing the time two analytes with similar mobilities have to move away from each before exiting the capillary. Tuning the magnitude and sometimes the direction of EOF is a critical part achieving a successful separation.

As EOF results from the excess charge on the capillary surface, it is strongly dependent on solution pH and its effect on the protonation state of the surface silanol groups. Figure 1.14 shows the dependence of EOF on the pH for different surface materials[113]. For silica capillaries, EOF becomes significant at pH values higher than 4 and increases until it plateaus at pH values greater than 8 or 9, once the surface silanols are fully deprotonated. The magnitude of EOF is also affected by the type, concentration and ionic strength of the electrolytes used in the separation buffer. High buffer concentration and ionic strength can be used to suppress EOF, but this approach is limited by Joule heating. The presence of additives, such as organic solvents, surfactants and other small molecules in the separation buffer will also have an effect on EOF. The magnitude of EOF can be expressed by the equation:

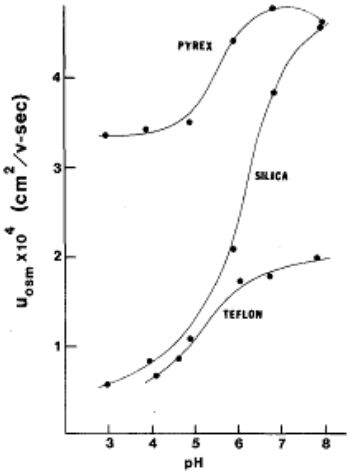

Figure 1.14. Effect of buffer pH on EOF for selected material (Lukacs, 1985).

$$\mu_{eo} = \frac{\epsilon\zeta}{4\pi\eta} \qquad \text{Eq.1.8}$$

Where ε is the solution dielectric and ζ is the zeta potential.

The potential difference that drives EOF is, unlike the pressure drop driving hydrodynamic flow, evenly distributed along the capillary. This results in a flat flow profile for EOF, in contrast with the parabolic flow profile resulting from pressure driven flow[111]. This means that EOF can be used as pump, to analyze cations, anions and neutral molecules in a single run with a negligible contribution to band broadening.

Band broadening in Capillary Electrophoresis

The total variance of an electrophoretic peak can be expressed as the sum of the variances that arise from the individual process that may contribute to band broadening, such as:

$$\sigma_{tot}^2 = \sigma_{diff}^2 + \sigma_{JH}^2 + \sigma_{inj}^2 + \sigma_{ads}^2$$

where the terms represent the variances due to diffusion (σ^2_{diff}), joules heating (σ^2_{JH}), injection plug length (σ^2_{inj}), and analyte adsorption (σ^2_{ads}). Each of these factors contributing to band broadening will be discussed in the sections below.

Axial diffusion

Under ideal conditions, the largest or even the only contributor to band broadening in CE is axial or longitudinal diffusion. The variance due to diffusion is proportional to the diffusion coefficient (*D*) of the analyte and the amount of time (*t*) it spends in the capillary (that is, its migration time):

$$\sigma^2 = 2Dt \qquad \text{Eq.1.9}$$

The velocity of an ion is given by:

$$v = (\mu_e + \mu_{eo})E \qquad \text{Eq.1.10}$$

where μ_{eo} is the ion's electroosmotic mobility. Its migration time is given by:

$$t = \frac{I}{v} \qquad \text{Eq.1.11}$$

where *I* is length of the capillary to the detector. The electric field *E* is:

$$E = \frac{L}{V} \qquad \text{Eq.1.12}$$

where L is the total length of the capillary and V is the applied voltage. Combining equations 1.10, 1.11 and 1.12 yields

$$t = \frac{IL}{(\mu_e + \mu_{eo})V} \qquad \text{Eq.1.13}$$

Substituting equation 1.13 into equation 1.9 yields

$$\sigma_{diff}^2 = \frac{2DIL}{(\mu_e + \mu_{eo})V} \qquad \text{Eq.1.14}$$

The efficiency of a column can be expressed by the equation

$$N = \left(\frac{l}{\sigma}\right)^2 \qquad \text{Eq.1.15}$$

Where N is the number of theoretical plates, I is the effective length of the capillary and σ is the standard deviation of the peak. Combining equations 1.14 and 1.15 results in the fundamental expression for separation efficiency in capillary electrophoresis:

$$N = \frac{(\mu_e + \mu_{eo})VI}{2DL} \qquad \text{Eq.1.16}$$

Joule heating

Equation 1.16 clearly shows that the plate number in electrophoretic separations is directly proportional to the applied voltage. That is, highest efficiency can be obtained by the highest voltage that can practically be used. The magnitude of the voltage that can be applied is limited not only by the power supply used, but by amount of heat generated by the current flowing through the conductive medium (i.e. separation buffer). This phenomenon is known as Joule heating. As heat is dissipated at the walls of the capillary,

regions near the wall will be cooler than regions near the center of the capillary. This temperature gradient will affect the viscosity at different positions along the capillary radius. Analyte molecules near the walls of the capillary will have different electrophoretic mobilities than those near the center, leading to band broadening. Moreover, EOF will no longer have a flat profile, contributing to further zone deformation.

Increasing the surface to volume ratio, by using capillaries with smaller inner diameters, can help reduce Joule heating significantly, though this could also have the effect of increasing wall-analyte interactions and lowering the limits of detection. Other strategies to limit the effect of Joule heating are decreasing the current by using lower ionic strength buffers and using active controls to remove heat from the capillary, such as flowing air or liquid coolant around it. Finally, the presence of Joule heating can be observed via an Ohm's law plot. According to Ohm's law, the current through a conductive medium is proportional to the voltage V and inversely proportional to the resistance, R ($I = V/R$). Plotting the current versus the applied voltage should show a linear relationship with slope 1/R. A positive deviation from this linear relationship indicates Joule heating.

Injection plug length

The contribution to the total peak variance for a rectangular injection plug is given by:

$$\sigma_{inj}^2 = \frac{w_{inj}^2}{12} \qquad \text{Eq.1.17}$$

where w_{inj} is the width of the injected plug. In order for the injection length to have a negligible effect on band broadening, it should be smaller than the diffusion width of the analyte zone[114]. In practice, however, size of the injection plug used will often be determined by the limits of detection of the analyte.

Analyte-wall interactions

Another potentially important contribution to band broadening results from the interactions between analyte and the surface of the silica capillary. Analyte molecules that become adsorbed and then desorbed will migrate more slowly than those that remain in solution, leading to band broadening and peak tailing. Adsorbed analytes will also affect the surface characteristics of the capillary leading to changes in EOF. Adsorption to capillary walls is particularly problematic for cationic solutes, which can interact with the surface silanol groups. Hydrophobic and hydrophilic interactions, however, can also result in adsorption leading to band broadening. The contribution of analyte-wall interactions to the total variance is given by:

$$\sigma_{ads}^2 = \frac{k' v_{eof} I}{(1+k')^2}\left(\frac{r^2 k'}{4D} + \frac{2}{K_d}\right) \qquad \text{Eq.1.18}$$

Where *k'* is the retention factor of the solute, *I* is the ionic strength of the buffer, v_{eof} is the velocity of the EOF, *D* is the diffusion coefficient of the analyte and K_d is its first order desorption constant. It can be seen from this equation that the variance is also proportional to the square of the capillary radius, *r*. So while reducing the capillary radius

will reduce the effect of Joule heating, the larger surface to volume ratio can result in increased analyte adsorption. As mentioned above, analyte-wall interactions can have a significant deleterious effect on the separation of biological molecules. Many strategies have been developed to reduce these interactions and will be discussed in more detail in another section.

Factors affecting resolution

As Jorgenson and Lukacs have pointed out[115], equation 1.16 seems to imply that separation efficiency can always be improved by increasing the EOF in the direction of the electrophoretic mobility. They have shown that this true only up to a point, after which high EOF velocity will degrade resolution. Starting with Giddings expression for resolution in electrophoresis

$$R_s = \frac{N^{1/2}}{4}\frac{\Delta v}{\bar{v}} \qquad \text{Eq.1.19}$$

(where Δv is the difference in velocity between two analyte zones and $\bar{v}$ is their average velocity) and combining it with equation 1.16 yields the following expression for resolution in terms of electrophoretic and electroosmotic mobilities

$$R_s = 0.177(\mu_1 - \mu_2)\left[\frac{V}{D(\bar{\mu} + \mu_{eo})}\right]^{1/2} \qquad \text{Eq.1.20}$$

This expression clearly shows that increasing EOF in the direction of the electrophoretic mobility, actually decreases resolution. That is, the faster the analytes migrate out of the capillary, the less time they have to resolve. Resolution, thus, will often have to be

balanced against analysis time. Another important point that can be observed from this equation is that unlike efficiency, resolution does not increase linearly with voltage. Instead, it increases only with the square root of voltage.

Capillary electrophoresis in the analysis of biomolecules

In the last two decades, CE has become an important method for the analysis of both small and large biological molecules. Studies have demonstrated CE to be particularly useful in growing fields like metabolomics[116] and glycomics[117]. It has also proven to be an essential tool in DNA sequencing [118, 119]. Because of its high separation efficiency and high throughput potential it is well suited for the analysis of complex protein samples, such as those common in proteomics research[120, 121]. Separation of protein samples, however, can be difficult as analyte adsorption to the fused silica capillary wall is a common problem[122]. Protein adsorption to the silica surface is due principally to hydrophobic and electrostatic forces[123]. Basic proteins are particularly problematic, due to interactions between the multiple positive charges on the analyte and the negatively charged silanols on the capillary surface[124, 125]

Strategies in reducing protein adsorption in fused silica capillaries

Minimizing analyte-wall interactions in CE is essential as these will degrade separation efficiency and resolution greatly[126]. In order to reduce detrimental interactions,

four strategies have been commonly used: the use of extreme pH, high ionic strength, buffer additives and a wide variety of coating methods[127].

pH, ionic strength and small molecule buffer additives.

At very low pH values (< pH 2.0) the majority of surface silanols are protonated. Thus, separation buffers with low pHs have been used successfully to reduce protein adsorption to the capillary walls[128]. At high pH values (much higher than the pI of the sample proteins) both proteins and walls will have the same charge, also reducing the electrostatic attraction between the two[129]. These extreme pH values, however, may have undesired effects on EOF and the stability of sample proteins. Increasing the ionic strength of the separation buffer by addition of alkali salts can also reduce protein adsorption[130]. This approach, however, limits the voltage that can be applied without Joule heating, and thus reduces efficiency and increase analysis time. Other small molecule additives such as amines and a variety of surfactants, such as Tween 20, Triton X-100, CTAB and DDAB, have also been shown to be effective at suppressing protein-wall interactions[127]. Structures for these and other commonly used surfactants can be seen in Figure 1.15. As the manipulation of pH and ionic strength as well as high surfactant concentrations may have unwanted effects on the folding state of the protein and separation efficiency, much effort has gone into the development of stable capillary coatings.

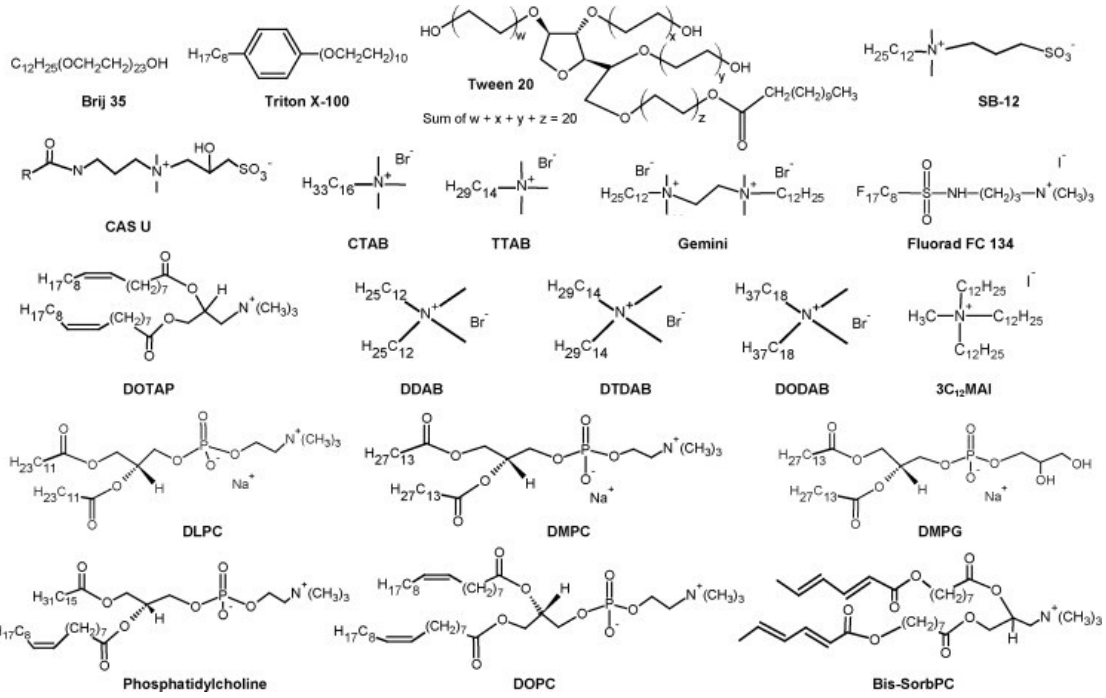

Figure 1.15 Structures of some common surfactants used in electrophoretic separations of biomolecules[127]

Covalently bound coatings.

CE coatings can be either covalently bonded or non-covalently attached to the silica surface[131]. Early in the development of CE, treatment of the capillary walls with silanizing agents such as trimethylchlorosilane and 3-glycidoxypropyltrimethoxysilane were shown to eliminate much of the surface charge and thus reduce amino acid and protein adsorption and EOF[108, 132]. Many other coating strategies have been developed since. The use of an i*n situ* polymerized, covalently bound polyacrilamide coating was first demonstrated by Hjerten[133]. Preformed, rather than *in situ* polymerized, covalently bound polymers such as polyacrylamide[134], poly(vinylpyrrolidone) (PVP) and poly(ethyleneoxide) (PEO)[131] have also been used as capillary coatings. The synthesis of covalent polymer coatings can often be labor intensive and involve multiple steps. Figure 1.16 shows the steps and reactions involved in a common procedure for the synthesis of a

polyacrylamide coating[135]. First, the silanol groups are chlorinated with thionyl chloride. With the excess thionyl chloride removed, the capillary is treated with a Grignard reagent. This step requires stringent control of humidity to avoid precipitation. After an overnight reaction, the capillary is rinsed with THF and water. Finally, the capillary is filled with a solution containing the acrylamide monomers and the catalysts persulfate and *N*,*N*,*N*′,*N*′-tetramethylethylenediamine (TEMED). After 3 hours for polymerization, the excess reagents can be rinsed away. The entire procedure requires at least two working days.

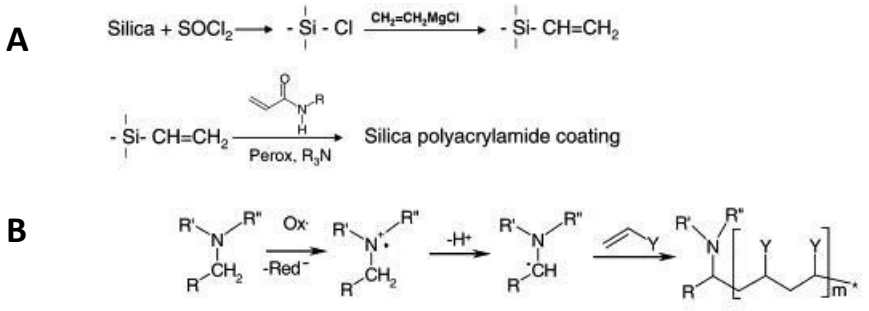

Figure 1.16. Procedure and reactions for a covalent polyacrylamide coating[136]**.** A) In the first step, surface silanols are chlorinated with $SOCl_2$. The capillary is then rinsed with a Grignard reagent and allowed to react overnight. After excess are rinsed away, the capillary is filled with the acrylamide monomers and the catalysts. B) Activation of TEMED during radical polymerization of acrylamide.

Non covalent coatings.

Non-covalent coatings can consist of small molecules, such as surfactants, or polymers adsorbed onto the surface by electrostatic interactions. Both small molecule and polymeric coatings can be further classified as dynamic or static. Dynamic coatings are generally water soluble polymers like polyvinyl alcohol[137] (PVA) or chitosan[138] that are included in the run buffer. Static coatings, composed of polymers like polyethethylene oxide[139, 140] (PEO) and polyethyleneimine[141] (PEI) are adsorbed onto the capillary walls via electrostatic forces and hydrogen bonds and are not included in the separation buffer. When static coatings are used, the capillary is rinsed with the polymer previous to sample

injection and normally needs to be recoated every few injections. Besides limiting analyte adsorption, coatings have also been used to suppress[124, 142], enhance, or even reverse[143, 144] electroosmotic flow (EOF) as the case may require. Structures for several polymeric coatings that have been used in CE can be seen in Figure 1.17.

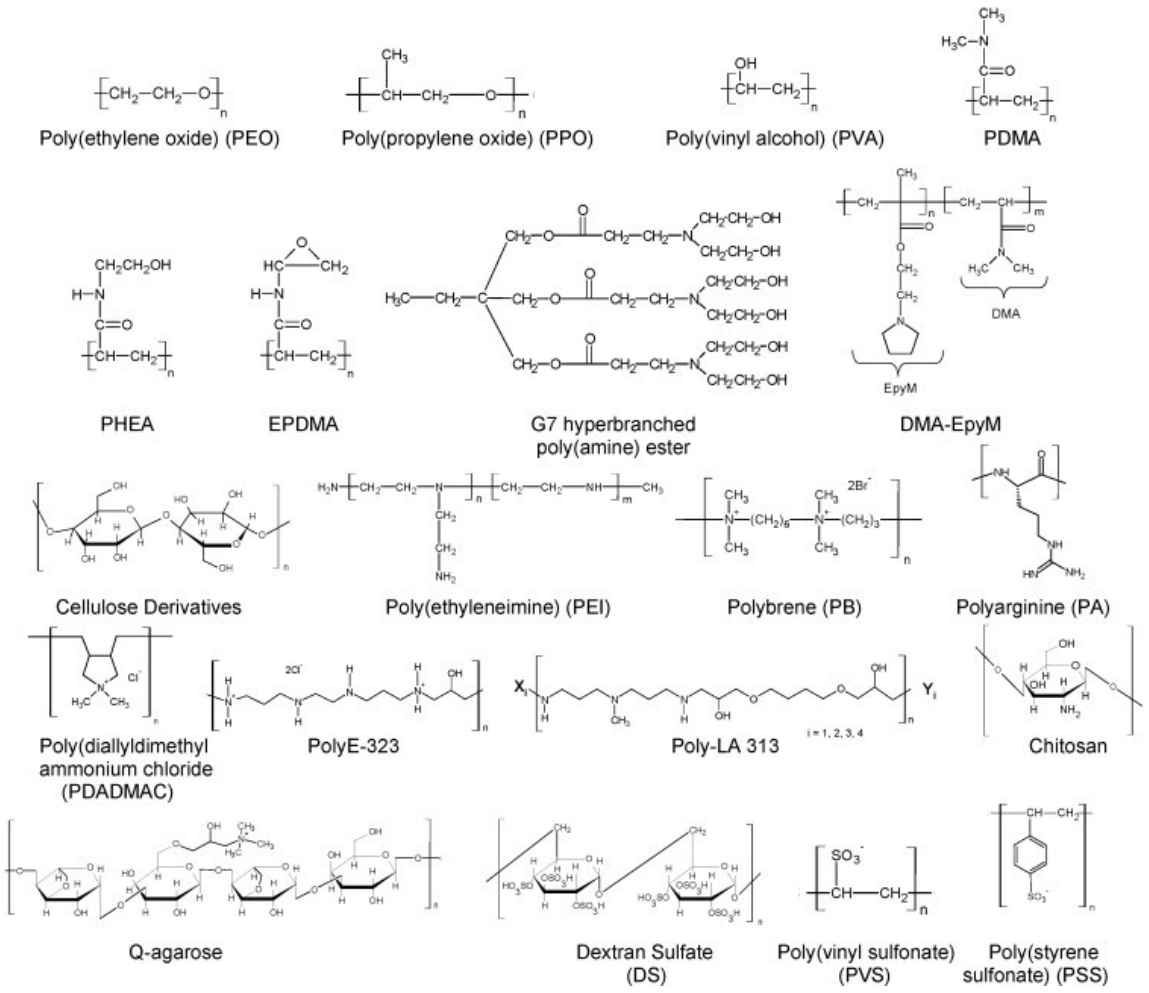

Figure 1.17 Structures of some commonly used polymeric coatings for CE[127].

Surfactants may be also used as dynamic coatings (if they are included in the separation buffer) or as semi-permanent coatings (if they are used to pre-treat the capillary and not subsequently included in the separation buffer).

Efficiency of coated capillaries

The improvement of separation efficiency with the use of capillary coatings can be remarkable. Basic proteins like cytochrome c and lysozyme are so readily absorbed that it takes repeated injections to fill all available binding sites before any detectable amount migrates from the capillary, and even then the separation will be poor. With the use of capillary coatings, both static and dynamic, separations of these proteins have been achieved with efficiencies of up to 1,000,000 theoretical plates/m. More commonly, plate counts between 50,000 and 300,000 theoretical plates/m have been reported[127]. The ideal coating will suppress both electrostatic and hydrophobic interactions. It should also be reproducible and stable over repeated injections. Finally, ease of application and cost must also be considered when assessing a coating's suitability.

Chapter II. Low-cost, fabrication-free approach to segmented flow microfluidics

Introduction

Two-phase or segmented flow has found a wide variety of analytical applications. A major advantage of segmented flow is that analytes can be compartmentalized and then transported and stored without concern for diffusional band broadening[58]. This property, for example, has been used to improve the temporal resolution of in vivo neurotransmitter monitoring assays, by allowing the compartmentalization of brain dialysate within droplets for their subsequent derivatization and analysis without band broadening[145, 146]. Segmented flow channels can also be patterned to ensure rapid mixing of reagents[147, 148]. Figure 2.1 shows one such application of rapid on-chip mixing to the development of a clinical assay. Ismagilov et al. have developed a segmented flow microfluidic device capable of rapid typing and subtyping of human erythrocytes[149].

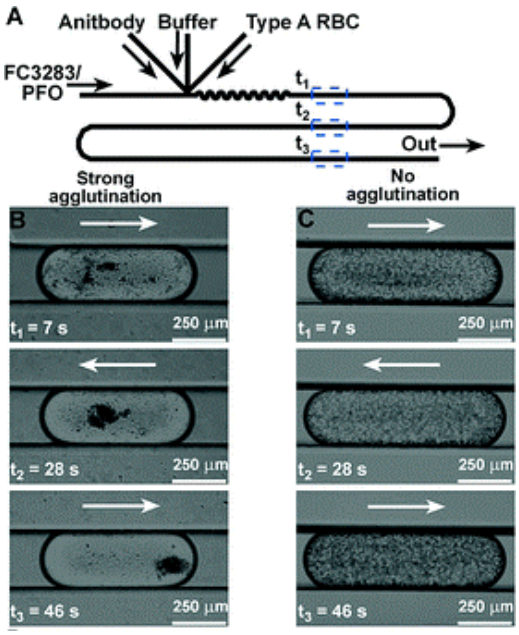

Figure 2.1 Sample application of lab-on-a-chip device in clinical diagnostics[149]. Top, Diagram of segmented flow microfluidic device for blood typing and subtyping. Bottom: Micrographs of droplets at three different time points of the device. An agglutination assay is carried on-line by mixing type A red

blood cells, buffer and an antibody solution. Agglutination is observed in the droplets when Anti-A is used (B). No agglutination is observed in droplets when Anti-B is used (C).

By adding T-junctions downstream from where the droplets are generated, reagents can also be easily and reproducibly introduced into existing droplets in precise sequences. This allows droplet-based chips to be used to carry out multiple step synthesis[51] and high throughput screening of target molecules against multiple reagents[49]. Segmented flow devices have also been used to optimize conditions for crystallization[50] and perform enzyme kinetics[52] assays. Unlike wells in microfluidic well-plates, the contents of droplets can be readily used for further analysis. Droplets can be collected for storage, sorted or injected onto on-chip channels for electrophoretic separation[53]. Finally, segmented flow has found application in assays that make use of what Ismagilov has termed "stochastic confinement". In these assays, individual cells are isolated within single droplets for analysis[38, 150]. This technique has been used to study the susceptibility of single bacteria to antibiotics[151] and to assay the contents of single cells for enzymes such as alkaline phosphatase[152], cytochrome c peroxidase (CCP)[153] and β-galactosidase[154].

Recently, it has been shown that the use of segmented flow does not require the fabrication of a microfluidic chip. Instead, several studies have reported the generation of microdroplet arrays inside commercial Teflon tubing. A segmented flow PCR amplification system using Teflon tubing has been demonstrated, although in this study droplets were not generated by flow focusing or a T-junction, but rather sequential injections from a PCR mix followed by injections from an oil reservoir[155]. Commercial T unions have also been used to generate droplets inside 500 μm ID Teflon tubing, for organic phase extractions[156]. More recently, a modular approach to segmented flow

assays has been shown by Trivedi et al[157]. Using commercial PEEK cross unions and Teflon tubing, they constructed a microfluidic system for the generation of droplets, mixing of reagents within them, and their subsequent analysis. With this system, shown in Figure 2.2, Trivedi et al. characterized droplet formation frequency, reproducibility of droplet size and droplet stability inside 1.5 mm, 500 μm and 150 μm ID Teflon tubing. Their results show that this approach is capable of generating droplet libraries with high frequency and reproducibility. In one interesting application, they were also able to culture cells inside their droplets and keep them viable for several days. A comparison between PDMS devices and commercial Teflon tubing systems reproduced in Table 2.1 shows that although the former can yield higher droplet formation frequencies and more complex channel geometries, the latter has some important advantages including ease of fabrication and solvent compatibility.

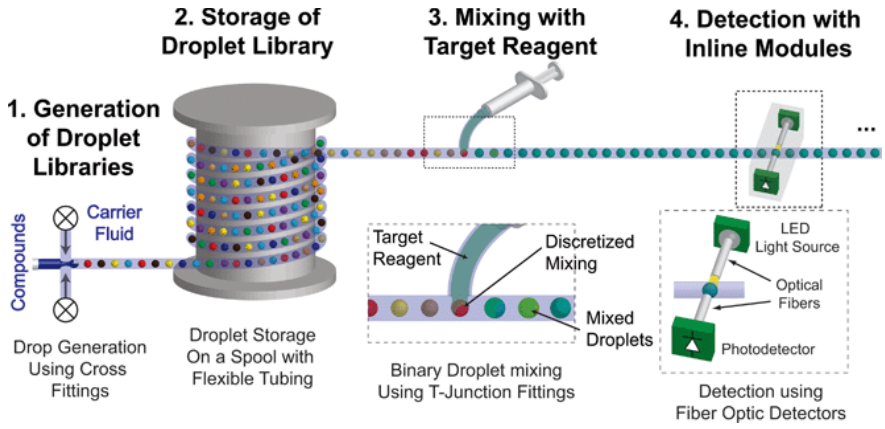

Figure 2.2 Schematic depiction of modular microfluidic system[157]. Droplets are generated by flow focusing using commercial cross fittings. These can be stored in a piece of spooled Teflon tubing. Reagents can be added to the droplets via a T-junction fitting placed downstream from the cross. Finally, the droplets can be analysed optically by an in-line detection module.

	PDMS/Soft Lithography	Modular using Teflon tubing (PTFE)
Water contact angle	109° native, 30° after O_2 plasma	110° native, 170° after O_2 plasmas
Drop volume	1 pL to 1 nL	65 pL to 2 μL
Drop generation rate	2000 drops per second	200 drops per second
Merging rates	100 drops per second (electrocoalescence)	10 drops per second (T-junction)
Detection	Microscope objectives	Fiber optic modules
Compatible fluid carriers	Compatible with a range of solvents; incompatible with silicone oil, pentane, xylenes	Inert to most chemicals
Optical properties	Transparent	Translucent
Gas permeable	Yes	Yes
Fabrication	Soft lithography (hours)	Hand assembled from commercial parts (minutes)
Complex geometries	Straightforward	Difficult, often impossible
Interconnect	Friction fittings, bonded nanoports	Commercially available barb, compression fittings
Maximum pressure	Up to 100 psi	>5000 psi

Table 2.1. Comparison between PDMS segmented flow microfluidic devices and modular system using Teflon tubing and commercial fittings[157].

As Trivedi et al. discuss, another potential advantage of using tubing is that it allows for the convenient storage of large libraries of droplets simply by wrapping the tubing segment around a spool. The low price of Teflon tubing (at the time of writing around $20 per 5 ft, when purchased from Upchurch/IDEX) further makes it a viable option for screening applications. The number of droplets that can fit in a meter of tubing is, of course, a function of its inner diameter; smaller ID tubing can accommodate more droplets. Trivedi et al. characterized tubing with IDs in the range of 1.5 mm to 150 μm. These dimensions represent minimal droplet volumes (for a perfectly spherical droplet inside the channel) of 2.65 μL and 2.65 nL respectively. Some applications of droplet arrays may require smaller volumes than these, either to increase the droplet capacity per length of tubing, to reduce the sample volume required or for other reasons, as in the case

single enzyme assays. In this work, we expand the characterization of Teflon capillary tubing as a means of generating droplet arrays using the smallest commercially available ID tubing and fittings.

Materials and methods

Reagents and materials

PEEK tee connectors with 100 μm ID were purchased from Vici Valco instruments (Houston, TX). Teflon tubing (360 μm OD, 100 μm ID) was from IDEX Health and Science (Oak Harbor, WA). Part numbers and manufacturers for parts used in assembly of droplet generator are described in Table 2.2. Perfluorodecalin, perfluorooctanol and fluorescein were all from Sigma Aldrich (St. Louis, MO). Gas tight syringes were purchased from Hamilton Co (Reno, NV). Fused silica capillary was from Polymicro Technologies (Phoenix, AZ). Fluorescein for experiments was dissolved in water purified with a Milli-Q water purification system (Millipore Corp, Bedford, MA).

	Part No.	Vendor
PEEK tee, 100 μm ID	C360QTPK4	Vici Valco Instruments
PEEK nut/ferrule assembly	C360NFPK	Vici Valco Instruments
Teflon tubing, 100 μm ID	1932	Upchurch

Table 2.2. List of parts and vendors used in segmented flow system.

Instruments and methods

Initial assessment of droplet size reproducibility and correlation to flow rate was done by fluorescence microscopy, as shown in Figure 2.3. A 50 μM solution of fluorescein in DI water was used as the aqueous dispersed phase and perfluorodecalin was used as the carrier phase. Gas tight syringes containing the two phases were loaded

onto two separate Pump 11 pico plus syringe pumps (Harvard Apparatus , Holliston, MA). Syringes were connected to a 100 μm ID PEEK Tee via two 10 cm pieces of 360 μm OD, 100 μm ID fused-silica capillary (Polymicro, Phoenix, AZ). A 50 cm piece of 360 μm OD, 100 μm ID Teflon tubing was connected to the third arm of the tee.

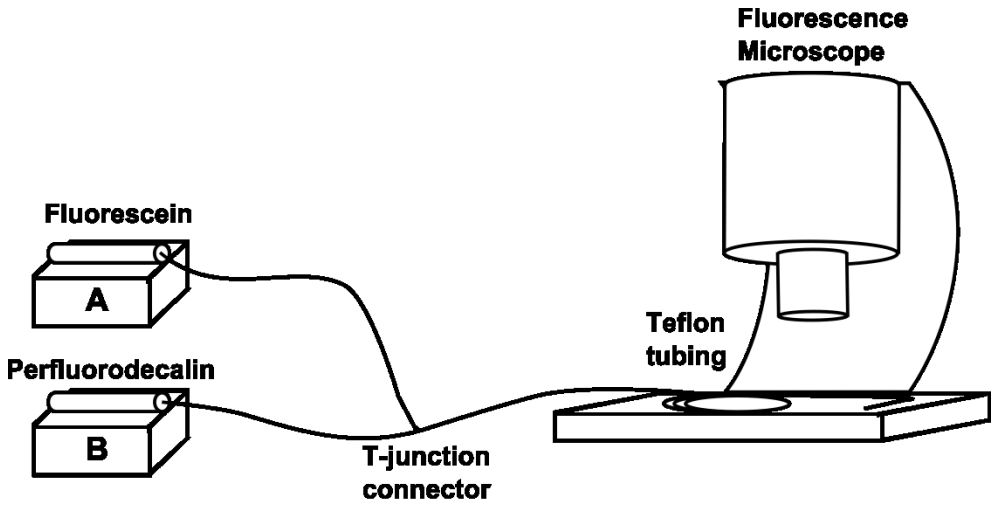

Figure 2.3 Droplet imaging system. Aqueous phase was delivered by pump A to the mixing tee, perpendicular to the perfluorodecaline stream delivered by pump B. Teflon tubing was connected to the third arm of the tee, also perpendicular to the flow of the aqueous phase. Droplets were imaged near the outlet of the tubing using a fluorescence microscope equipped with a CCD camera.

Figure 2.4 shows a schematic illustration of the PEEK tee assembly used for droplet generation. The Teflon tubing to be used for droplet storage and analysis was coiled and the outlet was placed in the viewing field of a Nikon SMZ1500 stereomicroscope. Droplet fluorescence was excited by an X-cite 120PC Q light source with a mercury vapor lamp (Lumen Dynamics, Mississauga, Canada). Light collected by microscope objective was filtered with a 520 nm band pass filter. Fluorescence images of the droplets were taken with a QuantEM 512SC CCD camera from Photometrics (Tucson, AZ) attached to the microscope. ImageJ open source software was used for image capture and processing.

For the flow rate experiments, droplets were generated in the same manner as described above but detection was done with a photomultiplier tube (PMT) from Hamamatsu (Figure 2.5). Fluorescent light was collected by an objective perpendicular to the excitation light and was filtered previous to detection with a 520 nm band pass filter from Intor (Socorro, NM). For excitation, a Cyan ™ 488 nm, 100 mW diode pumped solid state laser from Spectraphysics (Irvine, CA) was used.

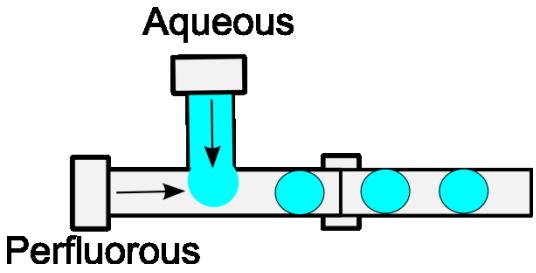

Figure 2.4 Diagram of PEEK tee used as droplet generator. One of the inlets of the tee is attached to a piece of fused silica capillary which delivers the carrier fluid (perfluorodecalin). The other inlet, perpendicular to the first, delivers the aqueous dispersed phase via another segment of fused silica capillary. The outlet of the tee is attached to a Teflon capillary in which the droplet array generated can be analysed or stored. Arrows indicate the direction of flow.

Laser light was expanded using a beam expander from Newport (Irvine, CA) and then focused directly onto the Teflon capillary using a focusing lens also from Newport. The Teflon capillary was held in place inside a home-built sheath-flow cuvette, and housed in a PEEK assembly. Water was allowed to flow through the sheath flow cuvette to remove the droplets as they exited the capillary and to reduce scatter at the Teflon capillary wall. Data collection was with a PC using LabView data acquisition hardware and software (National Instruments, Austin, TX).

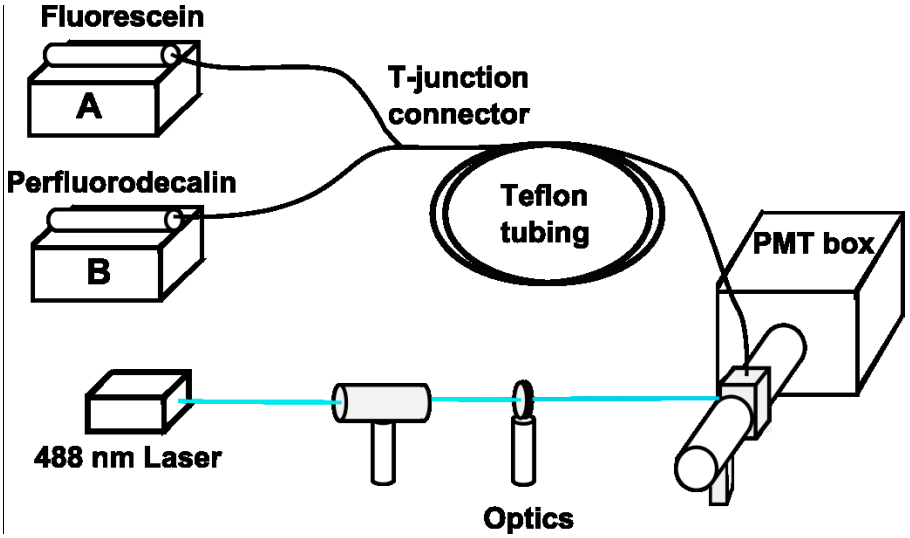

Figure 2.5 Flow rate and droplet scaling experiments. Droplets are generated as described above. Fluorescence detection, however, was done with a PMT placed perpendicular to a 488 nm laser line used for excitation. Laser beam was passed through a beam expander and a focusing lens. Collected light was filtered using a 520 nm band pass filter**.**

For the mixing experiments a second tee was added upstream of the droplet generator. Two syringes, one containing the 1 μM fluorescein solution, the other DI water, were loaded onto a single syringe pump. The two syringes were connected to the second tee, which was in turn connected to the droplet generating tee by a 3 cm piece of 360 μm OD, 100 μm ID fused-silica capillary, as shown in Figure 2.6. The two aqueous phases

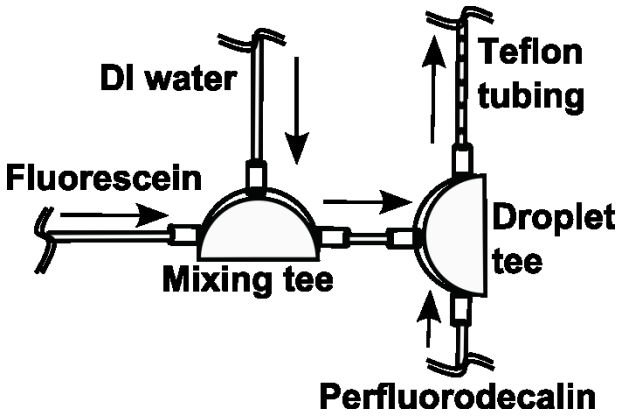

Figure 2.6 Droplet mixing experiments. Fluorescein solution and DI water were delivered to mixing tee via two pieces of fused silica capillary each connected to gas tight syringe. The mixing tee was connected to the droplet generator (T-junction) with a 3 cm piece of fused silica capillary. The T-junction was then used to generate droplets by mixing the two aqueous streams with a fluorous stream delivered perpendicularly via another segment of fused silica capillary connected to a third gas tight syringe. Droplets generated at the tee were collected in an array inside a piece of Teflon tubing connected to the outlet of the T-junction. Arrows indicate the direction of flow.

meet and begin to mix at the first tee and, as before, are dispersed into droplets at the second tee.

Results and Conclusions

Effect of flow rate on droplet size

Figure 2.7 shows fluorescent images of aqueous droplets generated at different flow rates. Exposure time for images was set at 100 milliseconds. For the first three captures, the flow rate of the aqueous phase (Q_w) was maintained constant at 800 nl/min while the flourous phase was set to 200, 400 and finally 800 nl/min. For the last three, the flow rate of the fluorous phase (Q_p) was kept constant at 800 nl/min, as the aqueous phase was set to 400, 200 and 100 nL/min. These settings correspond to flow rate ratios, Q_w/Q_p, of 4, 2, 1, ½, ¼ and 1/8 respectively. The system was allowed to stabilize for 1 hr between each flow rate setting. It can be seen in the images that the observed dependence of droplet size on Q_w/Q_p is in agreement with previous studies in microfabricated T-junctions[57-59]. From the literature value for the interfacial tension of perfluorodecalin with water (γ) of 56.6 dyn/cm[158] and the reported

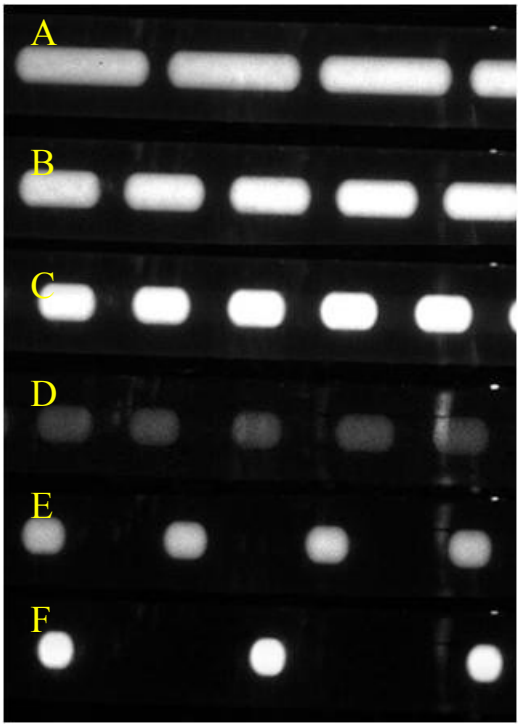

Figure 2.7 Fluorescence microscopy images of droplets generated under various flow rates. The aqueous to fluorous flow ratios (Q_w/Q_p) were as follows: A) 4, B) 2, C) 1, D) ½, E) ¼, F) 1/8. Droplets contained a 50 µM fluorescein solution.

value of the viscocity of perfluorodecalin (μ), 0.0551 dyn s/cm^2 we can use equation 1.1 to calculate the *Ca* for the flow rates used. The *Ca* values for these experiments were all calculated to be between 1.7×10^{-4} and 4.1×10^{-4}, well below the critical threshhold for stable droplet formation ($Ca < 0.015$)[60]. As is expected when working within the "squeezing" regime, droplet size decreases with Q_w/Q_p.

ImageJ software was used to measure the length of 20 droplets from the captured images at each of the different flow rate ratios. The average plug length for each flow ratio was plotted in Figure 2.8a. Figure 2.8b also shows the dimensionless plug length (*L/w*) versus Q_w/Q_p. The dashed line represents the theoretical relationship between *L/w* and Q_w/Q_p calculated from Eq. 1.2, for an α value of 1. The actual α value depends on the geometry of the channel, so our own data deviates slightly from the predicted ones. Our results, however, are in general agreement with the expected trend. That is, a linear increase of droplet length with Q_w/Q_p.

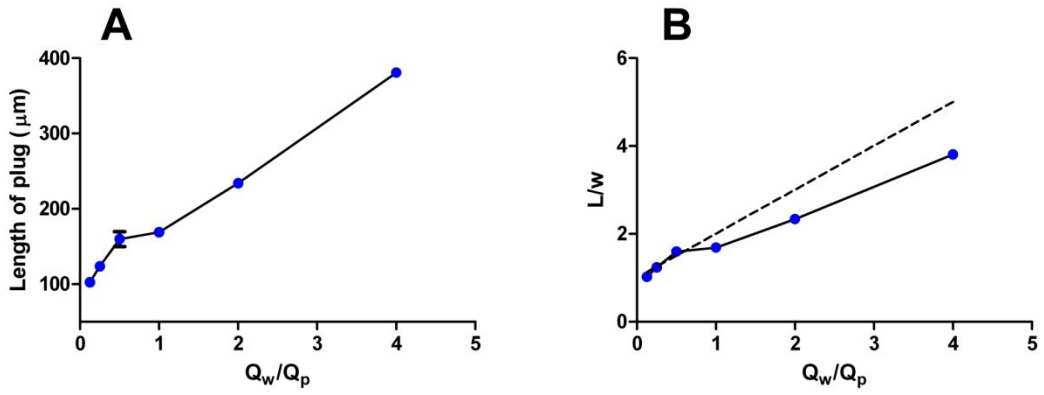

Figure 2.8. Flow rate experiments. A) Dependence of length of aqueous plug on flow rate ratio, Q_w/Q_p. B) Dimensionless plug length vs. Q_w/Q_p. Dashed line represents *L/w* predicted by model proposed by Whitesides et al. for α = 1.

Droplet size reproducibility

The reproducibility of the drop size was also assessed from these imaging experiments. For all observed flow rates, the RSD for the measured droplet lengths was less than 3% for all points except one, Q_w = ½, with an RSD of 6.17%. The measured droplet lengths and RSDs are shown in Table 2.3. Figure 2.9a is a plot of the effect Q_w on the droplet length RSD. For the first four flow rate ratio values (1/8, ¼, ½ and 1), Q_w was increased as Q_p was held constant, hence increasing Q_w also resulted in increasing total flow rate. It can be observed from the plot, that droplet length variance increases with Q_w and hence with the total flow rate, but it remains low throughout the flow rate range in which the experiments were carried out.

Droplet length (μ)	RSD	n
380.9	0.9	15
223.8	1.3	17
168.9	2.5	44
159.7	6.2	11
123.8	2.3	15
102.3	1.8	12

Table 2.3. Droplet lengths measured and reproducibility.

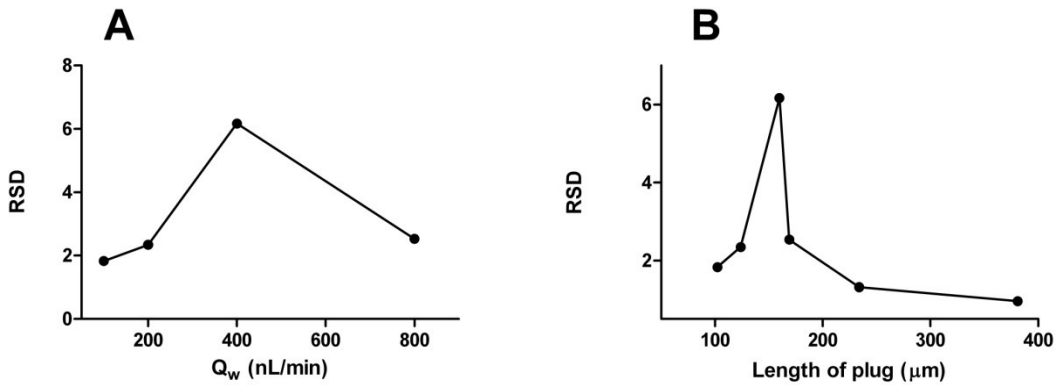

Figure 2.9. Droplet reproducibility. A) Plot of droplet length RSD vs. aqueous flow rate in nL/min. B) Plot of droplet length RSD vs. droplet length in μm.

Figure 2.9b shows the change in droplet length reproducibility as a function of droplet length. As plug length decreases, RSD initially increases, reflecting the trend

shown in Figure 2.9a where RSD increases with higher Q_w (and thus total flow rate), but then decreases again for longer droplet lengths.

Detection of droplets by LIF using a PMT detector

The use of fluorescence microscopy for droplet detection and analysis remains common in microfluidic application, particularly in those that require the visualization of the entire droplet or simultaneous analysis of more than one droplet at a time. In many instances, however, other detection methods may be desired. The exposure time required for detection by the CCD camera, for example, can sometimes limit the rate at which data can be acquired. A fluorescence microscope and CCD camera can also be expensive. LIF coupled to a PMT detector can increase assay sensitivity, increase data collection rate and can be a less expensive detection alternative. For the next set of experiments, the same previously described droplet generation module was adapted for use with a PMT detector and LIF. The details of this instrument are described in the previous section. Figure 2.10 shows a sample trace of droplet fluorescence as they flow past the detector.

Each peak in the trace represents a droplet containing 10 μM fluorescein as it passes the detector, and whose width is determined by the length of the droplet in the channel and the total flow rate through the channel. The baseline between each peak is given by the plugs of fluorous solvent separating each droplet. As can be seen in the figure, most of the peaks recorded also display a spike on the leading end. The likely cause for this is scatter due to a lensing effect at the aqueous/fluorous interface. These spikes can be observed on either the leading or trailing end of the droplets, depending on

the exact alignment of the laser. Like the previous experiments with CCD camera detection, the traces collected by LIF detection show high reproducibility in droplet size.

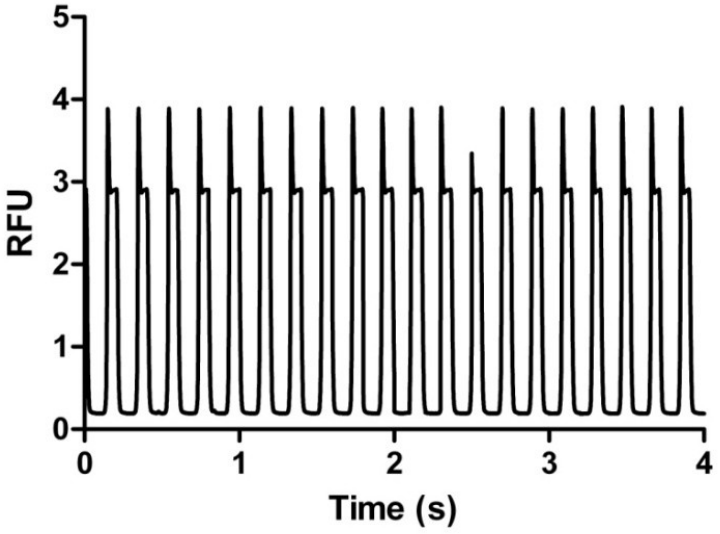

Figure 2.10 Trace of droplet fluorescence as they move past the detector. Each peak represents a single droplet containing 10μM fluorescein. Excitation was done with a 100 mW 488 nm diode pumped solid state laser. A PMT was used for detection.

As with fluorescence microscope detection, the effect of flow rate and flow rate ratio can be readily seen with the PMT detection system. Figure 2.11, shows the effect of increasing the aqueous flow rate as the fluorous flow rate is kept constant. As expected, as the total flow rate increases so does the droplet frequency. As the aqueous flow rate decreases and thus the Q_w/Q_p also decreases, the length of the fluorous plug between droplets becomes longer.

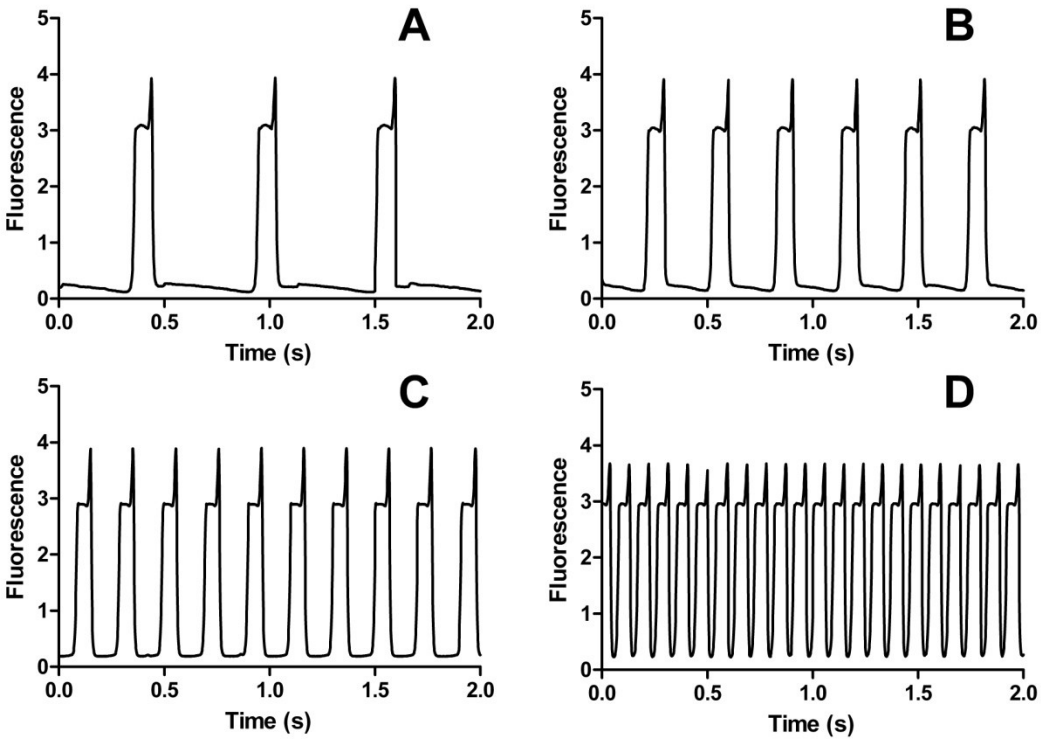

Figure 2.11 Effect of flow rate ratio on droplet frequency. For traces shown, fluorous flow rate was kept constant at 800 nL/min. Aqueous flow rates were as follows: A) 100 nL/min (Q_w/Q_p=1/8) B) 200 nL/min (Q_w/Q_p=1/4) C) 400 nL/.min (Q_w/Q_p=1/2) D) 800 nL/min (Q_w/Q_p= 1)

Figure 2.12 similarly shows the effect of changing the fluorous phase flow rate while maintaining the aqueous flow rate constant. As before, as the fluorous phase flow rate decreases, along with the total flow rate, the droplet frequency decreases as well. It can also be observed how the length of the aqueous plugs increases as the flow rate ratio Q_w/Q_p increases

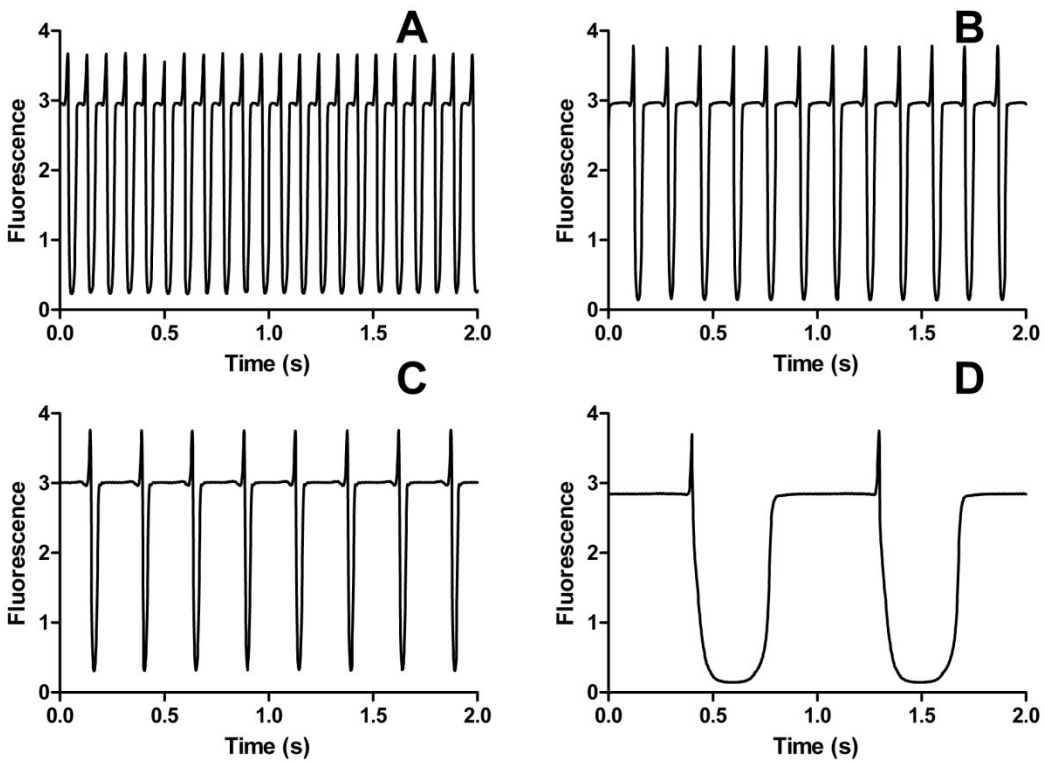

Figure 2.12. Effect of flow rate ratio on droplet droplet frequency and length. For traces shown, aqueous flow rate was kept constant at 800 nL/min. Fluorous flow rate was changed as follows: A) 800 nL/min ($Q_w/Q_p = 1$), B) 400 nL/min ($Q_w/Q_p = 2$), C) 200 nL/min ($Q_w/Q_p = 4$), and D) 100 nL/min ($Q_w/Q_p = 8$). A s the fluorous flow rate (Q_p), and the aqueous flow rate (Q_w) is held constant, the length of the a aqueous plug increases.

Frequency of droplet generation

Due to its capacity for high collection rates, the PMT detector was used to evaluate the effect of flow rate on the frequency of droplet formation using PEEK T-unions. Droplets were generated as previously described (see Figure 2.3). For the first set of collections, the total flow rate was increased while maintaining a constant ratio of aqueous to fluorous flow rates (Q_w/Q_p). Q_w/Q_p was held at 0.5 over a total flow rate range of 300 nL/min to 1500 nL/min. At each flow rate, the system was allowed to equilibrate for 30 minutes before data collection. Fluorescence data was collected for 60 seconds in triplicate runs. The peaks in each trace were detected and counted using LabView.

Figures 2.13a and 2.13b show the resulting droplet frequencies plotted against total flow rate and Q_w respectively.

For the second set of collections, the total flow rate was increased by increasing the aqueous flow rate (Q_w) while maintaining the fluorous flow rate (Q_p) constant. Q_p was held at 800 nL/min, while the Q_w was increased from 200 to 800 nL/min. Droplet generation data was collected as described above. Figures 2.13c and 2.13d show the resulting droplet frequencies plotted against total flow rate and Q_w respectively. Both sets of experiments, with constant and varying Q_w/Q_p, show the same trend of increasing generation frequency with increasing total flow rate. The magnitude of the increase in droplet generation frequency in the first case was almost ten-fold, from 1.36 ± 0.05 drops/s at 300 nL/min to 9.30 ± 0.16 drops/s nL/min at 1,500 nL/min. A similar, but smaller, increase was observed in the second case (varying Q_w/Q_p) from 3.18 ± 0.04 drops/s at 1000 nL/min to 10.37 ± 0.17 drops/s at 1,600 nL/min.

We have shown that, like in experiments using fabricated microfluidic chips, we are able to control the droplet frequency and droplet dimensions simply by adjusting the flow rates of the carrier and dispersed phases. This control is one of the principal advantages of segmented flow and crucial to many applications. Using a simple relation we can calculate the flow rate settings required to produce droplets with a desired volume. Furthermore, the size of the plug between the droplets is also easily adjusted, allowing for precise control of timing and the number of droplets per length of tubing. Highly reproducible droplets volumes are also important, particularly for applications in which the analyte concentration inside the droplet must be measured. That is, measured

differences in analyte concentration between droplets should not be the result of differences in droplet volume.

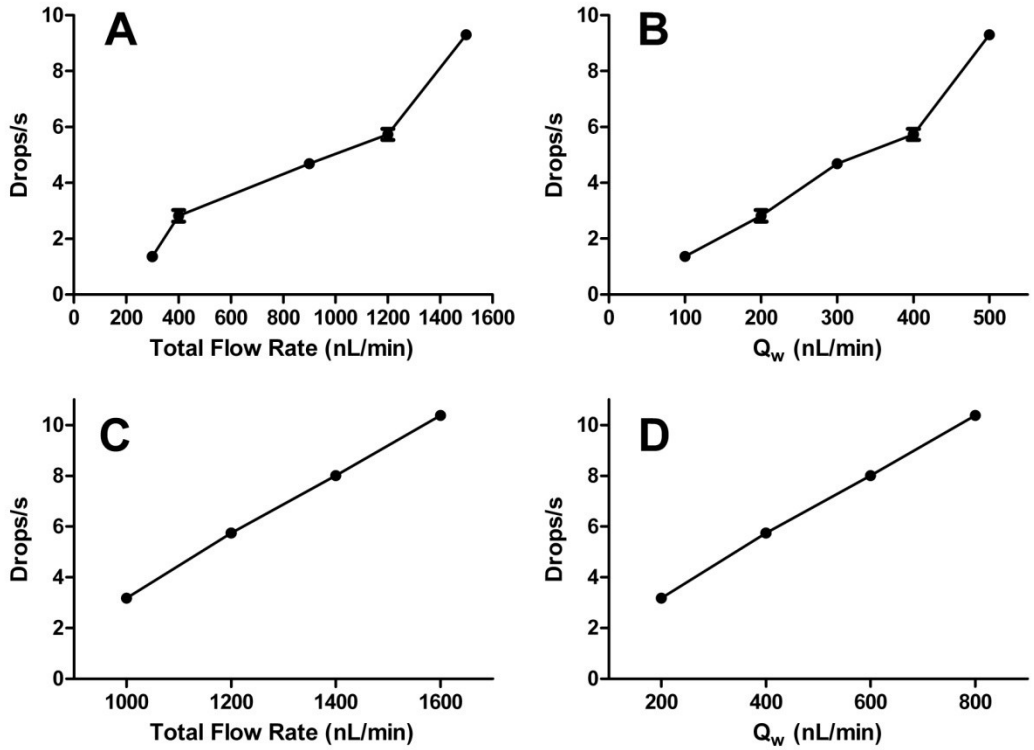

Figure 2.13 Effect of flow rate on droplet generation frequency. A) Droplet frequency as a function of total flow rate when Q_w/Q_p is kept constant at 0.5. B) Droplet frequency as a function of Q_w with same constant Q_w/Q_p.(=0.5) C) Droplet frequency as a function of total flow rate when Q_p is constant (=800 nL/min) and only Q_w is increased. D) Droplet frequency as a function of Q_w when Q_p is kept constant (=800 nL/min). For each flow rate, the number of droplets generated during 60 seconds was counted and averaged for triplicate 1 minute collections.

On-line mixing with segmented flow

Many applications of segmented flow arrays require the rapid mixing of reagents upon droplet generation. Mixing efficiency in the droplets generated by the PEEK T-unions was investigated experimentally as described in the *Instruments and Methods* section. Briefly, a second T-union was placed upstream of the droplet generator, perpendicular to the fluorous stream. This second T-union was used to mix two aqueous

streams: one containing a 1 μM fluorescein solution, the other containing only DI H_2O. The flow rates of these two aqueous streams were set to equal so that the resulting mixed solution was 500 nM fluorescein. The mixed stream was then dispersed into droplets at the first T-union. The blue trace in Figure 2.14 shows the fluorescence of a few droplets containing the mixed fluorescein solution. Using the same flow rate settings the experiment was repeated with the DI H_2O replaced with a second stream of 1 μM fluorescein, so that there was no 1:1 dilution. The red trace in Figure 2.14 shows the fluorescence of a few droplets containing the undiluted fluorescein solution. The fluorescence measured in the droplets containing the diluted fluorescein was 0.109 ± 0.004 RFU (n = 251) compared to 0.192 ± 0.006 RFU (n = 259) for the undiluted droplets, indicating good mixing of the two aqueous streams inside the droplets.

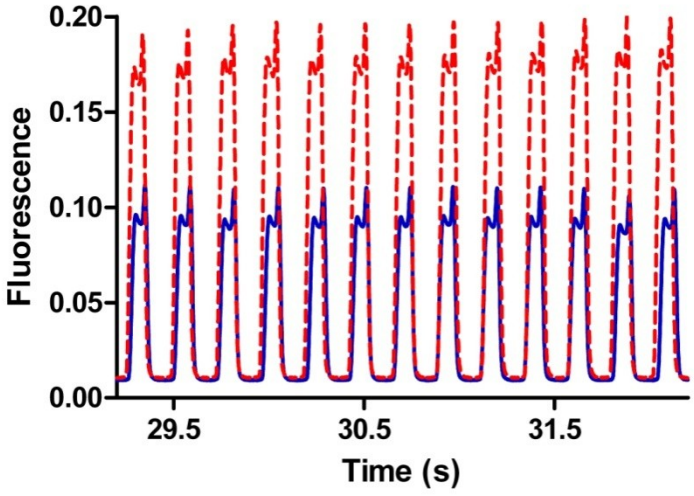

Figure 2.14 Comparison of traces from mixing experiments. The blue trace shows droplets generated by the on-line mixing a 1 μM solution of fluorescein with DI H_2O at the same flow rate, for an in-droplet concentration of 500 nM. Average droplet fluorescence was measured to be 0.109 ± 0.004 RFU (n = 251) The red trace shows droplets generated from a 1 μM solution of fluorescein with no mixing. Average droplet fluorescence was measured to be 0.192 ± 0.006 RFU (n = 259).

Long term droplet stability

One benefit of using Teflon tubing in segmented flow arrays is the ease of storing large droplet libraries for future analysis or other uses. Droplet arrays, for example, have been used for cell culturing. The long term stability of droplet arrays in 100 μm ID Teflon tubing was monitored over a period of a week. Figure 2.15 shows an image of droplets containing fluorescein after 7 days of storage. Droplets in storage show no sign of coalescence during this period.

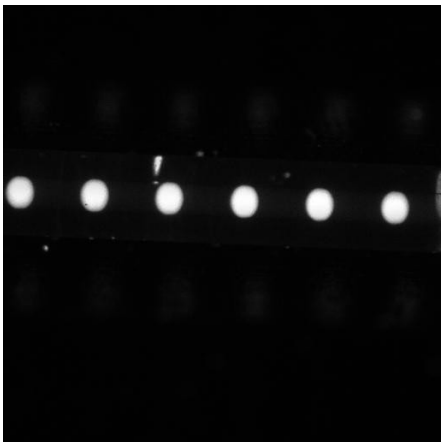

Figure 2.15 Image of fluorescent droplets inside Teflon tubing after storage for 7 days.

Conclusions

Modules featuring small diameter (100 μm) PEEK T-unions coupled to Teflon capillary tubing are a viable alternative for the generation and storage of droplet micro-arrays. This approach has been shown to produce highly reproducible droplets, whose volume can be readily manipulated by adjusting the flow rates of the carrier and dispersed phases. Simple dilution experiments have demonstrated fast mixing of reagents in the droplets, allowing their use as subnanoliter reactors. Finally, the droplet arrays are

stable and can be easily stored in a segment of coiled Teflon tubing for up to 7 days without observable aggregation.

Chapter III. Development of segmented-flow, single molecule alkaline phosphatase activity assay using Teflon tubing and commercial fittings.

Introduction

Alkaline phosphatase (AP) is an enzyme found ubiquitously in nature, common to both prokaryotic and eukaryotic organisms[159, 160]. It catalyzes the non-specific hydrolysis of phosphate monoesters to yield inorganic phosphate and an alcohol[159]. Its structure (shown in Figure 3.1) has been elucidated and its mechanism of catalysis studied extensively[161]. Despite its prevalence in nature the physiological role of AP continues to be poorly understood[162, 163]. Different isoforms of mammalian AP are believed to be involved in bone mineralization, intestinal absorption and immunity and endotoxin dephosphorylation[164-168]. AP has also been used as a biomarker for liver function and as a therapeutic agent for gastrointestinal disorders[166, 169-172]. AP from *E. Coli* has been called one of the most extensively studied enzymes and is believed to be involved in cellular phosphate regulation[162, 173-177]. AP is a homodimeric metalloenzyme with three metal binding sites, two for Zn^{2+} and one for Mg^{2+}[160, 178]. Each subunit is composed of 449 amino acid residues with a molecular weight of approximately 47,000 Da, though individual monomers do not display enzymatic activity[162, 179].

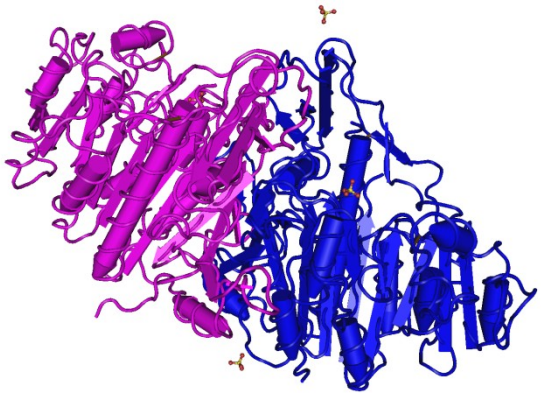

Figure 3.1. Structure of alkaline phosphatase dimer**.** Image from the RCSB PDB (www.pdb.org) of PDB ID 1ALK (Kim and Wyckoff, 1991)

Due to its high catalytic efficiency, AP is often used for signal amplification in assays that require high sensitivity. Thus, it has also found wide application in

biochemical and clinical assays. In particular, it has become a commonly used enzyme in immunoassays and related affinity techniques[180-186]. Given such interest, it is not surprising that a wide range of detection techniques for AP have been reported, including colorimetric[187], fluorescent[182, 188], electrochemical[189, 190], chemiluminescent[191, 192], phosphorescent[193] and using surface enhanced raman[184].

AttoPhos® as a fluorogenic substrate for AP

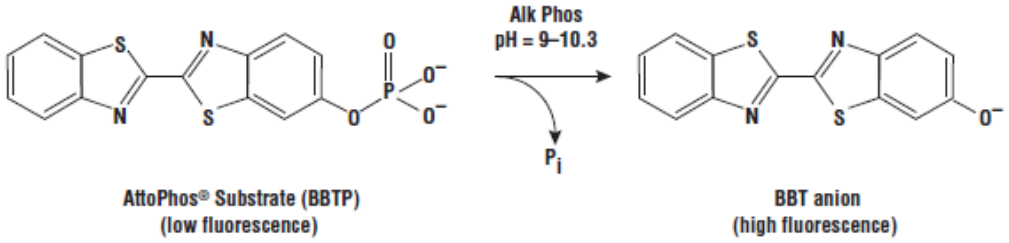

Figure 3.2. Alkaline phosphatase mediated hydrolysis of AttoPhos® substrate to yield BBT anion**.** From AttoPhos® AP Fluorescent Substrate System Technical Bulletin (Promega Part # TB280)

AttoPhos®, 2'-[2-benzthiazole]-6'-hydroxybenzthiazole phosphate, is a commonly use fluorogenic substrate for AP. Upon hydrolysis (Figure 3.2), the weakly fluorescent AttoPhos® is converted into the highly fluorescent product, the BBT anion (2'-[2-benzthiazole]-6'-hydroxybenzthiazole). Figure 3.3 shows excitation and emission spectra for the BBT

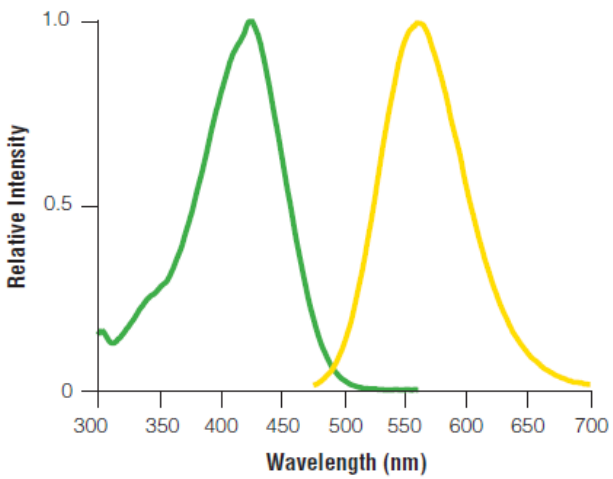

Figure 3.3. Excitation (green) and emission (yellow) spectra for BBT anion. From AttoPhos® AP Fluorescent Substrate System Technical Bulletin (Promega Part # TB280)

anion, with a maximum emission wavelength of 575 nm. A large Stoke's shift can be observed, allowing the use of AttoPhos® in highly sensitive assays.

Single enzyme studies with AP

Using a technique similar to Yeung et al's, Dovichi et al., were able to measure the activity of single molecules of calf intestinal alkaline phosphatase (CIAP)[14]. In these experiments, a solution of the fluorogenic substrate AttoPhos® and a dilute solution of CIAP were mixed off-line. A slug of the resulting mixture was rapidly injected onto a fused silica capillary with an ID of 10 μm. The concentration of the CIAP was low enough so that in each run an average of 11 enzyme molecules were injected onto the capillary. After injection, the enzyme molecules were allowed to react for a variable incubation time of between 14 and 30 minutes. During this time, each enzyme molecule present inside the capillary generated a discreet band of fluorescent product. After the incubation period, the product bands were moved electrophoretically to the outlet of the capillary for detection by LIF. The results of these experiments showed a 10-fold range of activity for the individual molecules observed. It was suggested by the authors that these differences in activity arise from heterogeneity in post-translational modification, particularly their state of glycosylation.

A later study, in which the single molecule activities of highly purified, non-glycosylated *E. Coli* AP were measured, seemed to offer confirmation of post-translational modification as the source of activity heterogeneity[84]. *E. Coli* AP is known to exist in three distinct isoforms. Previous to the activity assays, each isoenzyme was

purified by isoelectric focusing to guarantee enzyme homogeneity. In contrast to the previous experiment, the purified AP showed no heterogeneity of activity within experimental error. Finally, thermostable AP from *Thermus Thermophilus* grown at 70 °C has been shown to exhibit heterogeneity with regards to activity as well[194]. This report makes evident that even under more stringent growth conditions, multiple stable forms of AP exist at room temperature.

In this study, we apply the droplet generation and analysis system characterized in the previous chapter to the development of a microfluidic, segmented-flow single molecule AP assay. For this assay, a solution containing a very low concentration of the enzyme AP is mixed with a solution containing the fluorogenic substrate AttoPhos®. This reaction mixture is quickly dispersed into a droplet array stored inside a segment of Teflon tubing. When the concentration of AP in the original solution is low enough, only a fraction of the droplets generated will contain a single enzyme molecule while most will have none. In those droplets that do contain a single molecule of AP, that molecule will catalyze the formation of the fluorescent product, the BBT anion. After a suitable incubation period, unoccupied droplets will remain weakly fluorescent while occupied ones will show a measurably higher fluorescent intensity, proportional to the activity of the AP molecule contained within.

Materials and methods

Reagents and materials

AttoPhos® AP fluorescent substrate system was purchased from Promega (Madison, WI). Alkaline phosphatase from *E. Coli,* perfluorodecalin, perfluorooctanol and fluorescein were all from Sigma Aldrich (St. Louis, MO). Reaction buffer components, Tris base, $MgCl_2$, $ZnCl_2$, spermidine and Tween 20 were purchased from Sigma as well. PEEK tee connectors with 50 μm ID were purchased from Vici Valco instruments (Houston, TX). Teflon tubing (360 μm OD, 50 μm ID) was from IDEX Health and Science (Oak Harbor, WA). Product part numbers for tubing and connectors are shown in Table 3.1. 100 μL gas tight syringes were purchased from Hamilton Co (Reno, NV). Fused silica capillary was from Polymicro Technologies (Phoenix, AZ). All buffers for experiments were made in water purified with a Milli-Q water purification system (Millipore Corp, Bedford, MA).

	Part No.	Vendor
PEEK tee, 50 μm ID	C360QTPK2	Vici Valco Instruments
PEEK nut/ferrule assembly	C360NFPK	Vici Valco Instruments
Teflon tubing, 50 μm ID	1931	Upchurch

Table 3.1. List of parts and vendors used in segmented flow system.

Instruments and methods

A 2.0 mM working solution of AttoPhos® was made as per the manufacturer's instructions, using the AttoPhos® Buffer provided. The working solution was frozen and

stored in 500 μL aliquots at -70 °C until ready to be used. Before each experiment the AttoPhos® stock solution was diluted two-fold, to make a solution that when mixed with an equal volume of enzyme solution would result in an in-droplet concentration of 500 μM AttoPhos®. A 4× reaction buffer was made containing 200 mM Tris, 4 mM $MgCl_2$, 0.4 mM $ZnCl_2$ and 4 mM spermidine, with pH adjusted to 9.3. A 10% solution of Tween 20 in water was also made. All solutions were filtered using a 0.22 μm pore size nitrocellulose filter membrane. A stock solution of AP from *E. Coli* was made from the purchased suspension by diluting it in 1:1 glycerol and 1× reaction buffer. For experiments, enzyme dilutions were made sequentially from stock using 1× reaction buffer with 1% Tween 20. For the fluorous phase, a mixture of 10:1 perfluorodecaline: perfluorodecanol was made fresh every day.

On-line mixing and droplet generation

Two separate gas-tight syringes were used to deliver the aqueous solutions containing the enzyme and the fluorogenic substrate. The solutions were mixed on-line using a PEEK tee attached to each syringe via a piece of fused-silica capillary. The outlet of the mixing tee was then attached to a second tee which acted as the droplet generator. Perfluorodecalin was used as the carrier phase, delivered via a third gas-tight syringe attached to the second inlet of the droplet generator (Figure 3.4).

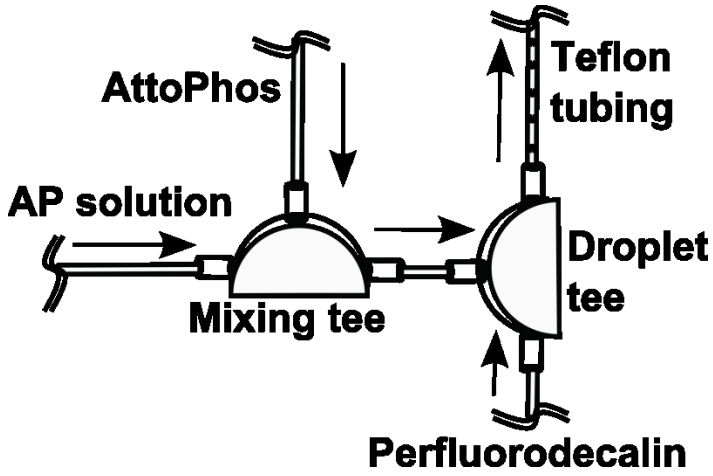

Figure 3.4. Loading single enzyme molecules into droplet arrays. Alkaline phosphatase solution and AttoPhos® solution were delivered to the mixing tee via two pieces of fused silica capillary each connected to a gas tight syringe. Mixing tee was connected to droplet generator (T-Junction) with a 3 cm piece of fused silica capillary. In the droplet generator, the two aqueous streams were mixed with a fluorous stream delivered perpendicularly via another segment of fused silica capillary connected to a third gas tight syringe. Droplets generated at the T-junction were collected in an array inside a piece of Teflon tubing connected to the outlet of the droplet generator. Arrows indicate the direction of flow.

The gas tight syringes containing the two aqueous phases and the perfluorodecalin were loaded onto two separate Pump 11 pico plus syringe pumps (Harvard Apparatus, Holliston, MA). The AttoPhos® and AP solution syringes were connected to a 100 μm ID PEEK Tee via two 10 cm pieces of 360 μm OD, 100 μm ID fused-silica capillary (Polymicro). A 3 cm piece of 100 μm ID fused-silica capillary was also used to join the outlet of the mixing tee to an inlet of the droplet generator tee (PEEK, 50 μm ID). Another 10 cm piece of fused silica capillary was attached to the second inlet of the droplet generator tee, and then connected to the perflourodecalin syringe. A 50 cm piece of 360 μm OD, 50 μm ID Teflon tubing was connected to the outlet of the droplet generator tee. The Teflon tubing was coiled and the outlet was placed inside a home built sheath-flow cuvette and housed in a PEEK assembly. Water was allowed to flow through the sheath-flow cuvette to remove the droplets as they exited the capillary and to reduce

scatter at the Teflon capillary wall. After droplet generation, pumps were stopped and syringes disconnected. The droplets inside the Teflon tubing were then allowed to incubate for a suitable period. After incubation, the pumps were turned on and reconnected to the tubing via a PEEK capillary tubing connector (Vici-Valco).

Droplet detection and analysis

On-capillary detection was done by LIF inside the cuvette. For excitation, a Cyan ™ 488 nm, 100 mW diode pumped solid state laser from Spectraphysics (Irvine, CA) was used. Laser light was expanded using a beam expander from Newport (Irvine, CA) and then focused directly onto the Teflon capillary using a focusing lens also from Newport. Fluorescent light was collected by an objective perpendicular to the excitation light and was filtered previous to detection with a 570 nm band pass filter from Intor (Socorro, NM). Fluorescence intensity data was collected with a PC using LabView data acquisition hardware and software. After each enzyme experiment, the entire system was rinsed with a solution of 7 M Urea and 100 mM KOH to remove any adsorbed enzyme. The entire system can be seen schematically in Figure 3.5.

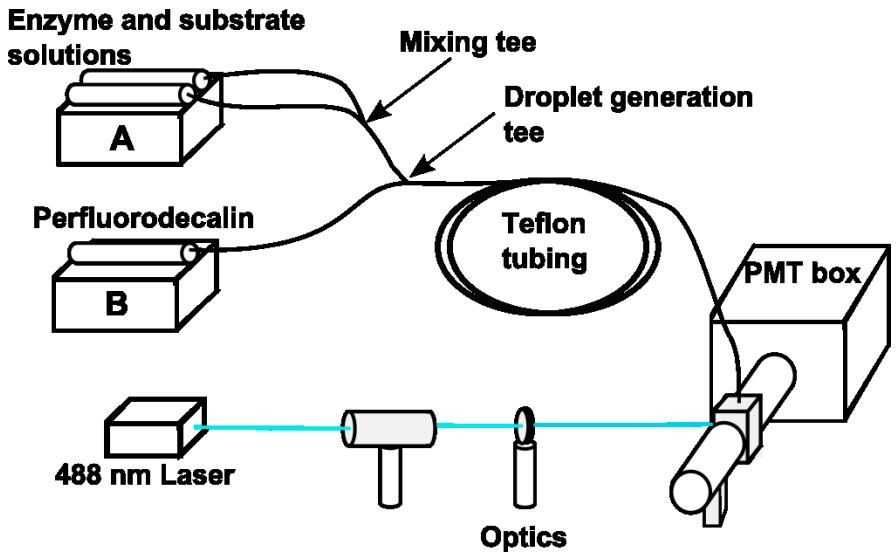

Figure 3.5 Diagram of droplet analysis system for single enzyme AP assays. Syringe pump A delivers the solutions containing AttoPhos and AP to a mixing tee. The mixing tee in connected to a second tee-junction which is in turn connected to syringe containing the fluorous phase (Syringe pump B). At this T-junction, aqueous and fluorous streams meet and generate a segmented flow array inside the Teflon tubing attached to the outlet of the T-junction. The outlet of the Teflon tubing is placed inside a sheath-flow cuvette, where droplets can be analyzed by LIF.

Results and Conclusions

Determination of droplet size, frequency and reproducibility

The fluorescence intensity of a droplet containing an enzyme molecule will depend on the concentration of fluorescent product molecules generated inside the droplet. The concentration of product, in turn, depends on the catalytic rate of the enzyme molecule and the volume of the droplet. In order to decrease analysis time, it is desirable to use the shortest incubation time necessary to detect enzyme activity. This means maintaining a low droplet volume. For this reason, the smallest ID Teflon tubing available was selected, 50 μm ID high purity Teflon tubing from Upchurch/IDEX. As in the previous chapter, the effect of flow rate on droplet size and reproducibility was

studied. In these experiments a 50 μm ID PEEK tee was used to generate droplets from an aqueous solution of 50 μM fluorescein at different flow ratios. Perfluorodecalin was used as the carrier phase. Aqueous and fluorous phases were delivered to the PEEK tee using separate syringe pumps. Droplet fluorescence was monitored by on-column LIF detection. Fluorescence data was collected and analysed using LabView. Figure 3.6 shows the traces of fluorescent droplets at several values of Q_w as Q_p is held constant at 300 nL/min.

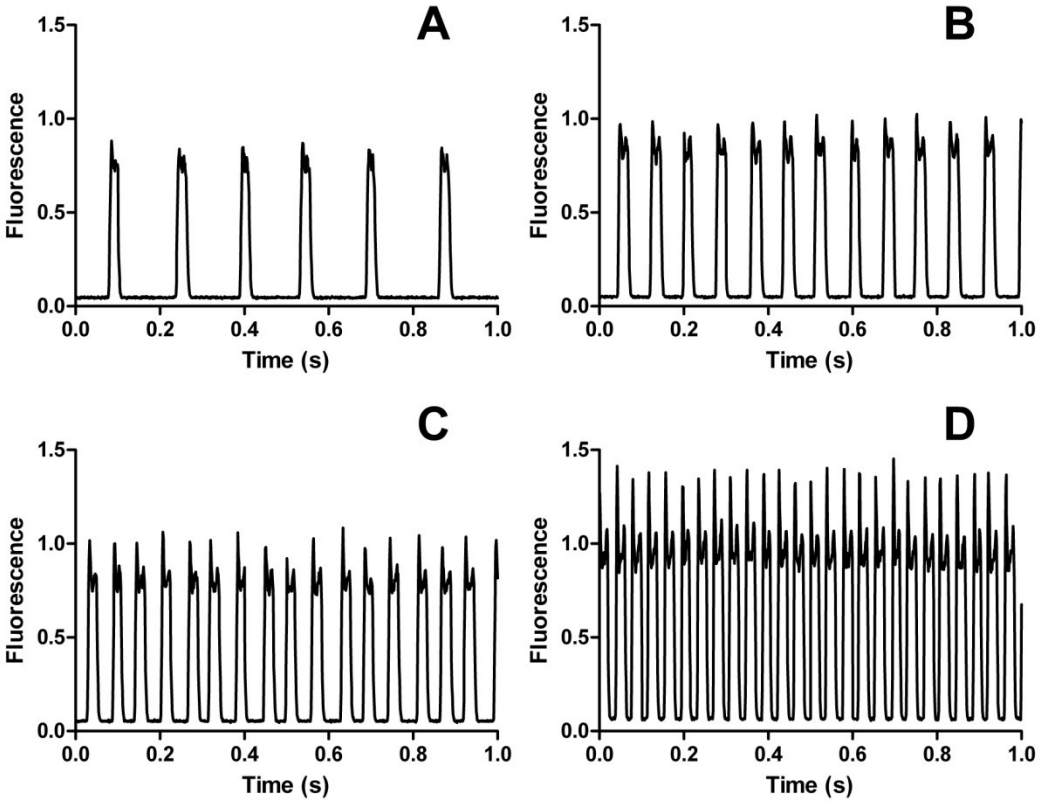

Figure 3.6. Effect of Q_w/Q_p on droplet frequency. For traces shown, Q_p was kept constant at 300 nL/min. Q_w was changed as follows: A) 50 nL/min (Q_w/Q_p = 1/6), B) 100 nL/min (Q_w/Q_p = 1/3), C) 150 nL/min (Q_w/Q_p = ½) and D) 300 nL/min (Q_w/Q_p = 1).

If the fluorescence intensity of the droplets is to be related to enzyme activity, droplet volume must be reproducible. The droplets generated in the 50 μm tubing were very reproducible. The RSD of the droplet lengths, as measured from droplet peak width, for all flow rates measured were under 5%. Figure 3.6 also shows that, as in the previous chapter, it is possible to control the length the fluorous plugs separating adjacent aqueous drops simply by adjusting the flow rate ratio. At a Q_w of 50 nL/min the droplets were observed to be nearly spherical. A perfectly spherical droplet with a radius of 50 μm has a volume of 98.17 pL. For the single enzyme experiments, a Q_w of 50 nL/min and a Q_p of 200 nL/min generated nearly spherical droplets. For the purpose of calculations the volume of these droplets was estimated to be 100 pL. The Q_w/Q_p of 1/4 was chosen to prevent possible droplet association due to proximity. This increased distance between droplets also seems to reduce the spikes associated with scattering at the aqueous/fluorous interface. The longer plugs, however, also reduce the number of aqueous droplets per length of tubing and so the chosen ratio must involve a compromise.

Incubation period estimation

In order to estimate the shortest adequate incubation period for the single enzyme experiments, conventional fluorescence assays were carried out first using a commercial plate reader. For these initial bulk enzyme experiments, the reaction conditions were the same as those to be used for the single enzyme experiments: 50 mM Tris, 1 mM $MgCl_2$, 0.2 mM $ZnCl_2$ and 1 mM spermidine, at a pH of 9.3. The reaction mixture also contained 500 μM of AttoPhos® fluorogenic substrate. The dilute AP solution was added last and

fluorescence readings were begun immediately after. The enzyme concentration in the final reaction mixture was 5.1×10^{-15} M, which corresponds to a target of 1 droplet out of 3 containing a single enzyme molecule (assuming a droplet volume of 100 pL). Figure 3.7 shows the results of these bulk assays. Fluorescence readings were taken every 2.5 minutes for a period of one hour. For the blank runs, the reaction mix was the same as described omitting only the AP enzyme added. After 60 minutes, the reaction sample shows an almost 4-fold increase in fluorescence over the blank. This, of course, represents an average activity over a very large number of molecules. It has been shown that individual molecules may display lower or higher activities than the average. It should also be noted that the effective concentration of the enzyme inside a droplet will also be higher or lower than in the bulk solution. That is, for a bulk solution with concentration 5.1×10^{-15} M about one droplet in three will contain a single AP molecule, with the rest remaining empty. In the empty droplets, the AP concentration is obviously zero. In the droplets that do contain an AP molecule, however, the concentration is three times the bulk concentration, 1.66×10^{-14} M. This is important, as in the following single enzyme experiments significantly lower bulk concentrations will be required in order to avoid

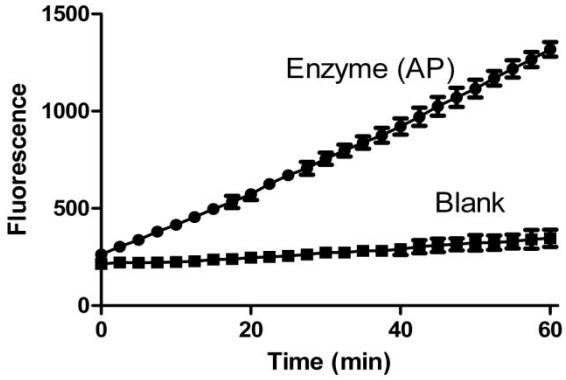

Figure 3.7. Bulk enzyme assay with AP and AttoPhos. Circles show fluorescence data for enzyme reaction over a period of 60 min. AttoPhos concentration was 500 μM and AP concentration was 5.1×10^{-15} M. Squares show fluorescence data for blank runs. Error bars shown are for n=3.

double or triple droplet occupancy. As the bulk enzyme concentration decreases, the proportion of occupied to unoccupied droplet also decreases, but the concentration of enzyme in an occupied droplet will never be less than 1.66×10^{-14} M (for a 100 pL droplet).

Distribution of enzyme molecules within the droplet array

As mentioned in the single enzyme assay introduction in Chapter I and alluded above, the observed distribution of enzyme molecules into the dispersed droplets follows a Poisson distribution. In general, a Poisson distribution gives the probability of a discreet number of independent events occurring at a given time or location, given a fixed average rate. The equation for such a distribution is shown below.

$$P(n) = \frac{\nu^n e^{-\nu}}{n!} \qquad \text{Eq. 3.1}$$

Where *P(n)* is the probability of *n*, *n* is the number of occurrences of the event and ν is the average rate with which the event occurs. Thus, the probability that a droplet in the array will contain a single enzyme molecule (*n*=1), or two (*n*=2), or three (*n*=3) and so on, can be calculated from the expected average number of enzyme molecules per droplet, ν. Figure 3.8 shows calculate Poisson distributions for several values of ν. It can be readily seen in Figure 3.8a that for low values of ν (ν = 0.1 or 1 in 10 droplets occupied) most droplets are, as expected, empty. In fact, the number of empty droplets is predicted to be very close (90.48%) to the target value of 90% (for ν = 0.1, one would expect 9 in 10 unoccupied droplets). Only 9.04% of the droplets will be singly occupied. Furthermore, there is a 0.45% probability of a droplet containing two enzyme molecules,

meaning such an event can be expected every 220 droplets. As ν increases so does the probability of more than one enzyme molecule occupying the same droplet. When ν = 0.50 (one in two occupied droplets), 60.65% of the droplets remain unoccupied and 7.58% of the droplets observed can be expected to contain two enzyme molecules. For large values of ν, the distribution becomes essentially a Gaussian with mean ν.

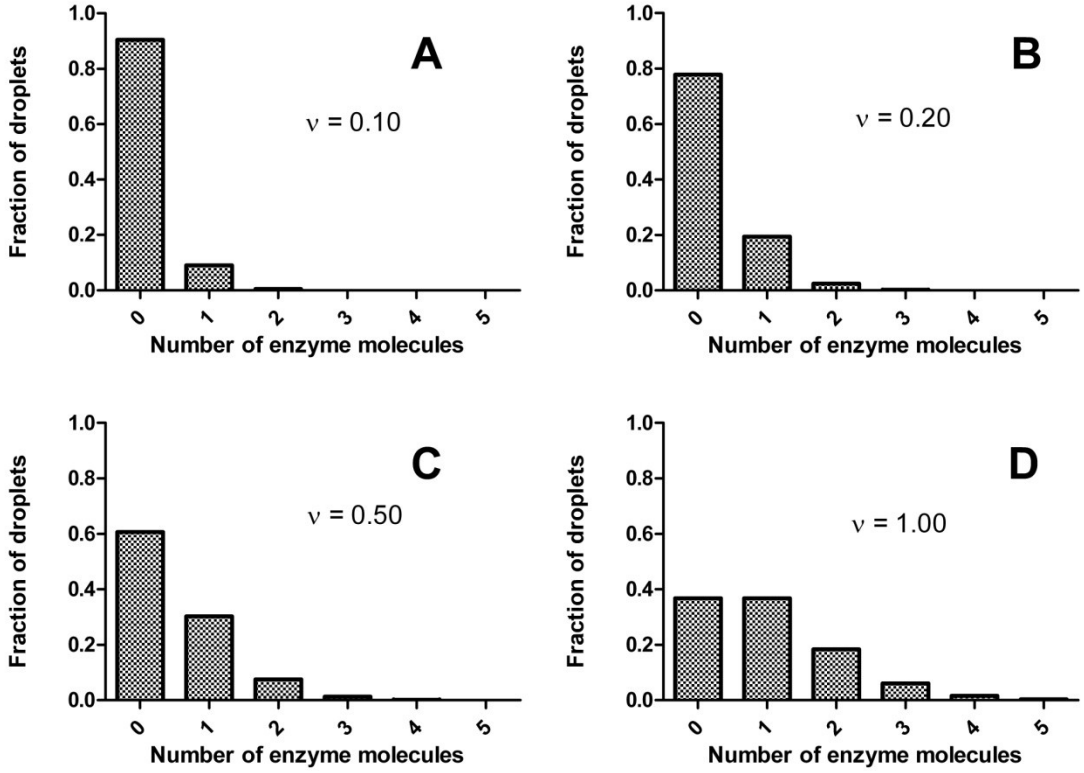

Figure 3.8. Calculated Poisson distributions for different occupied to unoccupied target ratios. The y-axis shows the probability of a droplet containing a given number of enzyme molecules (x-axis). The expected (or average) number of enzyme molecules per droplet are as follows: A) 0.10, B) 0.20, C) 0.50 and D) 1.00

Single enzyme molecules experiments

In order to study single enzyme molecules or single cells, then, studies that use stochastic confinement must use very low analyte concentrations in order to avoid or at least reduce the numbers of droplets with multiple analytes. For the initial single enzyme experiments an AP concentration of 3.3×10^{-15} M was selected, to give an expected 1 in 5 occupied droplets ($\nu = 0.2$). The experiment was carried out as described in the experimental section. The dilute enzyme solution was mixed with the substrate solution on-line using a PEEK T-junction. The droplets were allowed to incubate for 2 hrs and then pushed past the LIF detector using a syringe pump. The result, as in the previous chapter, is a plot analogous to a chromatrogram or electropherogram, in which each peak represents a droplet moving past the detector. Figure 3.9 shows one such trace. Significant differences in droplet fluorescence can be readily seen in this figure, increased fluorescence indicating the activity of a single enzyme molecule. For

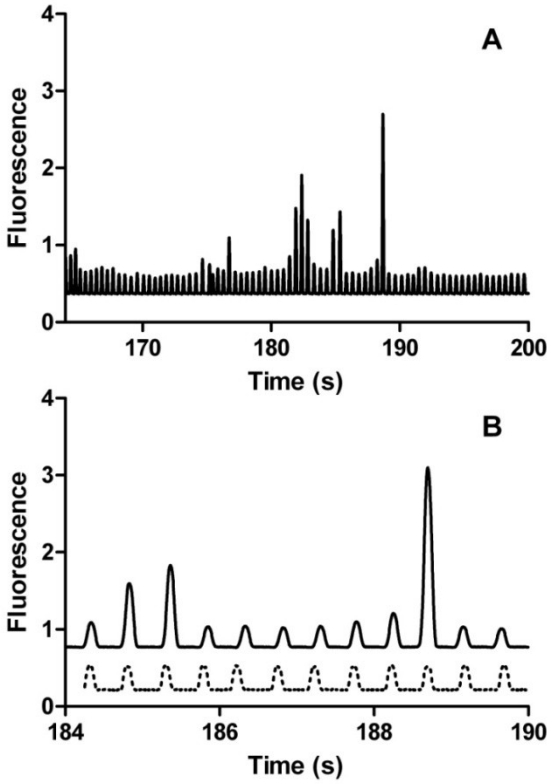

Figure 3.9. Plot of fluorescence intensity vrs. time. A) Each peak shown represents a droplet moving past the detector. Highly fluorescent peaks indicate the presence of single molecule of AP. B) Enlarged segment of trace above. Blank run is included as a broken line trace.

comparison, a blank run is included (shown as a broken line). The experimental procedure for the blank run was the same, except that no enzyme was included in the reaction solutions.

After the data collection, LabView was used for peak detection and analysis. Peak fluorescence measurements were sorted into a histogram as shown in Figure 3.10. This figure shows the fluorescence distribution of 220 droplets after an incubation period of 2 hrs. As stated above, the concentration of AP in the final solution was 3.3×10^{-15} M, for an expected 1 in 5 occupied droplets ($\nu = 0.2$). As expected, most of the droplets are only weakly fluorescent (due to trace amounts of BBT anion present in the AttoPhos® as impurities and also to the non-enzymatic hydrolysis of AttoPhos®), and clustered between fluorescence values 0f 0.62 and 0.74 RFU. These droplets, in fact, account for 79.45% of the total number of droplets analysed, very close to the 81.78% unoccupied droplets predicted by the Poisson distribution for a target ratio of 1 enzyme molecule per 5 droplets ($\nu = 0.20$). Figure 3.10b, shows the same histogram without the unoccupied droplets. An almost 3-fold difference in magnitude of the measured fluorescence for the droplets containing an AP molecule can be observed. Poisson statistics predict a 1.36% probability of any single droplet containing 2 enzyme molecules (for $\nu=0.2$), meaning that for a population of 220 droplets, only 3.6 double-enzyme droplets should be expected. Since most of the single enzyme droplets are clustered between fluorescence values of 0.98 and 1.20 RFU, it is likely that the droplets between 1.94 and 2.42 RFU represent double enzyme droplets. The rest of the variance in droplet fluorescence must be due to differences in enzymatic activity between individual AP molecules.

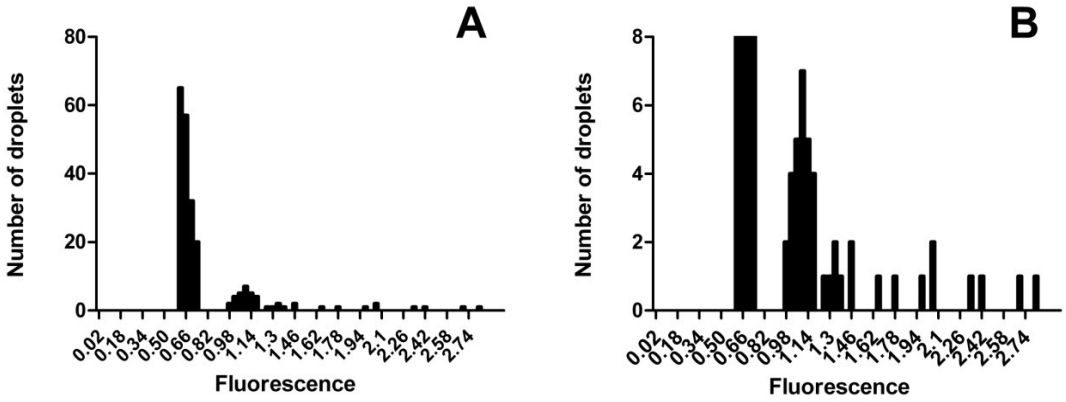

Figure 3.10 Distribution of droplet fluorescence intensities for a single enzyme assay. X axis shows values of fluorescence, while y-axis values reflect the number of droplets at each fluorescence magnitude. A) At a target ratio of 1 in 5 ($\nu = 0.2$), most droplets are empty as can be seen by the large number of weakly fluorescent droplets below 0.78 fluorescence units. B) Shows the same histogram with the unoccupied droplets removed. An almost 3-fold range of fluorescence intensity can be observed.

Next, further single enzyme experiments were carried out at different target ratios to observe if distribution of AP molecules changes as predicted by Poisson statistics and to confirm that the variance in fluorescence measurements is due to differences in single molecule activity. Enzyme solutions to yield occupied to unoccupied ratios of 0.05, 0.10, 0.20 and 0.50 were made and used to generate droplet arrays as detailed in the previous experiments. Droplets were allowed to incubate for 2 hours and then analyzed. Between each single enzyme run, the entire system was rinsed with a KOH and urea solution, followed by a methanol rinse, to avoid carry-over effects. Droplets were rinsed from the capillary at the same flow rate, and fluorescence data was collected and analyzed as before. Droplet fluorescence distributions are shown in Figure 3.11.

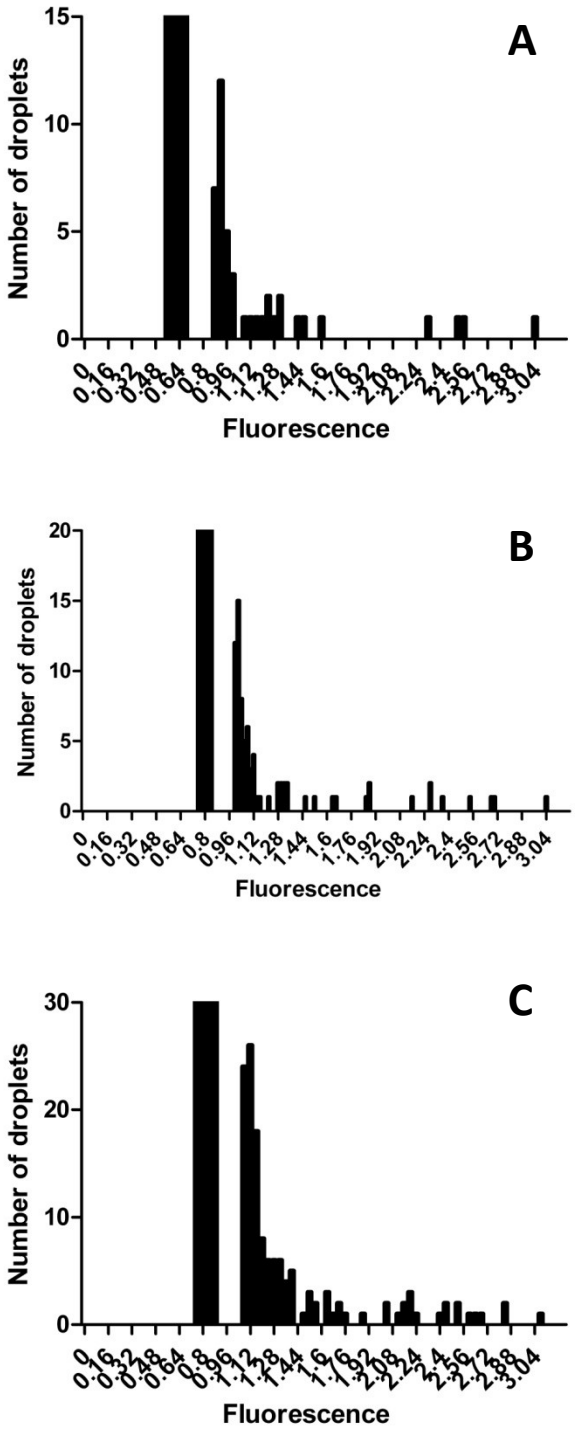

Figure 3.11. Fluorescence intensity distributions for single enzyme experiments at various values of ν. A) ν = 0.05 B) ν= 0.10 C) ν = 0.20. It can be seen that the range of droplet fluorescence remains unchanged as the target occupation rate is decreased down to 0.05. This indicates that the differences in fluorescence observed reflect differences in single enzyme activity, and not just the presence of more than one enzyme molecule in some droplets.

As can be seen, at low enzyme to droplet ratios (0.05 to 0.20) the range of observed fluorescence remains largely invariant at close to 3-fold. This is as expected as even at a ratio of 0.20 AP molecules per droplet and for the number of droplets observed, no droplets containing more than three enzyme molecules are predicted. As the ratio is lowered to 0.10 AP molecules per droplet, the predicted number of doubly occupied droplets (for the observed 956 droplets) is only 4.32. Figure 3.11b, however, shows that at least 11 droplets have a fluorescence intensity higher than 1.66 RFU. This indicates that most of the droplets at the higher fluorescence range cannot be explained by the presence of multiple enzyme molecules and must be due to single enzyme activity heterogeneity. Similarly, at the ratio of 0.05 molecules per droplet, though there are fewer droplets at the higher end of the fluorescence measurement range, the range itself remains unchanged.

In order to confirm that the enzyme molecules are indeed distributed in the droplet arrays as predicted by Poisson statistics, the observed ratio of occupied droplets was plotted against the expected or average ratio, ν. The results are shown in Figure 3.12. From equation 3.1, the probability of a droplet remaining unoccupied ($n = 0$) is equal to $e^{-\nu}$, where ν is the expected fraction of occupied droplets. Figure 3.12 also includes a least squares regression of the data points to a simple exponential decay equation. The equation gives an excellent fit to the data with an R^2 value of 0.96. At very low enzyme concentration (that is, low rates of droplet occupation, ν) this plot is nearly linear as the observed occupied to unoccupied ratio is close to the expected average ratio. At higher droplet occupation rates, however, the two begin deviate as the number of unoccupied

droplets remains higher than ν. Figure 3.8, for example, shows that for a ν of 0.50 (50 % occupied droplets) the number of unoccupied droplets is predicted by the Poisson distribution to be closer to 60%. This trend is also confirmed by experimental observation.

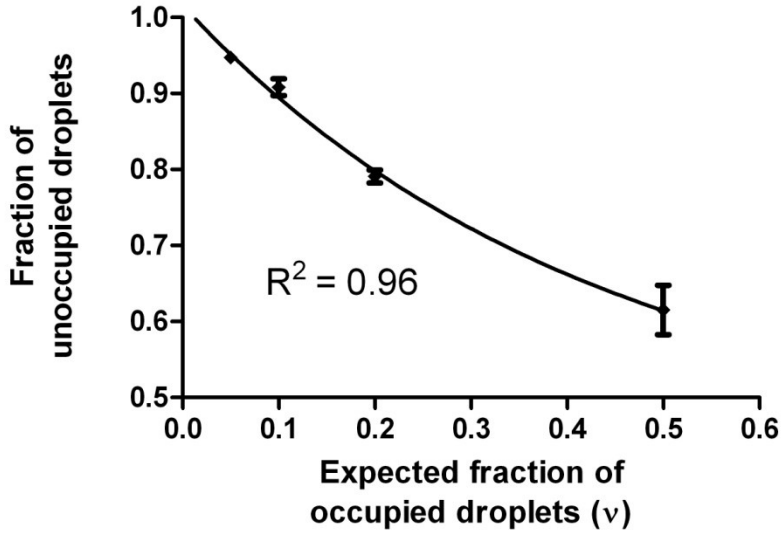

Figure 3.12. Plot of observed droplet occupation rate vrs expected average rate ν. Error bars are for n=3. Solid line represents the least-squares fit of a simple exponential decay equation to the experimental data.

Finally, there was a question as to whether the 2 hour incubation time is adequate to observe the enzyme's full range of activity. It is possible that, for example, very low activity conformations of the enzyme exist which would only be measured on longer incubation periods. If such is not the case, it could then be possible to shorten the incubation time without losing the ability to detect all occupying enzyme molecules. With this in mind, the effect of incubation time on the observed number of enzyme molecules was investigated. Single enzyme molecule assay were performed as described for the previous experiments, using a target occupation rate of 1 in 5 droplets (ν = 0.20). The droplet arrays were allowed to incubate in the tubing for periods of 30, 60, 120 and

240 minutes. Triplicate runs were done for each incubation time. For each run the number of occupied droplets was measured. The results are shown in Figure 3.13.

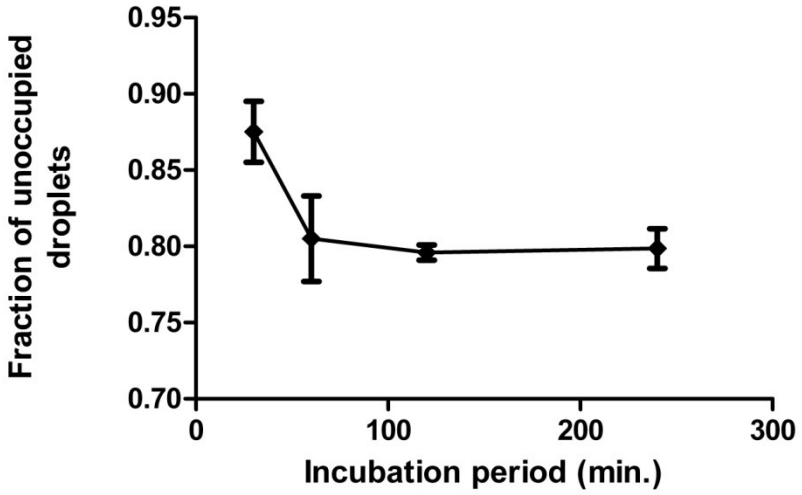

Figure 3.13. Effect of incubation period on number of occupied droplets. For each incubation period, the average of three experiments is shown. For all experiments, expected occupation rate was 1 occupied droplet in 5 ($\nu = 0.20$).

The fraction of unoccupied droplets for the 30 minutes incubation is significantly higher (0.86 ± 0.02) than that for the longer incubation times and the value predicted by Poisson statistics, 0.818. It is clear that incubation period much shorter than 1 hour do not allow enough time for the detection of some of the lower activity AP molecules. For the 60 minute incubation period the average measured unoccupied fraction was 0.81 ± 0.03, not statistically different than the values for 120 minutes (0.796 ± 0.005) and 240 minutes (0.80 ± 0.01). The 60 minute incubation, however, has a larger variance. This is due to lower fluorescence intensity of the enzyme containing droplets, which makes it more difficult to distinguish from the empty droplets. It is also noted that there are no further increases in the number of occupied droplets for the 240 minute incubation. This

indicates that the presence of low activity molecules is unlikely and incubation times longer than 2 hours are unnecessary.

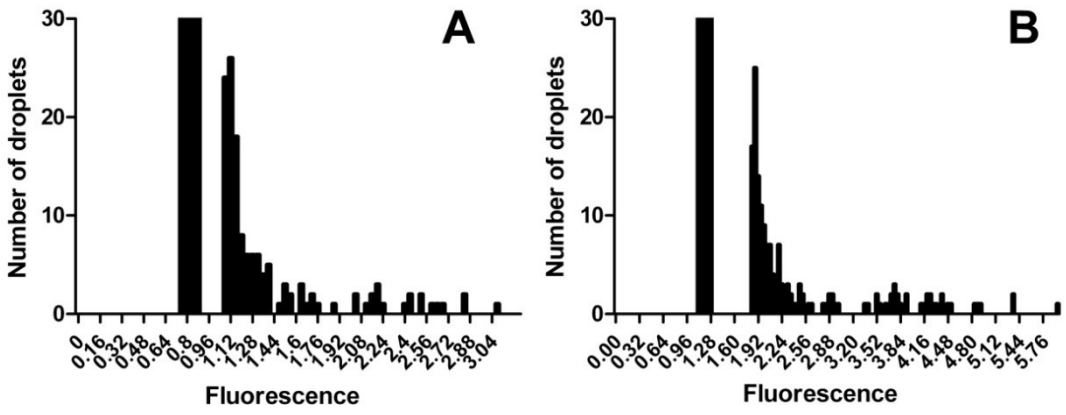

Figure 3.14. Droplet fluorescence distributions at different incubation times. A) 2 hours incubation B) 4 hours incubation.

Figure 3.14 shows fluorescence histograms for incubation times of 2 and 4 hours. A shift in the droplet intensity distribution can be observed in the longer incubation time. As enzyme molecules have more time to generate product, the droplet fluorescence increases along with the range of the distribution. The range of the observed droplet fluorescence increases from 1.08 - 3.08 RFU to 1.84 - 5.96 RFU. Similarly, the median fluorescence for the two distributions increases from 1.16 RFU in the 2 hr incubation to 2.06 RFU in the 4 hr incubation. This is consistent with the presence of activity heterogeneity and not with other possible interpretations such as differences in the rate of enzyme degradation/unfolding.

In conclusion, it has been shown that the proposed segmented flow assay can be used to detect the activity of single enzyme molecules of AP. Single enzyme experiments

were performed with a range of concentration and incubation times. Heterogeneity with respect to activity has been observed. When corrected for the background fluorescence, a 9-fold difference in occupied droplet fluorescence was observed, in agreement with previously reported 10-fold activity differences for single AP molecules[14]. For a 50 cm piece of Teflon tubing, each 2 hour incubation can produce up to 3,000 droplets for analysis. The droplet generation platform here detailed can be assembled in minutes from commercially available parts, without the need for the fabrication of a complex microfluidic device. Such a system could be useful in extending the use of segmented flow assays into areas and research labs where, due to cost or lack of facilities and fabrication experience, they have previously been absent.

Chapter IV. Use of commercial glass treatment for the coating of fused silica capillaries improves separation efficiency of basic proteins in Capillary Electrophoresis

Introduction

Aquapel is available commercially as a water repellant glass treatment for windshields. It consists of a fluorous polymer dissolved in a volatile solvent. The treatment is applied to a glass surface and the solvent is allowed to evaporate, depositing a polymer layer onto the surface. Aquapel has been used in microfluidic applications to render the surface of PDMS channels more hydrophobic for segmented flow applications[195-197]. Due to their low reactivity, fluorous surfactants have been previously used as dynamic coating agents with good results[198-200]. As a fluorous polymer, Aquapel is a good candidate for reducing both electrostatic and lipophilic interactions. However, since the specifics of the composition of Aquapel are proprietary, the nature of the coating's interactions with the silica surface and its effect on EOF are unknown. Ideally, the coating would reduce protein adsorption without entirely suppressing EOF making possible the separation of both basic and acidic proteins. In the present study we have evaluated the suitability of Aquapel as a CE coating, with respect to its effect on EOF and on protein adsorption. The coating can be easily applied simply by rinsing the capillary with the Aquapel solution, without the need for more complicated polymer synthesis or silanization reactions. The effect of pH on the EOF generated by Aquapel coated capillaries was measured. Reduction of analyte adsorption was assessed by monitoring peak efficiencies of three basic proteins. Long term coating stability was also determined by measuring the variance of analyte migration times over repeated injections.

Materials and method

Chemicals and materials.

Aquapel Applicator Pack was purchased from Pittsburgh Glass Works, LLC (Pittsburgh, PA). The applicator consists of a glass vial which must be broken before use. The Aquapel solution was extracted from the vial and placed in a stoppered flask which was stored at 2 °C to prevent solvent evaporation. Lysozyme from chicken egg white, cytochrome c from bovine heart and α-chymotrypsinogen from bovine pancreas were all obtained as lyophilized powder from Sigma Aldrich (St. Louis, MO) and used without further purification. Protein samples were dissolved in water at a concentration of 5 mg/ml. DMSO (Sigma Aldrich, St. Louis, MO) was used as neutral marker in 0.2 % solution with H_2O. pH 4.0 and 5.0 buffers were made with 20 mM sodium acetate. pH 6.0 and 7.0 buffers were made with 20 mM sodium phosphate . As best results were observed when the separation buffer contained a small amount of surfactant, all buffers also contained 10 μM Brijj 35 (This is well below the CMC of 50 to 100 μM[124]). Buffer reagents as well as NaOH and concentrated HCl for pretreatment solutions were also from Sigma Aldrich (St. Louis, MO). All buffers were made in deionized water filtered with a Milli-Q water purification system (Millipore Corp, Bedford, MA).

Coating procedure.

360 μm OD, 75 μm ID fused silica capillaries were purchased from Polymicro Technologies (Molex, Phoenix, AZ). As studies suggest that conditioning of capillaries with HCl and NaOH improve stability of polymer coatings and EOF reproducibility, all

capillaries used were subjected to the following pretreatment[201, 202]: First, a 60 minute 6 M HCl rinse at 16 µl/min, followed by a 30 minute DI H_2O rinse at 16 µl/min. Then, a 60 minute 1 M NaOH rinse at 16 µl/min, followed by a 30 minute DI H_2O rinse at 16 µl/min. The capillaries were purged with N_2 at 40 psi for 10 minutes, then dried overnight at 200 °C. The following day, the capillaries were rinsed with Aquapel at 8 µl/min for 20 min. Next, excess Aquapel was flushed away with N_2 at 20 psi for 10 minutes. Finally, the capillaries were dried at 90 °C for 2 hours. Rinses for capillary pretreatment and coating were done using a syringe pump (Harvard Instruments, Holliston MA).

CE system and separation conditions.

Protein separations and EOF measurements were carried out on a P/ACE MDQ capillary electrophoresis system (Beckman Coulter, Inc. Fullerton, CA). All capillaries used were 40.2 cm total length (30 cm to detector). The detection window on the capillary was made by manually burning away a section of the polyimide coating. Peak migration was monitored by UV at 220 nm. Migration times and separation efficiency were obtained using P/ACE 32 Karat software. Coated and uncoated capillaries were pre-rinsed with separation buffer for 45 minutes at 20 psi before use. A separation voltage of +20 kV was applied during all experiments. Protein samples and neutral marker solutions were injected by pressure at 0.2 psi for 2 seconds. Capillary temperature was maintained at 25 °C.

Results and discussion

Effect of pH on EOF and separation efficiency

In order to determine the effect of the Aquapel coating on EOF, migration times of a neutral marker (0.2% DMSO in water) were measured at pH values of 4.0, 5.0, 6.0 and 7.0. At each pH, three neutral marker injections were averaged to calculate the EOF. To eliminate capillary to capillary variance, all measurements were done on the same capillary. Previous to the injections the capillary was rinsed with pH 4.0 buffer for 45 min at 20 psi. The injections were done at 0.2 psi for 2 seconds and the applied voltage was +20 kV. Between injections the capillary was rinsed for 5 minutes at 20 psi with the pH 4.0 buffer. After three injections, the capillary was rinsed with the pH 5.0 buffer for 10 minutes at 20 psi. The procedure was repeated for the rest of the buffers. As shown in Figure 4.1a, EOF in the coated capillary is reduced but still present with a slight but significant increase from 5.6 ± 0.3 to 8.0 ± 0.2 10^{-9} m^2/Vs. This residual EOF is not unusual for adsorbed polymeric coating and is likely due to incomplete coverage of the surface by the deposited polymer or imperfect shielding of the surface charges. For comparison, Figure 4.1b shows the same plot including measured EOF values for an uncoated capillary at pH values of 4.0 and 7.0. At pH 4.0, EOF in the uncoated capillary is low and only slightly higher than in the coated capillary at 6.1 ± 0.3 10^{-9} m^2/Vs. At pH 7.0, however, there is a more than four-fold difference in EOF magnitude between coated and uncoated capillaries.

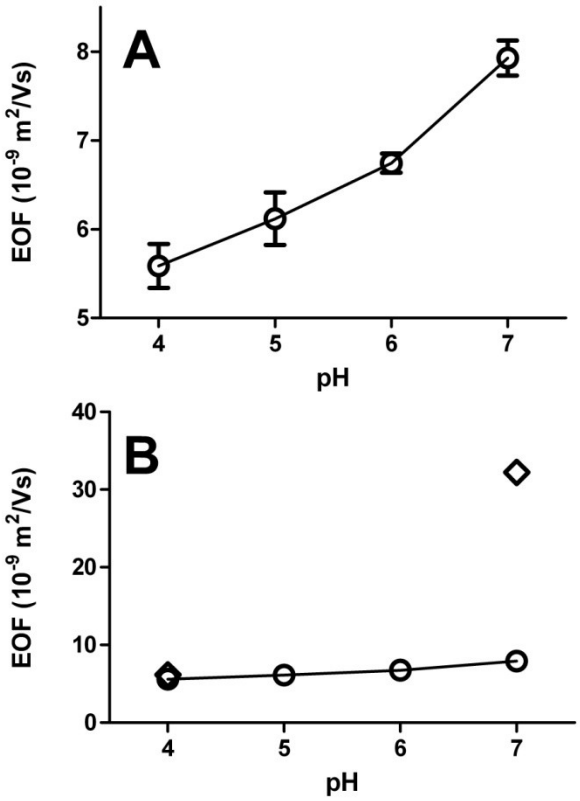

Figure 4.1 EOF measurements. A) Effect of pH on EOF for an Aquapel coated 75 μm I.D. fused silica capillary. 0.5% DMSO in H_20 was used as a neutral marker. pH 4.0 and 5.0 buffers were 20 mM sodium acetate. pH 6.0 and pH 7.0 buffers were 20 mM sodium phosphate. Separation voltage was +20kV. B) Comparison of EOF in coated and uncoated capillaries. The diamonds represent EOF measured at pH values of 4.0 and 7.0 in an uncoated fused silica capillary. The circles are EOF values measured in coated capillary.

To assess the effect of the Aquapel coating on protein adsorption, a set of three basic proteins was chosen. Lysozyme, cytochrome c and α-chymotrypsinogen all have pI values above 9.0 (Table 4.1) and are known to be have low recoveries on bare fused silica capillaries. They have also been used widely as a test

Protein	pI	MW
Lysozyme	11.0	14,000
Cytochrome C	10.2	12,200
α-Chymotrypsinogen	9.2	25,000

Table 4.1. Molecular weights and isoelectric points of proteins used in capillary coating performance experiments.

set for capillary coatings[124-127, 139, 201, 203-208]. Figure 4.2 shows electropherograms comparing the separation of the sample proteins in coated and uncoated capillaries.

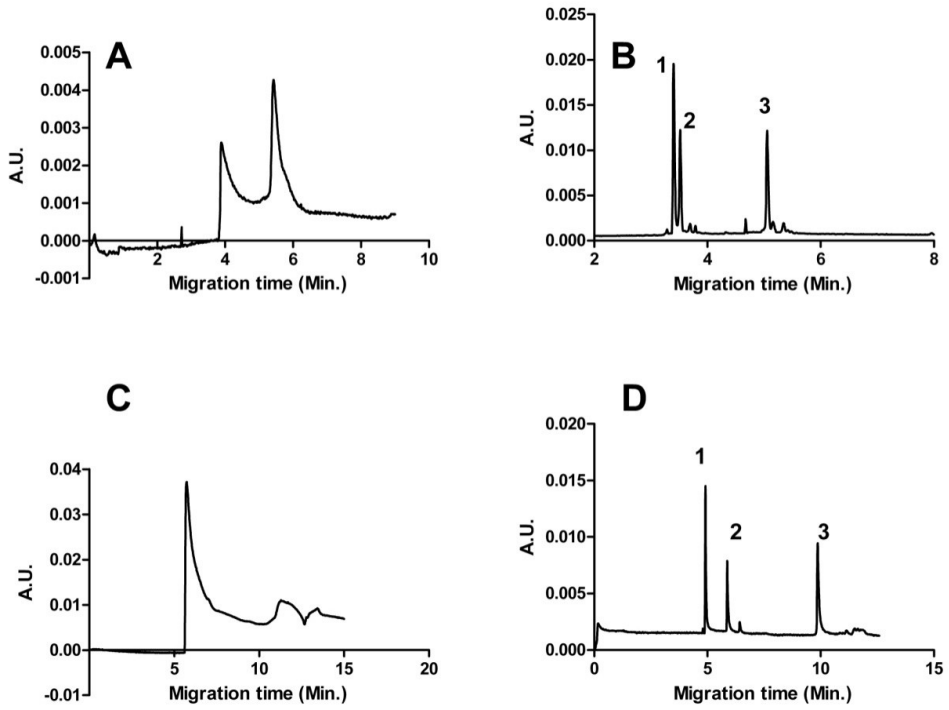

Figure 4.2 Separation of basic proteins on Aquapel coated and bare fused silica capillaries. A) Uncoated 75 µm ID capillary, 20 mM sodium acetate at pH 4.0. B) Coated 75 µm ID capillary, 20 mM sodium acetate at pH 4.0 C) Uncoated 75 µm ID capillary, 20 mM sodium phosphate at pH 7.0. D) Coated 75 µm ID capillary at pH 7.0. Separation voltage for all separations was +20 kV. Protein samples were injected by pressure at 0.2 psi for 2 seconds, for all electropherograms except d for which samples were injected for 6 seconds at 0.5 psi. Sample proteins: 1 = lysozyme, 2 = cytochrome C, 3 = α-chymotrypsinogen. All buffers contained 10 µM Brijj 35.

Figure 4.2a was obtained only after several injections on a bare fused-silica capillary at a separation pH of 4.0, presumably after all surface binding sites had been saturated. Figure 4.2b shows a separation under the same conditions with an Aquapel coated capillary. The Aquapel coating has allowed the separation of three fully resolved peaks in less than 7 minutes. Figure 4.2c shows another separation of the same three proteins on an uncoated capillary, this time at pH 7.0. As in the previous separation using an uncoated capillary at pH 4.0, this electropherogram was only obtained after several

large injections. No useful data can be obtained from this electropherogram, as no components of the protein mixture can be resolved. As can be seen in Figure 4.2d, Aquapel also greatly improves the separation of the basic proteins at pH 7.0. Peak resolution was also improved by changing the pH of the separation buffer from 4.0 to 7.0

As pH is a critical parameter in optimizing protein separations, its effect on peak efficiency was investigated on the Aquapel coated capillary. As with the EOF measurements, protein separations at different pH values were done with a single capillary, starting with pH 4.0. Separation conditions were the same as for the EOF experiments. Peak efficiency values reported are the averages of three injections. Between separations, the capillary was rinsed with run buffer at 20 psi for 5 minutes and for 10 minutes when changing buffers. Cytochrome c and α-chymotrypsinogen show a similar trend of increasing peak efficiency with pH, with the highest theoretical plate counts achieved at pH 6.0 (Figure 4.3). Cytochrome c, however, exhibits the largest change going from the lowest efficiency measured for all proteins of 27,000 ± 7,000 theoretical plates at pH 4.0 to the highest of 130,000 ± 2,000 plates at pH 6.0. Plate counts for lysozyme remain, within error of the measurements, unaffected by pH over the range examined. Except for the lower plate counts measured for cytochrome c at pH 4.0, the three proteins were separated at all pH values with good resolution and good peak efficiency. Separation efficiencies achieved with the Aquapel coating are comparable to those reported for other surfactant and polymeric coatings. For physically adsorbed neutral polymeric coatings, for example, efficiencies for cytochrome c under a variety of separation conditions have been reported in the range between 11,000 and 400,000

theoretical plates[209], with more typical values between 35,000[210] and 200,000 plates[127, 211]. Many of these coatings, however, may be more laborious or require more expensive reagents than coating with Aquapel.

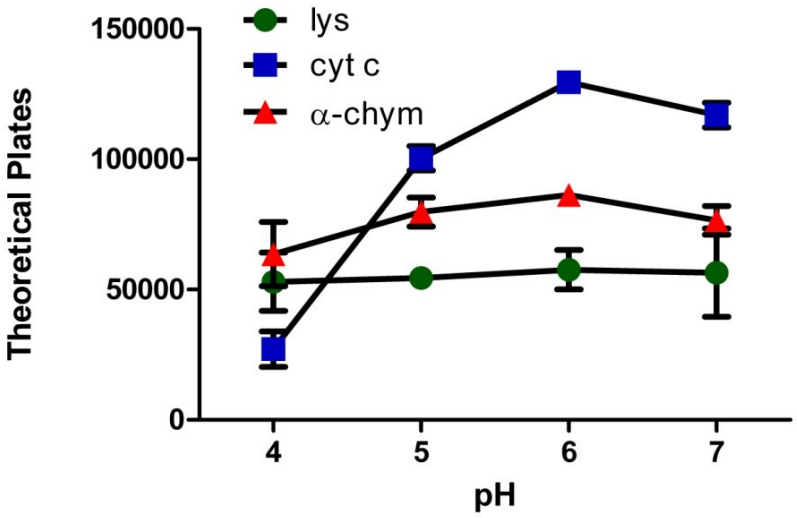

Figure 4.3 Effect of pH on an Aquapel coated capillary. pH 4.0 and 5.0 buffers were 20 mM sodium acetate. pH 6.0 and pH 7.0 buffers were 20 mM sodium phosphate. Separation voltage was +20 kV. Protein samples were injected by pressure at 0.2 psi for 2 seconds.

Coating stability and reproducibility

Having achieved a successful separation of the test protein set, the stability of the coating upon repeated injections was investigated. Since protein adsorption leads to changes in EOF, the reproducibility of analyte migration time is commonly used as a measure of coating stability. A series of 62 injections, with 20 mM sodium phosphate at pH 7.0 as the separation buffer, were performed on the same Aquapel coated capillary over a period of two days. The applied voltage was +20 kV and the protein samples were injected by pressure at 0.2 psi for 2 seconds. The first 34 injections were done overnight on day one over a period of about 14 hours. The following morning, with a two hour pause after the end of the previous sequence, 28 more injections were performed. Over

the 62 injections, the migration times of lysozyme and cytochrome c showed RSD values of 1.5% and 1.8% respectively (Figure 4.4). α-Chymotrypsinogen, however, had higher migration time RSD at 3.4%.

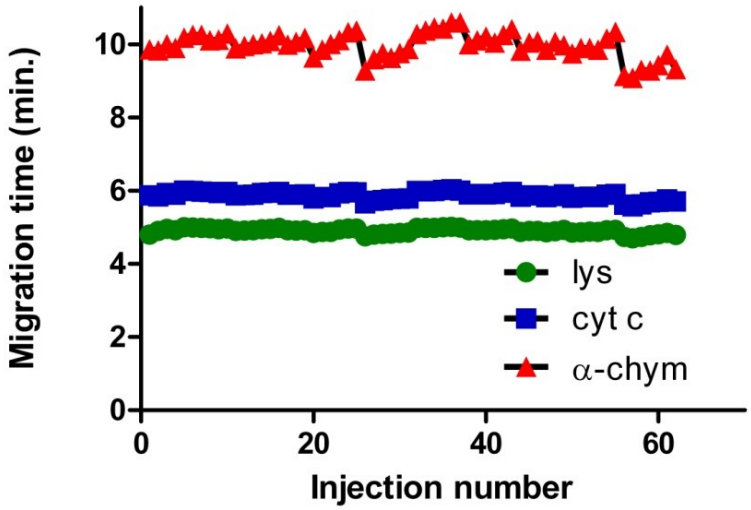

Figure 4.4 Migration time stability over 62 protein injections. Separation buffer was 20 mM sodium acetate at pH 7.0. Separation voltage was +20 kV. Protein samples were injected by pressure at 0.2 psi for 2 seconds**.**

As separation efficiency is another important parameter in evaluating the long term performance of a capillary coating, peak plate counts were also calculated for the three proteins over the 62 injections (Figure 4.5). Separation efficiency was highest during the first 17 injections, during which plate counts for all proteins averaged 81,000 to 92,000 plates. Peak efficiency fell between the 17^{th} and 19^{th} injection for all three proteins and stabilized for the rest of the experiment. The largest change is observed for cytochrome c, which has the highest initial average efficiency (92,000 ± 11,000 plates, n=17) and then the lowest (40,000 ± 8,000 plates, n=45). The other proteins also exhibit similar, but smaller, drops in separation efficiency: 85,000 ± 8,000 plates (n=17) to

56,000 ± 9,000 plates (n=45) for lysozyme and 81,000 ± 7,000 plates (n=17) to 63,000 ± 8,000 plates (n=45) for α-chymotrypsinogen. Though a similar change is not observed in the protein migration times, this decrease in efficiency likely indicates residual protein adsorption. Rinsing the capillary with SDS every few injections could improve the stability of peak efficiency without much of an increase in analysis time.

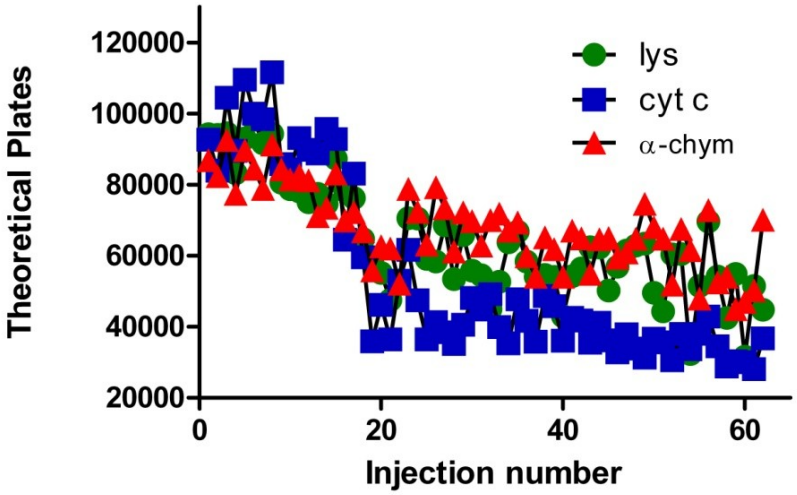

Figure 4.5 Peak efficiency of model proteins over 62 protein injections. Separation buffer was 20 mM sodium acetate at pH 7.0. Separation voltage was +20 kV. Protein samples were injected by pressure at 0.2 psi for 2 seconds.

The reproducibility of migration times in different coated capillaries was also investigated. Using the 20 mM sodium phosphate separation buffer (pH 7.0), three separate injections were performed on three separately coated capillaries. The separation voltage for all runs was +20 kV and protein injections were done hydrodynamically at 0.2 psi for 2 seconds. Run to run reproducibility in each individual capillary was good, less than 3% for all proteins. However, capillary to capillary reproducibility was lower at just over 10% (Table 4.2). A more rigorous control over the coating procedure, such as

keeping a constant time between the drying and Aquapel coating steps could improve coating reproducibility.

	Lysozyme (min)	Cytochrome C (min)	Chymotrypsinogen (min)
Capillary 1	4.76 ± 0.01	5.64 ± 0.01	9.00 ± 0.01
Capillary 2	4.90 ± 0.07	5.87 ± 0.11	9.97 ± 0.34
Capillary 3	5.73 ± 0.1	6.72 ± 0.14	10.82 ± 0.3
Average	5.14	6.08	9.91
RSD	10.10%	6.40%	10.36%

Table 4.2. Run to run and capillary to capillary reproducibility of migration times for model proteins. Migration times for proteins are in minutes.

Conclusions

The commercial glass treatment Aquapel can be used as a capillary coating agent in CE. EOF within the coated capillary is reduced compared to bare silica, but not fully suppressed and so should allow the separation of anionic and neutral species. The remnant EOF is likely due to incomplete surface coverage by the Aquapel coating. Basic proteins have been separated successfully over a pH range of 4.0 to 7.0, with good separation efficiency and reproducibility. The greatest improvements in separation efficiency were observed for pH values 6.0 and 7.0. Further optimization of separation conditions such as buffer type, ionic strength and surfactant concentration could yield even higher plate counts. With only a brief buffer rinse between injections, the Aquapel coating is stable for over 60 injections though with some loss of efficiency over time. Alternative separation protocols, such as rinsing the coated capillary with SDS between injections could improve the performance and lifetime of the coating. Separation

efficiencies for the basic proteins studied are comparable to previously reported values for polymeric and non-polymeric coatings. Aquapel's relative ease of application, availability and low cost makes it a useful addition to the field of capillary coatings.

References

(1) Effenhauser, C. S.; Manz, A.; Widmer, H. M. *Analytical Chemistry* **1993**, *65*, 2637-2642.
(2) Alberts, B. *Molecular biology of the cell*, 4th ed.; Garland Science: New York, 2002.
(3) Berg, J. M.; Tymoczko, J. L.; Stryer, L. *Biochemistry*, 5th ed.; W.H. Freeman: New York, 2002.
(4) Doyle, D. A.; Cabral, J. M.; Pfuetzner, R. A.; Kuo, A. L.; Gulbis, J. M.; Cohen, S. L.; Chait, B. T.; MacKinnon, R. *Science* **1998**, *280*, 69-77.
(5) Gilman, A. G. *Annual Review of Biochemistry* **1987**, *56*, 615-649.
(6) Anderson, N. L.; Anderson, N. G. *Electrophoresis* **1998**, *19*, 1853-1861.
(7) Blackstock, W. P.; Weir, M. P. *Trends in Biotechnology* **1999**, *17*, 121-127.
(8) JAMES, P. *Quarterly Reviews of Biophysics* **1997**, *30*, 279-331.
(9) Turner, A. J.; Hooper, N. M. *Trends in Pharmacological Sciences* **2002**, *23*, 177-183.
(10) van der Weide, J.; Steijns, L. S. W. *Annals of Clinical Biochemistry* **1999**, *36*, 722-729.
(11) Antoon, J. W.; White, M. D.; Burow, M. E.; Beckman, B. S. *Oncology Reports* **2012**, *27*, 1779-1786.
(12) Yan, G. W.; Chen, Y.; Li, Y. X.; Chen, H. F. *Chemical Biology & Drug Design* **2012**, *79*, 916-925.
(13) Buroni, S.; Pasca, M. R.; Ribeiro, A. L. D. L.; Degiacomi, G.; Molteni, E.; Riccardi, G. *Applied Microbiology and Biotechnology* **2012**, *94*, 907-916.
(14) Craig, D. B.; Arriaga, E. A.; Wong, J. C. Y.; Lu, H.; Dovichi, N. J. *Journal of the American Chemical Society* **1996**, *118*, 5245-5253.
(15) Xue, Q. F.; Yeung, E. S. *Nature* **1995**, *373*, 681-683.
(16) Whitesides, G. M. *Nature* **2006**, *442*, 368-373.
(17) *Advanced Science Letters*, *4*, 150-155.
(18) McDonald, J. C.; Duffy, D. C.; Anderson, J. R.; Chiu, D. T.; Wu, H. K.; Schueller, O. J. A.; Whitesides, G. M. *Electrophoresis* **2000**, *21*, 27-40.
(19) Kovacs, G. T. A.; Petersen, K.; Albin, M. *Analytical Chemistry* **1996**, *68*, 407A-412A.
(20) Petersen, K. E. *Proceedings of the IEEE* **1982**, *70*, 420-457.
(21) Herold, K. E.; Rasooly, A. *Lab on a chip technology*; Caister Academic Press: Norfolk, UK, 2009.
(22) Manz, A.; Miyahara, Y.; Miura, J.; Watanabe, Y.; Miyagi, H.; Sato, K. *Sensors and Actuators B: Chemical* **1990**, *1*, 249-255.
(23) Woolley, A. T.; Lao, K. Q.; Glazer, A. N.; Mathies, R. A. *Analytical Chemistry* **1998**, *70*, 684-688.
(24) Harrison, D. J.; Fluri, K.; Seiler, K.; Fan, Z. H.; Effenhauser, C. S.; Manz, A. *Science* **1993**, *261*, 895-897.

(25) Yao, S.; Anex, D. S.; Caldwell, W. B.; Arnold, D. W.; Smith, K. B.; Schultz, P. G. *Proceedings of the National Academy of Sciences of the United States of America* **1999**, *96*, 5372-5377.
(26) Woolley, A. T.; Hadley, D.; Landre, P.; deMello, A. J.; Mathies, R. A.; Northrup, M. A. *Analytical Chemistry* **1996**, *68*, 4081-4086.
(27) Waters, L. C.; Jacobson, S. C.; Kroutchinina, N.; Khandurina, J.; Foote, R. S.; Ramsey, J. M. *Analytical Chemistry* **1998**, *70*, 5172-5176.
(28) Woolley, A. T.; Mathies, R. A. *Analytical Chemistry* **1995**, *67*, 3676-3680.
(29) Burns, M. A.; Mastrangelo, C. H.; Sammarco, T. S.; Man, F. P.; Webster, J. R.; Johnson, B. N.; Foerster, B.; Jones, D.; Fields, Y.; Kaiser, A. R.; Burke, D. T. *Proceedings of the National Academy of Sciences of the United States of America* **1996**, *93*, 5556-5561.
(30) Simpson, P. C.; Roach, D.; Woolley, A. T.; Thorsen, T.; Johnston, R.; Sensabaugh, G. F.; Mathies, R. A. *Proceedings of the National Academy of Sciences* **1998**, *95*, 2256-2261.
(31) Hadd, A. G.; Raymond, D. E.; Halliwell, J. W.; Jacobson, S. C.; Ramsey, J. M. *Analytical Chemistry* **1997**, *69*, 3407-3412.
(32) Becker, H.; Gärtner, C. *Electrophoresis* **2000**, *21*, 12-26.
(33) Xia, Y. N.; Whitesides, G. M. *Annual Review of Materials Science* **1998**, *28*, 153-184.
(34) McDonald, J. C.; Whitesides, G. M. *Accounts of Chemical Research* **2002**, *35*, 491-499.
(35) Effenhauser, C. S.; Bruin, G. J. M.; Paulus, A.; Ehrat, M. *Analytical Chemistry* **1997**, *69*, 3451-3457.
(36) Sanders, G. H. W.; Manz, A. *TrAC Trends in Analytical Chemistry* **2000**, *19*, 364-378.
(37) Khandurina, J.; Guttman, A. *Journal of Chromatography A* **2002**, *943*, 159-183.
(38) Dittrich, P. S.; Manz, A. *Nature Reviews Drug Discovery* **2006**, *5*, 210-218.
(39) Watts, P.; Haswell, S. J. *Current Opinion in Chemical Biology* **2003**, *7*, 380-387.
(40) Kobayashi, J.; Mori, Y.; Okamoto, K.; Akiyama, R.; Ueno, M.; Kitamori, T.; Kobayashi, S. *Science* **2004**, *304*, 1305-1308.
(41) Marcy, Y.; Ishoey, T.; Lasken, R. S.; Stockwell, T. B.; Walenz, B. P.; Halpern, A. L.; Beeson, K. Y.; Goldberg, S. M. D.; Quake, S. R. *PLoS Genet* **2007**, *3*, e155.
(42) Nagaki, A.; Kawamura, K.; Suga, S.; Ando, T.; Sawamoto, M.; Yoshida, J.-i. *Journal of the American Chemical Society* **2004**, *126*, 14702-14703.
(43) Hansen, C. L.; Skordalakes, E.; Berger, J. M.; Quake, S. R. *Proceedings of the National Academy of Sciences of the United States of America* **2002**, *99*, 16531-16536.
(44) Clark, R. A.; Hietpas, P. B.; Ewing, A. G. *Analytical Chemistry* **1997**, *69*, 259-263.
(45) Weibel, D. B.; DiLuzio, W. R.; Whitesides, G. M. *Nature Reviews Microbiology* **2007**, *5*, 209-218.
(46) Nagai, H.; Murakami, Y.; Yokoyama, K.; Tamiya, E. *Biosensors and Bioelectronics* **2001**, *16*, 1015-1019.

(47) Ali, M. F.; Kirby, R.; Goodey, A. P.; Rodriguez, M. D.; Ellington, A. D.; Neikirk, D. P.; McDevitt, J. T. *Analytical Chemistry* **2003**, *75*, 4732-4739.
(48) Rondelez, Y.; Tresset, G.; Tabata, K. V.; Arata, H.; Fujita, H.; Takeuchi, S.; Noji, H. *Nature Biotechnology* **2005**, *23*, 361-365.
(49) Zheng, B.; Ismagilov, R. F. *Angewandte Chemie* **2005**, *117*, 2576-2579.
(50) Zheng, B.; Roach, L. S.; Ismagilov, R. F. *Journal of the American Chemical Society* **2003**, *125*, 11170-11171.
(51) Shestopalov, I.; Tice, J. D.; Ismagilov, R. F. *Lab on a Chip* **2004**, *4*, 316-321.
(52) Roach, L. S.; Song, H.; Ismagilov, R. F. *Analytical Chemistry* **2004**, *77*, 785-796.
(53) Chiu, D. *Analytical and Bioanalytical Chemistry*, *397*, 3179-3183.
(54) Garstecki, P.; Gitlin, I.; DiLuzio, W.; Whitesides, G. M.; Kumacheva, E.; Stone, H. A. *Applied Physics Letters* **2004**, *85*, 2649-2651.
(55) Anna, S. L.; Bontoux, N.; Stone, H. A. *Applied Physics Letters* **2003**, *82*, 364-366.
(56) Xu, Q. Y.; Nakajima, M. *Applied Physics Letters* **2004**, *85*, 3726-3728.
(57) Thorsen, T.; Roberts, R. W.; Arnold, F. H.; Quake, S. R. *Physical Review Letters* **2001**, *86*, 4163-4166.
(58) Song, H.; Tice, J. D.; Ismagilov, R. F. *Angewandte Chemie-International Edition* **2003**, *42*, 768-772.
(59) Garstecki, P.; Fuerstman, M. J.; Stone, H. A.; Whitesides, G. M. *Lab on a Chip* **2006**, *6*, 437-446.
(60) De Menech, M.; Garstecki, P.; Jousse, F.; Stone, H. A. *Journal of Fluid Mechanics* **2008**, *595*, 141-161.
(61) Schneider, T.; Burnham, D. R.; VanOrden, J.; Chiu, D. T. *Lab on a Chip*.
(62) van Steijn, V.; Kleijn, C. R.; Kreutzer, M. T. *Lab on a Chip* **2010**, *10*, 2513-2518.
(63) Ward, T.; Faivre, M.; Abkarian, M.; Stone, H. A. *Electrophoresis* **2005**, *26*, 3716-3724.
(64) Koshland, D. E., Jr. *J Cell Physiol Suppl* **1956**, *47*, 217-234.
(65) Albery, W. J.; Knowles, J. R. *Biochemistry* **1976**, *15*, 5631-5640.
(66) Pocker, Y.; Janjic, N. *Biochemistry* **1987**, *26*, 2597-2606.
(67) Goli, U. B.; Galardy, R. E. *Biochemistry* **1986**, *25*, 7136-7142.
(68) Chang, C. F.; Ho, C. W.; Wu, C. Y.; Chao, T. A.; Wong, C. H.; Lin, C. H. *Chemistry & Biology* **2004**, *11*, 1301-1306.
(69) Lee, J. H.; An, C. S.; Yun, B. S.; Kang, K. S.; Lee, Y. A.; Won, S. M.; Gwag, B. J.; Cho, S. I.; Hahm, K. B. *Eur. J. Pharmacol.*, *687*, 28-38.
(70) Schiemann, S.; Luhn, S.; Alban, S. *Analytical Biochemistry*, *427*, 82-90.
(71) Gajda, A. D.; Pawelczak, M.; Drag, M. *Plant Physiol. Biochem.*, *54*, 6-9.
(72) Mafakheri, A.; Siosemardeh, A.; Bahramnejad, B.; Struik, P. C.; Sohrabi, Y. *Aust. J. Crop Sci.*, *5*, 1255-1260.
(73) La Torre, G. L.; Lagan 胨, G.; Bellocco, E.; Vilasi, F.; Salvo, F.; Dugo, G. *Food Chemistry* **2004**, *85*, 259-266.
(74) Jin, J.; Mazon, H.; van den Heuvel, R. H. H.; Janssen, D. B.; Fraaije, M. W. *Febs Journal* **2007**, *274*, 2311-2321.
(75) Feijoo-Siota, L.; Villa, T. G. *Food Bioprocess Technol.*, *4*, 1066-1088.
(76) Khoufi, S.; Hamza, M.; Sayadi, S. *Bioresource Technology*, *102*, 9050-9058.

(77) Damasceno, F. R. C.; Cammarota, M. C.; Freire, D. M. G. *Colloid Surf. B-Biointerfaces*, *95*, 241-246.
(78) Sun, Y.; Cheng, J. *Bioresource Technology* **2002**, *83*, 1-11.
(79) Yin, D.; Jing, Q.; AlDajani, W. W.; Duncan, S.; Tschirner, U.; Schilling, J.; Kazlauskas, R. J. *Bioresource Technology*, *102*, 5183-5192.
(80) Rotman, B. *Proceedings of the National Academy of Sciences* **1961**, *47*, 1981-1991.
(81) Rotman, B.; Zderic, J. A.; Edelstein, M. *Proceedings of the National Academy of Sciences* **1963**, *50*, 1-6.
(82) Huang, Z. J. *Biochemistry* **1991**, *30*, 8535-8540.
(83) Hofmann, J.; Sernetz, M. *Analytical Biochemistry* **1983**, *131*, 180-186.
(84) Polakowski, R.; Craig, D. B.; Skelley, A.; Dovichi, N. J. *Journal of the American Chemical Society* **2000**, *122*, 4853-4855.
(85) Craig, D. B.; Dovichi, N. J. *Canadian Journal of Chemistry-Revue Canadienne De Chimie* **1998**, *76*, 623-626.
(86) Rissin, D. M.; Gorris, H. H.; Walt, D. R. *Journal of the American Chemical Society* **2008**, *130*, 5349-5353.
(87) Gorris, H. H.; Walt, D. R. *Journal of the American Chemical Society* **2009**, *131*, 6277-6282.
(88) Chen, A. Y.; Jani, A. S.; Zheng, L.; Burke, P. J.; Brody, J. P. *Biotechnology Progress* **2009**, *25*, 929-937.
(89) Craig, D. B.; Hall, T. *Journal of Clinical Laser Medicine & Surgery* **2000**, *18*, 209-213.
(90) Craig, D. B.; Nachtigall, J. T.; Ash, H. L.; Shoemaker, G. K.; Dyck, A. C.; Wawrykow, T. M. J.; Gudbjartson, H. L. *Journal of Protein Chemistry* **2003**, *22*, 555-561.
(91) Craig, D. B. *Protein Journal* **2010**, *29*, 55-61.
(92) Nichols, E. R.; Craig, D. B. *Protein Journal* **2008**, *27*, 376-383.
(93) Shoemaker, G. K.; Juers, D. H.; Coombs, J. M. L.; Matthews, B. W.; Craig, D. B. *Biochemistry* **2003**, *42*, 1707-1710.
(94) Nichols, E. R.; Gavina, J. M. A.; McLeod, R. G.; Craig, D. B. *Protein Journal* **2007**, *26*, 95-105.
(95) Craig, D. B.; Haslam, A. M.; Silverstein, H. J.; Chikamatsu, M.; Shadabi, E.; Nichols, E. R. *Protein Journal* **2010**, *29*, 398-406.
(96) Nichols, E. R.; Shadabi, E.; Craig, D. B. *Biochemistry and Cell Biology-Biochimie Et Biologie Cellulaire* **2009**, *87*, 517-529.
(97) Craig, D. B.; Haslam, A. M.; Coombs, J. M. L.; Nichols, E. R. *Biochemistry and Cell Biology-Biochimie Et Biologie Cellulaire* **2010**, *88*, 451-458.
(98) Craig, D. B.; Nichols, E. R. *Electrophoresis* **2008**, *29*, 4298-4303.
(99) Nichols, E. R.; Craig, D. B. *Electrophoresis* **2008**, *29*, 4257-4269.
(100) Tan, W. H.; Yeung, E. S. *Analytical Chemistry* **1997**, *69*, 4242-4248.
(101) Rissin, D. M.; Walt, D. R. *Nano Letters* **2006**, *6*, 520-523.
(102) Rissin, D. M.; Walt, D. R. *Journal of the American Chemical Society* **2006**, *128*, 6286-6287.

(103) Rissin, D. M.; Kan, C. W.; Campbell, T. G.; Howes, S. C.; Fournier, D. R.; Song, L.; Piech, T.; Patel, P. P.; Chang, L.; Rivnak, A. J.; Ferrell, E. P.; Randall, J. D.; Provuncher, G. K.; Walt, D. R.; Duffy, D. C. *Nature Biotechnology* **2010**, *28*, 595-U525.
(104) Sakakihara, S.; Araki, S.; Iino, R.; Noji, H. *Lab on a Chip* **2010**, *10*, 3355-3362.
(105) Tiselius, A. *Transactions of the Faraday Society* **1937**, *33*, 524-531.
(106) Gordon, M. J.; Huang, X. H.; Pentoney, S. L.; Zare, R. N. *Science* **1988**, *242*, 224-228.
(107) Mikkers, F. E. P.; Everaerts, F. M.; Verheggen, T. P. E. M. *Journal of Chromatography* **1979**, *169*, 11-20.
(108) Jorgenson, J. W.; Lukacs, K. D. *Analytical Chemistry* **1981**, *53*, 1298-1302.
(109) Heiger, D. N. *High performance capillary electrophoresis : an introduction*, 2nd ed.; Hewlett Packard Co.: [France?], 1992.
(110) Berli, C. L. A.; Piaggio, M. V.; Deiber, J. A. *Electrophoresis* **2003**, *24*, 1587-1595.
(111) Pretorius, V.; Hopkins, B. J.; Schieke, J. D. *Journal of Chromatography A* **1974**, *99*, 23-30.
(112) Hiemenz, P. C. *Principles of colloid and surface chemistry*, 3rd ed., rev. and expanded / ed.; Marcel Dekker: New York, 1997.
(113) Lukacs, K. D.; Jorgenson, J. W. *Journal of High Resolution Chromatography & Chromatography Communications* **1985**, *8*, 407-411.
(114) Huang, X. H.; Coleman, W. F.; Zare, R. N. *Journal of Chromatography* **1989**, *480*, 95-110.
(115) Jorgenson, J. W.; Lukacs, K. D. *Clinical Chemistry* **1981**, *27*, 1551-1553.
(116) Monton, M. R. N.; Soga, T. *Journal of Chromatography A* **2007**, *1168*, 237-246.
(117) Volpi, N.; Maccari, F. *Journal of Chromatography B-Analytical Technologies in the Biomedical and Life Sciences* **2006**, *834*, 1-13.
(118) Song, L. G.; Liang, D. H.; Fang, D. F.; Chu, B. *Electrophoresis* **2001**, *22*, 1987-1996.
(119) Dovichi, N. J. *Electrophoresis* **1997**, *18*, 2393-2399.
(120) Shen, Y. F.; Smith, R. D. *Electrophoresis* **2002**, *23*, 3106-3124.
(121) Song, E. J.; Babar, S. M. E.; Oh, E.; Hasan, M. N.; Hong, H. M.; Yoo, Y. S. *Electrophoresis* **2008**, *29*, 129-142.
(122) Bonvent, J. J.; Barberi, R.; Bartolino, R.; Capelli, L.; Righetti, P. G. *Journal of Chromatography A* **1996**, *756*, 233-243.
(123) Stutz, H. *Electrophoresis* **2009**, *30*, 2032-2061.
(124) Towns, J. K.; Regnier, F. E. *Analytical Chemistry* **1991**, *63*, 1126-1132.
(125) Cifuentes, A.; Santos, J. M.; Defrutos, M.; Diezmasa, J. C. *Journal of Chromatography A* **1993**, *652*, 161-170.
(126) Towns, J. K.; Regnier, F. E. *Analytical Chemistry* **1992**, *64*, 2473-2478.
(127) Lucy, C. A.; MacDonald, A. M.; Gulcev, M. D. *Journal of Chromatography A* **2008**, *1184*, 81-105.
(128) Mccormick, R. M. *Analytical Chemistry* **1988**, *60*, 2322-2328.
(129) Lauer, H. H.; Mcmanigill, D. *Analytical Chemistry* **1986**, *58*, 166-170.
(130) Green, J. S.; Jorgenson, J. W. *Journal of Chromatography* **1989**, *478*, 63-70.

(131) Doherty, E. A. S.; Meagher, R. J.; Albarghouthi, M. N.; Barron, A. E. *Electrophoresis* **2003**, *24*, 34-54.
(132) Jorgenson, J. W.; Lukacs, K. D. *Science* **1983**, *222*, 266-272.
(133) Hjerten, S. *Journal of Chromatography* **1985**, *347*, 191-198.
(134) Schmalzing, D.; Piggee, C. A.; Foret, F.; Carrilho, E.; Karger, B. L. *Journal of Chromatography A* **1993**, *652*, 149-159.
(135) Gelfi, C.; Curcio, M.; Righetti, P. G.; Sebastiano, R.; Citterio, A.; Ahmadzadeh, H.; Dovichi, N. J. *Electrophoresis* **1998**, *19*, 1677-1682.
(136) Righetti, P. G.; Gelfi, C.; Sebastiano, R.; Citterio, A. *Journal of Chromatography A* **2004**, *1053*, 15-26.
(137) Cifuentes, A.; Rodriguez, M. A.; GarciaMontelongo, F. J. *Journal of Chromatography A* **1996**, *742*, 257-266.
(138) Yao, Y. J.; Li, S. F. Y. *Journal of Chromatography A* **1994**, *663*, 97-104.
(139) Iki, N.; Yeung, E. S. *Journal of Chromatography A* **1996**, *731*, 273-282.
(140) Preisler, J.; Yeung, E. S. *Analytical Chemistry* **1996**, *68*, 2885-2889.
(141) Erim, F. B.; Cifuentes, A.; Poppe, H.; Kraak, J. C. *Journal of Chromatography A* **1995**, *708*, 356-361.
(142) He, Y.; Wei, Y. M.; Zheng, X. H.; Zheng, J. B. *Electrophoresis* **2010**, *31*, 630-633.
(143) Hardenborg, E.; Zuberovic, A.; Ullsten, S.; Soderberg, L.; Heldin, E.; Markides, K. E. *Journal of Chromatography A* **2003**, *1003*, 217-221.
(144) Boonyakong, C.; Tucker, S. A. *Journal of Separation Science* **2009**, *32*, 3489-3496.
(145) Wang, M.; Roman, G. T.; Perry, M. L.; Kennedy, R. T. *Analytical Chemistry* **2009**, *81*, 9072-9078.
(146) Wang, M.; Slaney, T.; Mabrouk, O.; Kennedy, R. T. *Journal of Neuroscience Methods* **2010**, *190*, 39-48.
(147) Bringer, M. R.; Gerdts, C. J.; Song, H.; Tice, J. D.; Ismagilov, R. F. *Philosophical Transactions of the Royal Society of London Series a-Mathematical Physical and Engineering Sciences* **2004**, *362*, 1087-1104.
(148) Song, H.; Bringer, M. R.; Tice, J. D.; Gerdts, C. J.; Ismagilov, R. F. *Applied Physics Letters* **2003**, *83*, 4664-4666.
(149) Kline, T. R.; Runyon, M. K.; Pothiawala, M.; Ismagilov, R. F. *Analytical Chemistry* **2008**, *80*, 6190-6197.
(150) Vincent, M. E.; Liu, W.; Haney, E. B.; Ismagilov, R. F. *Chem Soc Rev*, *39*, 974-984.
(151) Boedicker, J. Q.; Li, L.; Kline, T. R.; Ismagilov, R. F. *Lab Chip* **2008**, *8*, 1265-1272.
(152) Huebner, A.; Olguin, L. F.; Bratton, D.; Whyte, G.; Huck, W. T.; de Mello, A. J.; Edel, J. B.; Abell, C.; Hollfelder, F. *Anal Chem* **2008**, *80*, 3890-3896.
(153) Thorsen, T.; Maerkl, S. J.; Quake, S. R. *Science* **2002**, *298*, 580-584.
(154) Schmitz, C. H.; Rowat, A. C.; Koster, S.; Weitz, D. A. *Lab Chip* **2009**, *9*, 44-49.
(155) Curcio, M.; Roeraade, J. *Analytical Chemistry* **2002**, *75*, 1-7.
(156) Lucy, C. A.; Yeung, K. K. C. *Analytical Chemistry* **1994**, *66*, 2220-2225.

(157) Trivedi, V.; Doshi, A.; Kurup, G. K.; Ereifej, E.; Vandevord, P. J.; Basu, A. S. *Lab on a Chip* **2010**, *10*, 2433-2442.
(158) Nishikido, N.; Mahler, W.; Mukerjee, P. *Langmuir* **1989**, *5*, 227-229.
(159) McComb, R. B.; Bowers, G. N.; Posen, S. *Alkaline phosphatase*; Plenum Press: New York, 1979.
(160) Kim, E. E.; Wyckoff, H. W. *Clinica Chimica Acta* **1990**, *186*, 175-187.
(161) Kim, E. E.; Wyckoff, H. W. *Journal of Molecular Biology* **1991**, *218*, 449-464.
(162) Wilcox, D. E. *Chemical Reviews* **1996**, *96*, 2435-2458.
(163) Crawford, K.; Weissig, H.; Binette, F.; Millan, J. L.; Goetinck, P. F. *Developmental Dynamics* **1995**, *204*, 48-56.
(164) Millan, J. L. *Purinergic Signal* **2006**, *2*, 335-341.
(165) Poelstra, K.; Bakker, W. W.; Klok, P. A.; Kamps, J. A. A. M.; Hardonk, M. J.; Meijer, D. K. F. *American Journal of Pathology* **1997**, *151*, 1163-1169.
(166) Poelstra, K.; Bakker, W. W.; Klok, P. A.; Hardonk, M. J.; Meijer, D. K. F. *Laboratory Investigation* **1997**, *76*, 319-327.
(167) Poelstra, K.; Bakker, W. W.; Hardonk, M. J.; Meijer, D. K. F. *Hepatology* **1996**, *24*, 802-802.
(168) Chen, K. T.; Malo, M. S.; Beasley-Topliffe, L. K.; Poelstra, K.; Millan, J. L.; Mostafa, G.; Alam, S. N.; Ramasamy, S.; Warren, H. S.; Hohmann, E. L.; Hodin, R. A. *Digestive Diseases and Sciences* **2011**, *56*, 1020-1027.
(169) Tuin, A.; Poelstra, K.; de Jager-Krikken, A.; Bok, L.; Raaben, W.; Velders, M. P.; Dijkstra, G. *Gut* **2009**, *58*, 379-387.
(170) Tuin, A.; de Jager-Krikken, A.; Bok, L.; Raaben, W.; Velders, M. P.; Meijer, D. K. F.; Poelstra, K.; Dijkstra, G. *European Journal of Gastroenterology & Hepatology* **2008**, *20*, A35-A36.
(171) Tuin, A.; De Jager-Krikken, A.; Bok, L.; Willem, R.; Velders, M. P.; Meijer, D. K.; Poelstra, K.; Dijkstra, G. *Gastroenterology* **2007**, *132*, A231-A231.
(172) Tuin, A.; Huizinga-van der Vlag, A.; van Loenen-Weemaes, A. M.; Verweij, W. R.; Olinga, P.; Meijer, D. K.; Poelstra, K. *Hepatology* **2004**, *40*, 701a-701a.
(173) Horiuchi, T.; Horiuchi, S.; Mizuno, D. *Nature* **1959**, *183*, 1529-1530.
(174) Annamaria, T. *Biochimica Et Biophysica Acta* **1960**, *38*, 460-469.
(175) AMMERMAN, J. W.; AZAM, F. *Science* **1985**, *227*, 1338-1340.
(176) Dhaked, R. K.; Alam, S. I.; Dixit, A.; Singh, L. *Enzyme and Microbial Technology* **2005**, *36*, 855-861.
(177) O'Brien, P. J.; Herschlag, D. *Biochemistry* **2002**, *41*, 3207-3225.
(178) Hehir, M. J.; Murphy, J. E.; Kantrowitz, E. R. *Journal of Molecular Biology* **2000**, *304*, 645-656.
(179) Mangani, S.; Carloni, P.; Viezzoli, M. S.; Coleman, J. E. *Inorganica Chimica Acta* **1992**, *191*, 161-165.
(180) Benez, A.; Geiselhart, A.; Handgretinger, R.; Schiebel, U.; Fierlbeck, G. *Journal of Clinical Laboratory Analysis* **1999**, *13*, 229-233.
(181) Inouye, K.; Ueno, I.; Yokoyama, S.; Sakaki, T. *Journal of Biochemistry* **2002**, *131*, 97-105.

(182) Martin, K.; Hart, C.; Liu, J. X.; Leung, W. Y.; Patton, W. F. *Proteomics* **2003**, *3*, 1215-1227.
(183) Han, Z. Z.; Karatan, E.; Scholle, M. D.; McCafferty, J.; Kay, B. K. *Combinatorial Chemistry & High Throughput Screening* **2004**, *7*, 55-62.
(184) Ruan, C. M.; Wang, W.; Gu, B. H. *Analytical Chemistry* **2006**, *78*, 3379-3384.
(185) Kaatz, M.; Schulze, H.; Ciani, I.; Lisdat, F.; Mount, A. R.; Bachmann, T. T. *Analyst* **2012**, *137*, 59-63.
(186) Nistor, C.; Emneus, J. *Analytical Communications* **1998**, *35*, 417-419.
(187) Stinson, R. A. *Clinical Chemistry* **1993**, *39*, 2293-2297.
(188) Craig, D. B.; Wong, J. C. Y.; Dovichi, N. J. *Analytical Chemistry* **1996**, *68*, 697-700.
(189) Ito, S.; Yamazaki, S.; Kano, K.; Ikeda, T. *Analytica Chimica Acta* **2000**, *424*, 57-63.
(190) Sun, X. M.; Gao, N.; Jin, W. R. *Analytica Chimica Acta* **2006**, *571*, 30-33.
(191) Bronstein, I.; Martin, C. S.; Fortin, J. J.; Olesen, C. E. M.; Voyta, J. C. *Clinical Chemistry* **1996**, *42*, 1542-1546.
(192) Sergienko, E. A.; Millan, J. L. *Nature Protocols*, *5*, 1431-1439.
(193) Liu, J. M.; Huang, X. M.; Liu, Z. B.; Lin, S. Q.; Li, F. M.; Gao, F.; Li, Z. M.; Zeng, L. Q.; Li, L. Y.; Ouyang, Y. *Analytica Chimica Acta* **2009**, *648*, 226-234.
(194) Dyck, A. C.; Craig, D. B. *Luminescence* **2002**, *17*, 15-18.
(195) Abbyad, P.; Tharaux, P. L.; Martin, J. L.; Baroud, C. N.; Alexandrou, A. *Lab on a Chip* **2010**, *10*, 2505-2512.
(196) Baret, J. C.; Miller, O. J.; Taly, V.; Ryckelynck, M.; El-Harrak, A.; Frenz, L.; Rick, C.; Samuels, M. L.; Hutchison, J. B.; Agresti, J. J.; Link, D. R.; Weitz, D. A.; Griffiths, A. D. *Lab on a Chip* **2009**, *9*, 1850-1858.
(197) Stapleton, J. A.; Swartz, J. R. *Plos One* **2010**, *5*, -.
(198) Muijselaar, W. G. H. M.; Debruijn, C. H. M. M.; Everaerts, F. M. *Journal of Chromatography* **1992**, *605*, 115-123.
(199) Hult, E. L.; Emmer, A.; Roeraade, J. *Journal of Chromatography A* **1997**, *757*, 255-262.
(200) Emmer, A.; Roeraade, J. *Electrophoresis* **2001**, *22*, 660-665.
(201) Cifuentes, A.; Canalejas, P.; Ortega, A.; Diez-Masa, J. C. *Journal of Chromatography A* **1998**, *823*, 561-571.
(202) Gomez, J. E.; Sandoval, E. *Electrophoresis* **2008**, *29*, 381-392.
(203) Engelhardt, H.; Cunatwalter, M. A. *Journal of Chromatography A* **1995**, *716*, 27-33.
(204) Bernal, J.; Rodriguez-Meizoso, I.; Elvira, C.; Ibanez, E.; Cifuentes, A. *Journal of Chromatography A* **2008**, *1204*, 104-109.
(205) Gilges, M.; Kleemiss, M. H.; Schomburg, G. *Analytical Chemistry* **1994**, *66*, 2038-2046.
(206) Haselberg, R.; de Jong, G. J.; Somsen, G. W. *Journal of Separation Science* **2009**, *32*, 2408-2415.
(207) Hjerten, S.; Kubo, K. *Electrophoresis* **1993**, *14*, 390-395.

(208) Towns, J. K.; Bao, J. M.; Regnier, F. E. *Journal of Chromatography* **1992**, *599*, 227-237.
(209) Busch, M. H. A.; Kraak, J. C.; Poppe, H. *Journal of Chromatography A* **1995**, *695*, 287-296.
(210) Albarghouthi, M. N.; Stein, T. M.; Barron, A. E. *Electrophoresis* **2003**, *24*, 1166-1175.
(211) Ng, C. L.; Lee, H. K.; Li, S. F. Y. *Journal of Chromatography A* **1994**, *659*, 427-434.